THE ROLE OF SORPTIVE PROCESSES IN THE ORGANIC CARBON AND NITROGEN CYCLES OF THE AMAZON RIVER BASIN

Anthony Keith Aufdenkampe

A dissertation submitted in partial fulfillment
of the requirements for the degree of

Doctor of Philosophy

University of Washington

2002

Program Authorized to Offer Degree: School of Oceanography

University of Washington
Graduate School

This is to certify that I have examined this copy of a doctoral dissertation by

Anthony Keith Aufdenkampe

and have found that it is complete and satisfactory in all respects,
and that any and all revisions required by the final
examining committee have been made.

Chair of Supervisory Committee:

_____
John I. Hedges

Reading Committee:

_____
John I. Hedges

_____
Richard G. Keil

_____
Paul D. Quay

Date: _____

In presenting this dissertation in partial fulfillment of the requirements for the Doctoral degree at the University of Washington, I agree that the Library shall make its copies freely available for inspection. I further agree that extensive copying of the dissertation is allowable only for scholarly purposes, consistent with "fair use" as prescribed in the U.S. Copyright Law. Requests for copying or reproduction of this dissertation may be referred to ProQuest Information and Learning, 300 North Zeeb Road, Ann Arbor, MI 48106-1346, to whom the author has granted "the right to reproduce and sell (a) copies of the manuscript in microform and/or (b) printed copies of the manuscript made from microform."

Signature: _____

Date: _____

University of Washington

ABSTRACT

THE ROLE OF SORPTIVE PROCESSES IN THE ORGANIC CARBON AND NITROGEN CYCLES OF THE AMAZON RIVER BASIN

Anthony Keith Aufdenkampe

Chair of the Supervisory Committee:

Professor John I. Hedges
School of Oceanography

Dissolved, mineral-associated, and mineral-free particulate organic matter (OM) fractions are compositionally distinct from one another in a wide range of aquatic and terrestrial environments. In the Amazon River Basin in particular, differences in elemental (C, N), isotopic (^{13}C, ^{14}C) and biochemical (amino acid, carbohydrate, lignin) compositions are greater between these three OM fractions than the variability within a fraction along the 1,800-km reach of the lower Amazon and its major tributaries. The overall goal of this dissertation has been to determine the extent to which sorption and related processes might contribute to these consistent compositional differences.

To test these questions I conducted a suite of laboratory experiments, in which natural suspended river sediments and organic-free kaolinite were mixed with various natural dissolved OM samples from throughout the Amazon. The first round of experiments demonstrated that sorption and related processes were responsible for essentially all of the characteristic organic nitrogen compositional patterns observed

in the Amazon River System. Total nitrogen, total hydrolyzable amino acids, basic amino acids and hydrophobic amino acids were all preferentially taken into the mineral-associated OM fraction relative to the parent DOM, whereas non-protein amino acids preferentially remained in solution. The second round of experiments compared sorption incubations that were inoculated with a native microbial community to sterile controls. Results demonstrated that the microbial community plays an important role in determining the extent of OM association with minerals as well as its elemental and isotopic composition, despite the fact that biomass is an insignificant fraction of this OM. Furthermore, this study presents conclusive evidence that sorption and related processes are responsible for 1-3 ‰ enrichments of ^{13}C of mineral-associated OM relative to the initial DOM.

Observations of OM composition in 18 rivers from the Andean headwaters to the Amazon lowlands of Peru were placed into the context of results from laboratory experiments. Downstream trends in elemental, isotopic, amino acid, and lignin compositions suggest that sorption and related processes are important to the evolution of organic matter in large rivers and that exchanges between phases are rapid relative to transport times within the river system.

TABLE OF CONTENTS

LIST OF FIGURES

Page

LIST OF TABLES

Page

ACKNOWLEDGEMENTS

I wish to express sincere gratitude for the guidance and opportunities provided by my advisor John Hedges and by the PI of CAMREX, Jeffrey Richey. Committee members Richard Keil, Paul Quay and John Barross have provided assistance in countless ways. I have also learned much from Allan Devol and James Murray. I also wish to thank the National Science Foundation's Program for Ecosystem Studies and NASA's Office of Earth Science for financial support of my research and studies.

Many others have contributed to the work presented in this thesis. Fieldwork would not have been possible without helpful facilitation by B. Forsberg, C. Llerena, and A. V. Krusche. Many thanks to T. Pimental, J. L. Semizo, B. J. Dickson for additional assistance in the field. E. Tsmakis and J. Gudeman performed most of the amino acid and lignin analyses presented in Chapter 5, S. Carpenter counted bacteria for Chapter 4, and M. Peterson, A. Knapp and many others provided an invaluable hand with many tasks in the lab. I owe much to the graduate students who "showed me the ropes" during my early years, M. McClain, S. Wilhelm, M. McCarthy and P. Hernes, to friends from my cohort, J. Schmidt and C. P. Sarason, and to all members of the Marine Organic Geochemsitry Group at UW. My thinking about the Amazon has especially benefited from collaboration with E. Mayorga.

I owe the most gratitude to Bonnie, who has nourished and supported me in so many indescribable ways during my graduate studies.

DEDICATION

To my parents, their parents and those before.

To Bonnie and to Lily

CHAPTER 1: INTRODUCTION

The driving question behind this dissertation is: What processes determine observed contrasts in the elemental, isotopic and biochemical compositions of dissolved versus co-existing mineral-associated organic matter in aquatic systems? Studies of natural organic matter (OM) in the environment have long used compositional characteristics to distinguish potential biological sources and infer the diagenetic state of OM. However, most studies - whether they focused on petroleum, soils, sediments, lakes or oceans - generally considered only particulate OM or only dissolved OM but rarely both. These choices were made because one phase most often dominates within a particular environmental system. Rivers however carry roughly equal amounts of dissolved versus particulate organic matter to the ocean (Meybeck 1982; Ludwig and Probst 1996). Thus, those who studied rivers were perhaps the first to notice that coexisting dissolved and particulate OM consistently exhibited considerably different compositions (Williams 1968). Interpreting compositional signatures based on studies of soil and sedimentary OM, it was inferred that dissolved organic matter (DOM) was more degraded and possibly came from different sources than fine particulate organic matter (FPOM) in the same waters (Williams 1968; Hedges et al. 1994).

In the last decade however, one of the most important new insights into organic matter dynamics has been an understanding of the critical role of organo-mineral associations. Within soils, suspended river sediments and marine shelf sediments, greater than 85% of fine particulate organic carbon (POC) is in intimate physical association with minerals [Trumbore, 1993 #187; Mayer, 1994 #33; Keil,

1997 #189 (Mayer 1994b; Bergamaschi et al. 1997). The organic carbon content of these associations is often strongly correlated with mineral surface area within (Keil et al. 1994b; Mayer 1994a; Hedges and Keil 1995; Mayer and Xing 2001), with observed loadings of 0.5-1.1 mg OC m^{-2}. Furthermore, the association with minerals appears to protect otherwise labile organic matter from degradation (Keil et al. 1994a; Nelson et al. 1994; Baldock and Skjemstad 2000). Thus, not only are sorption and related organo-mineral formation processes ubiquitous and quantitatively important in most natural systems, but also whether or not an organic molecule becomes associated with a mineral surface has a critical effect on the transport and fate of that molecule.

Different types of molecules, however, have different affinities for surfaces. Selective partitioning behavior has long been understood for small, discrete inorganic and organic molecules. Several studies have explored how such molecular selectivity might apply to the larger and more diverse organic molecules found dissolved in nature. Experimental and spectroscopic evidence suggests the preferential sorption of higher molecular weight, more aromatic and carboxyl rich, and more hydrophobic fractions of natural OM (Davis and Gloor 1981; Jardine et al. 1989; McKnight et al. 1992; Day et al. 1994). More recent evidence confirms that competition for mineral binding sites between different components of DOM enhances the sorptive fractionation of natural OM during sorption (Gu et al. 1995; Gu et al. 1996; Kaiser and Zech 1997). However, previous studies did not investigate the effect of sorption compositional signatures that are commonly used to distinguish sources or infer the extent of degradation of OM.

This leads us back to the central question of this dissertation. More specifically, do sorption and related processes produce compositional signatures that are discernable in dissolved and particulate natural organic matter fractions within the Amazon Basin? If so, how do patterns of selective partitioning affect signatures related to source or diagenesis? To answer these questions, I employed all three facets of research – detailed literature review, controlled laboratory experiments and field observations. These research efforts are presented in the following five chapters. Chapter 2 presents a geographic overview of the Amazon River system and synthesizes results from previous biogeochemical studies into a conceptual model of the processes controlling bioactive elements. Chapter 3 reports the results from my first experiments, designed to elucidate the role of sorption in determining compositional signatures related to organic nitrogen. Chapter 4 builds on the experimental methods and findings from Chapter 3, to determine the extent to which bacteria might mediate observed selective partitioning and also to test the hypothesis that sorptive processes are associated with isotopic shifts. Chapter 5 examines the compositions of organic matter fractions from 18 sites along a transect from the Andean headwaters to the Amazon lowlands of Peru, in order to assess where OM signatures are imprinted within the Amazon river system and whether these signatures evolve downstream. Chapter 6 summarizes previous chapters and describes implications for other natural systems.

CHAPTER 2: BIOACTIVE ELEMENTS IN THE AMAZON RIVER SYSTEM: THE ROLE OF SIZE ON FATE AND TRANSPORT

INTRODUCTION

The Amazon Basin drains a vast and heterogeneous region of Northern South America, encompassing large areas of seven nations and important population centers such as Manaus, Porto Velho, Iquitos, Cusco, and La Paz (Fig. 2.1). Despite the acceleration of human impact in the form of deforestation and land use change, mining and oil extraction, dam construction, and urbanization, larger tracts remain relatively pristine, and the main river channels remain largely unaffected by engineering (Lewis et al. 1995; Richey et al. 1997). The Amazon is of undeniable importance for local communities in particular, and Amazonian nations in general; but as the largest river system in the world it also plays a significant continental and global role in modulating climate, biogeochemical cycles, and terrestrial inputs to the ocean (Devol et al. 1994; Meade 1994; Devol and Hedges 2001; Marengo and Nobre in press).

An understanding of biogeochemical dynamics and controls in river systems is a central requirement of any effort to rationally manage fluvial resources and minimize the impact of human activity on riverine ecosystems. The cycling of bioactive materials (oxygen, carbon, nitrogen, phosphorus, etc.) in rivers, however, is mediated by physical and biological components, such as hydrology, sediment dynamics, and bacterial metabolism. In addition, the linkages between a river and the land it drains are often complex. An integrated approach that crosses disciplinary and

landscape boundaries is required to fully elucidate the biogeochemistry of a river system.

In this chapter I review and synthesize current understanding of the biogeochemistry of the Amazon River system. My goal is to provide a conceptual framework for subsequent chapters, rather than summarize all available data as has been done in the extensive reviews by Guyot (1993) and Lewis et al. (1995). In this overview, which was condensed from my contributions to a book chapter (Mayorga and Aufdenkampe in press), no new data or analyses are presented nor are observations discussed in extensive detail. Rather, numerous references are provided to the many papers that do so. After a brief introduction to the geography of the Amazon Basin, the remainder of the chapter describes the principal fractions of bioactive materials carried by rivers – their characteristics, sources and interactions – paying special attention to the role of size in fate and transport. While I refer to relevant research by other groups, I write this chapter from my perspective as a member of the CAMREX (**C**arbon in the **AM**azon **R**iver **EX**periment) project, with origins in oceanography that are evident in my view of river processes.

THE AMAZON RIVER AND ITS BASIN

The Amazon basin covers a continental-scale region of approximately six million km^2 (not including the Tocantins basin; Fig. 2.1 and 2.2). Such a large area will inevitably encompass very dissimilar environments, climates, and ecosystems. The main physiographic features of the basin and the river system have been extensively reviewed elsewhere (Sternberg 1975; Sioli 1984b; Lewis et al. 1995), and I provide only a brief outline. The main structural elements include the Precambrian,

highly weathered Guayana and Brazilian Shields, the Andean mountains to the west, the Andean alluvial foreland, and a central continental alluvium or trough (Fig. 2.1). Soils in the lowlands are generally deep and highly weathered, with prominent occurrences of sandy podzols in the shields. The soils in floodplains and alluvial regions around mainstems draining the Andes originate in the cordillera and are much less weathered. The climate is generally humid, with mean annual rainfall of approximately 2000 mm. However, precipitation in some regions in the northwest and the Andean piedmont can be much larger, whereas large regions in the east, south, and the high Andes can be drier or arid. More specifically, 10 -15% of the basin receives less than 1,500 mm of rainfall per year, while 6 -10% receives at least 3,000 mm of rainfall per year (unpub. data). The length of the dry season in particular has a large role in determining that type of vegetation that may be sustained. The lowlands are primarily covered by evergreen to semi-deciduous rain forest, but large regions have distinct savanna-like vegetation systems, often seasonally inundated in low-lying areas. River discharge generally displays strong seasonality, with changes in stage height of as much as 10 meters in the Amazon mainstem driving changes in the extent of inundation within the central lowlands from 100,000 km^2 in November to 350,000 km^2 in May (Richey et al. In Press). Discharge to the ocean is approximately 220,000 $m^3 s^{-1}$.

The variety of environments, massive scale of drainage areas and rivers, and relatively low levels of human impacts, has long attracted geochemical and ecological researchers to the region. Initial investigations centered on large rivers in the Brazilian Amazon, especially the Solimões-Amazonas mainstem, surrounding floodplains and major tributaries, and the region around Manaus (Sioli 1984b). Early

observations of three types of river water based on color (Wallace 1853) were later developed extensively and systematized by H. Sioli (Furch 1984; Sioli 1984a). Whitewater rivers have a characteristic muddy color, relatively high concentrations of dissolved solids, and alkaline to neutral pH; their high sediment load originates in Andean or alluvial regions. Examples include the Rios Solimões and Madeira, and other lowland rivers draining mountainous Andean regions. Blackwater rivers are tea-colored from high concentrations of dissolved organic matter (DOM), have negligible suspended sediment loads and medium transparencies, are very dilute in dissolved ions, and are usually acidic; they typically drain areas of low relief and sandy podzol soils. The Rio Negro is the classic example. Finally, clearwater rivers can have high transparencies and are clear or olive-green in color. Their dissolved load is typically low but varies across systems, and they have a wide range in pH, from acidic to alkaline, and low suspended sediment loads. Examples are the Rios Tapajos and Xingu.

THREE DISTINCT PHYSICAL SIZE CLASSES OF MATERIALS TRANSPORTED IN RIVERS

Riverine transport of bioactive elements from land to sea forms a major link in the global biogeochemical system. The diversity of matter carried within river water is extraordinary – weathered products of rocks and plants sustain all forms of living organisms. The entire continuum of material size is represented, ranging from individual molecules to boulders and trees. Early on in the study of rivers, materials in water were separated into fractions by size (Williams 1968; Meybeck 1982). Coarse particulate, fine particulate, and dissolved fractions were thus operationally defined using sieve pore sizes ranging from 20 to 65 μm to separate particulate

fractions, and filter pore sizes ranging from 0.1 to 1.0 μm to isolate dissolved constituents. These exact size cutoffs often differ slightly between research groups, chosen arbitrarily and largely out of convenience. In nature the size distribution of materials across these ranges is actually quite smooth. Despite this, the three size classes – coarse, fine and dissolved – consistently exhibit very distinct transport dynamics, degradation patterns and compositional characteristics. In addition, these three fractions remain compositionally distinct despite interacting with each other on a continual basis (Fig. 2.3, 2.4, 2.5).

COARSE PARTICLES

Essentially all the material transported by rivers starts out in the coarse particulate size class. Rock and decaying vegetation are physically and chemically weathered and eroded until they finally reach the river. While the coarse size class includes boulders and dead trees, most riverine studies have focused on sand sizes (defined as 63 μm – 2 mm within CAMREX). Because these coarse suspended sediments (CSS) settle quickly to the streambed, suspended concentrations are strongly dependent on stream flow velocities (Meade et al. 1985; Devol et al. 1995) and increase substantially with depth in the river (Curtis et al. 1979; Richey et al. 1986). Thus CSS transport is highly episodic or seasonal, with most occurring during flood events. For instance, the mainstem of the Amazon near Manaus has depth averaged CSS concentrations of 10-20 mg L^{-1} during low water and 45-70 mg L^{-1} at high water (Devol et al. 1995). The bedload, or the CSS travelling very close to, or even as part of, the fluid riverbed, is estimated to be a small fraction of total coarse sediment flux in the Amazon mainstem (Dunne et al. 1998) but it may be important in

smaller rivers. As for all the size classes, coarse particulates consist of both inorganic mineral material and organic material derived from the remains of living organisms.

Within the Amazon Basin, quartz is the dominant mineral in CSS with 25-75% of the total (Gibbs 1967); other primary silicates such as feldspars, micas, and chlorite comprise the remainder at 2-25% each. These primary minerals in rivers, surrounding soils and aquifers each exhibit distinctive weathering rates and products. Thus through weathering processes, the lithology, relief and climate of a watershed together determine the composition of the finer, secondary minerals such as alumino-silicate clays and iron and aluminum oxides and the composition of major dissolved inorganic ions, such as Ca^{2+}, Na^{+}, Mg^{2+}, HCO_3^{-}, Cl^{-} and Si species (Fig. 2.3) (Stallard and Edmond 1981; Stallard and Edmond 1983, 1987). The composition of CSS as a function of hydrograph remains unstudied, but hydrodynamic sorting of CSS components would be expected to produce spatial and temporal variations in CSS composition within a reach.

In the Amazon mainstem and other large turbid rivers, organic matter (OM) is a small but important portion of the CSS fraction, comprising only 0.6-3.3% by mass (Richey et al. 1990; Devol et al. 1995). However as CSS concentrations decrease in rivers, OM contributions increase to as high as 10-30% in the clearest waters (Hedges et al. 1994, and unpublished data). In all cases, microscopic studies reveal that most coarse particulate organic matter (CPOM) in rivers resembles partially degraded plant fragments, often retaining visible cell structure (Keil et al. 1997). CPOM is less dense than mineral grains of the same size, hence explaining its higher contribution to CSS in river channels under low flow. 10-20% of CPOM can be identified biochemically as amino acids, carbohydrates and lignins – the primary molecular

building blocks of living organisms – relative to 25-60% within biomass sources (Fig. 2.5) (Hedges et al. 1986a; Hedges et al. 1994; Hedges et al. 2000). Biochemical source indicators, such as carbon to nitrogen ratio and the ratio of cinamyl to vanilyl lignin phenols, all show that Amazon Basin CPOM is primarily derived from tree leaves (Fig. 2.6a) (Devol and Hedges 2001). Several other lines of evidence, including stable carbon isotope compositions, confirm these conclusions but also show minor contributions from grasses for certain rivers (data not shown Quay et al. 1992; Victoria et al. 1992). Biochemical indicators of degradation, such as the contribution of fucose and rhamnose sugars to total carbohydrates and acid to aldehyde ratios in lignin phenols, all support evidence from microscopic studies and major biochemical composition that CPOM is sparingly degraded and rather fresh (Fig. 2.6b). Radiocarbon analysis of CPOM and low density soil POM confirms their recent origin (Hedges et al. 1986b; Trumbore et al. 1995). It is clear that CPOM is actively degrading and leaching, supplying microbes with substrate and releasing dissolved organic and inorganic compounds into the river. These rates have not been directly measured, but are likely to be quite high. Stream and river budgets suggest that CPOM continuously enters the river mostly from bank vegetation and detritus falling directly into the water (McClain et al. 1997).

Coarse suspended river sediments are thus a heterogeneous mixture of sand sized mineral grains and discrete plant fragments (Fig. 2.3). Both inorganic and organic constituents of CSS are generally fresh and supply the dissolved component (or “pool”) as they degrade. CSS deposits on the river bed and in sand bars form a relatively porous sediment buffer or “hyporheic” zone (Boulton et al. 1998) that acts

as a biological reactor, supplying the river with its products and forming new riverine environments that can be colonized by vegetation.

FINE PARTICLES

Fine suspended sediments (FSS) consist of clays and silts, material between 0.45 and 63 μm in size as defined by CAMREX. Maintained in suspension by the slightest turbulence, FSS is often referred to as the "wash load" by geomorphologists, because once introduced to a stream or river, FSS will generally not settle. Notable environments that often prevent FSS from washing directly out to sea are lakes, reservoirs, and floodplains. For instance, evidence suggests that within the Amazon – with its extensive annually flooded plains – a typical FSS particle passes through floodplain deposits several times between the Peruvian border and the Atlantic (Martinelli et al. 1993; Dunne et al. 1998). Given the patterns of channel migration, each cycle of floodplain deposition and re-suspension requires a few thousand years (Mertes et al. 1996). Because FSS is mobilized by erosion events, concentrations are also a function of river discharge, although the tendency for FSS to not be redeposited results in weaker correlations than those observed for CSS (Devol et al. 1995). The mainstem of the Amazon near Manaus exhibits FSS concentrations of 70-120 mg L^{-1} during low water and annual maximums of 210-340 mg L^{-1} during the rising hydrograph (Devol et al. 1995).

Mineralogy within the FSS fraction can be quite diverse. Silt size grains (5-63 μm) often retain many of the characteristics of the CSS fraction while at the same time showing signs of being more weathered (Fig. 2.4a). Fine quartz is important in more weathered lowland basins whereas other primary silicate minerals dominate in

rivers draining the Andes (Gibbs 1967). Clays and oxides are aggregated with the larger minerals in important quantities. The clay size fraction (0.45-5 μm) is composed mostly of phylo alumino-silicate clay minerals, which are the weathering products of primary silicates (Fig. 2.3, 2.4b). As can be seen in figures 4a and 4b, mineral diversity within FSS is very large and depends on the geology (source minerals) and climate (weathering rates) of the watershed. As a result, mineralogical compositions within the Amazon are constantly evolving downstream with inputs from tributary watersheds and from weathering during temporary storage in the floodplain (Johnsson and Meade 1990; Martinelli et al. 1993). All FSS samples do have common characteristics however. This size fraction is generally high in surface area and high in cation and anion exchange capacity. As such, significant quantities of certain inorganic ions (e.g. NH_4^+, PO_4^{3-} and most metals) and organic compounds (e.g. natural organic matter, contaminants, etc.) can potentially be adsorbed to the mineral surfaces of FSS. Thus FSS actively interacts with the dissolved fraction, often acting as a buffer or reservoir for dissolved compounds (Fig. 2.3).

As with the CSS, organic matter contributes only a small fraction of FSS, generally 0.5-2.0% by weight in turbid rivers (Richey et al. 1990; Devol et al. 1995). Unlike CPOM however, fine particulate organic matter (FPOM) is tightly associated with the mineral phase (Fig. 2.3). In the Amazon and other rivers of the world, generally over 90% of the FPOM can not be physically separated from the mineral material (Keil et al. 1997; Mayer et al. 1998). With low-density material removed, the organic surface loadings of these sediments is consistently 0.5-1.1 mg C m^{-2} of mineral surface area, leading in part to the conclusion that sorption of natural DOM to minerals is the primary pathway in which FPOM is formed (Mayer 1994b; Hedges

and Keil 1995). Evidence suggests however that mineral-associated organic matter does not form uniform coatings over the surfaces, but rather as organic gel-like assemblages that cover <20% of the surfaces (Mayer 1999; Filius et al. 2000). However, sorbed organic matter affects mineral surface properties significantly by increasing cation exchange capacity and by offering hydrophobic phases into which organic contaminants (e.g. pesticides, petroleum products, etc.) and heavy metals readily sorb (Benedetti et al. 1995). Biochemically, a smaller fraction of FPOM is identifiable as carbohydrates or lignins when compared to CPOM (Fig. 2.5), but often a larger fraction is identifiable as amino acids. FPOM appears to come largely from leaf material as does CPOM (Fig. 2.6a), but often falls slightly outside of the biochemical range that is possible by mixing biomass alone, as might be expected of diagenetically altered material (Devol and Hedges 2001). Specific degradation parameters show this clearly (Fig. 2.6b), however riverine FPOM is still relatively fresh compared to riverine DOM or deep-sea sediments (Hedges et al. 1994). This appears to be the result of physical protection from microbial attack that is offered by the intimate association of FPOM with mineral surfaces (Keil et al. 1994a; Baldock and Skjemstad 2000; Kaiser and Guggenberger 2000).

FSS is thus a diverse but tightly associated mixture of minerals and organic matter that interacts strongly with other size fractions (Fig. 2.3). Fine minerals are formed from the weathering of coarse minerals, and FPOM largely results from sorptive interactions with dissolved organics. However, the major characteristics of FPOM most likely form within soils prior to erosion into rivers. Mineralogical and biochemical evidence all points to this conclusion (Devol and Hedges 2001), including carbon-14 dates hundreds to thousands of years old (Hedges et al. 1986b,

and unpublished data). However, whereas high relief source basins are the ultimate source for >90% of river-borne FSS (Meade 1994), stable carbon isotopes show that at Obidos >60% of the associated FPOM originates in the lowlands (Quay et al. 1992; Hedges et al. 2000). With such high levels of surface exchange and activity, deposited FSS forms highly fertile soils and sediments, often far from the river channel.

DISSOLVED MATTER

Just as for the particulate size classes, the dissolved fraction (<0.45 μm as defined by CAMREX) is composed of matter spanning a continuum of sizes, from truly dissolved individual molecules to colloidal minerals and organic gels. The distinguishing physical feature of material in the <0.45 μm size class is that it will stay in suspension indefinitely due to Brownian motion alone. Thus, the transport of material in the dissolved pool is determined by the advection and mixing of the waters that carry it. However, fluxes are not only determined by hydrology but also by processes that transfer material in and out of the dissolved phase, such as degradation, adsorption and coagulation. Perhaps the most important characteristic of dissolved material is that it has the potential to be directly bioavailable. Microbial organisms, plant roots, and many animal tissues will transport dissolved molecules across cellular membranes, both passively and actively. Likewise, contaminants exhibit their highest toxicity when in the dissolved phase. The only way to measure the mass of the entire dissolved pool is by evaporation, however it is much more typical to measure the concentration of individual compounds or compound classes.

The inorganic material within the dissolved fraction includes all major ions, nutrients, dissolved gases, and colloidal minerals. The major inorganic ion composition of the Amazon mainstem is very similar to the world river average, dominated by HCO_3^-, Ca^{2+}, Na^+, $Si(OH)_4 + SiO(OH)_3^-$, Cl^-, Mg^{2+} and SO_4^{2-} in order of importance (Stallard and Edmond 1983). Diversity within the Amazon basin parallels the pattern of other rivers of the world, with a wide range of ionic compositions and concentrations controlled largely by geology and weathering regime with minor inputs from precipitation (Stallard and Edmond 1983, 1987). Once within the river, these ions mix conservatively, such that conductivity and alkalinity serve as excellent tracers for water sources (Stallard and Edmond 1983; Devol et al. 1995). Of the bioactive compounds, phosphate shows the least systematic variability, generally 0.4-2.0 μM in turbid rivers as a result of buffering with larger mineral-bound reservoirs in the FSS (Forsberg et al. 1988; Devol et al. 1995). On the other hand, inorganic nitrogen compounds – NO_3^- and NH_4^+ – cycle rapidly via remineralization of organic matter and other microbial process such as nitrification and denitrification (McClain et al. 1994; Brandes et al. 1996; Boulton et al. 1998). Dynamics of dissolved gasses, such as O_2 and CO_2, are also largely controlled by the respiration of organic matter because river, floodplain and lake waters are dominantly heterotrophic (Cole et al. 1994; Cole and Caraco 2001). These within-river fluxes (more below) are in quasi- steady state balance with atmospheric gas exchange (Quay et al. 1992; Devol et al. 1995). Waters of the Amazon are characteristically supersaturated in CO_2 with respect to atmospheric equilibrium (by commonly a factor of 20-50) and act as a significant source of CO_2 to the atmosphere (Richey et al. In Press). Thus the dissolved inorganic constituents of river waters are

constantly evolving as a result of interactions with non-dissolved phases within the river corridor.

Dissolved organic matter (DOM) exists as a mixture of simple molecules, complex biomacromolecules, their partial degradation products and molecular assemblages or gels. Total concentrations, measured as dissolved organic carbon (DOC), depend strongly upon the mineralogy of the basin, highlighting the importance of sorption to DOM dynamics. Watersheds with soils dominated by quartz sands having low surface area produce black water rivers with 7-40 mg L^{-1} of DOC, whereas watersheds rich in clays produce surface waters with low DOC (2-7 mg L^{-1}) (Sioli 1984a; Nelson et al. 1993; McClain et al. 1997). To better understand the composition and dynamics of DOM, ultrafiltration techniques have employed membranes with pores as small as 1 nm to separate and concentrate DOM into various size fractions (Hedges et al. 1994; Küchler et al. 1994; Amon and Benner 1996a, b; Mounier et al. 1999; Patel et al. 1999). Generally, ultrafiltered DOM (UDOM) refers to organic material with molecular weights >1000 g mol^{-1} or daltons (HMW, or high molecular weight DOM in the CAMREX convention), including very high molecular weight subsets variously named VHMW DOM or colloidal organic carbon (COC) by different research groups (1000 dalton is approximately equivalent to a molecule of 1 nm diameter). Inorganic colloids also appear in UDOM fractions, comprising from 5-10% of the total mass in the Amazon lowlands to as much as 80-90% in the high Andes (Hedges et al. 2000).

In Amazon lowland rivers, 70-90% of total DOM can be isolated as UDOM (Hedges et al. 1994; Amon and Benner 1996a, b), with yields decreasing upstream to 40-50% in the Andes (Hedges et al. 2000). Relative to the two particulate classes,

UDOM contains the smallest fraction, 2.5-4.5%, identifiable as major biochemicals (Fig. 2.5), although UDOM also appears to be largely derived from tree leaves (Fig. 2.6a). DOM shows the most extensive signs of degradation of all three fractions (Fig. 2.6b) (Ertel et al. 1986; Hedges et al. 1986a; Hedges et al. 1994), yet radiocarbon analysis places the average age to be less than decades (Hedges et al. 1986b, and unpublished data).

Cumulative evidence suggests that DOM is produced largely from the degradation and/or leaching of leaf detritus similar to that in CPOM (Devol and Hedges 2001). Once in solution, biomacromolecules such as proteins and carbohydrates are easily hydrolyzed (a least partially) by exoenzymes for subsequent microbial uptake. As a result degradation tends to decrease both the size and bioavailability of HMW DOM to form the low molecular weight (LMW, ~200-1000 daltons) fraction (Amon and Benner 1996a). However, as all particulate and dissolved organic carbon fractions degrade, microbial activity and photochemistry can generate a pool of the smallest molecules (<200 daltons) – free amino acids, free sugars, and organic acids such as acetate and citrate (Amon and Benner 1996b; Moran and Zepp 1997). Despite the likelihood that this very low molecular weight (VLMW) DOM represents an exceedingly small proportion of total DOM in rivers, these compounds are generally extremely bioavailable and could drive significant biological fluxes. The relative proportions of VHMW, HMW, LMW and VLMW DOM fractions would be expected to evolve down river as a result of their different degradation rates. Coagulation and disassociation of DOM in and out of colloidal gel phases or mineral surfaces complicates these size dynamics significantly however, as

many of these processes respond to changes in pH and to ratios of polyvalent to monovalent ions in solution (such as Ca^{2+}/Na^{+}) (Chin et al. 1998; Kaiser 1998).

The dissolved fraction is particularly characterized by diversity and contrasts (Fig. 2.3). Organics and inorganics exist in both truly dissolved and colloidal phases. This mixture contains the most labile material carried by the river (e.g. NH_4^+, free amino acids, etc.) and also relatively non-labile weathering end-products (e.g. inorganic ions that determine alkalinity, LMW DOM, etc.). Some material is swept away with the water directly to sea, whereas transit times for other components are delayed considerably by interactions with mineral particles.

River metabolism

The CSS, FSS and dissolved fractions are compositionally distinct, yet interact with each other on a continual basis through the processes of degradation and sorption. The dynamics of one fraction can not be completely understood without considering the dynamics of the other two. Likewise, when considering whole-river processes, such as river metabolism, all three fractions must be considered together because nutrients and substrates (or pollutants) can reside in more than one fraction. A notable omission in the above discussion of river-borne material is microorganisms. Bacterial biomass accounts for only 15-50 μg OC L^{-1} (0.75-2.5 $x10^9$ cells L^{-1}) or <5% of total organic carbon (Wissmar et al. 1981; Benner et al. 1995), thus contributing insignificantly to the mass of any fraction. However, the microbial community mediates nearly all biochemical transformations in the natural environment, including the weathering of rocks, and as such the activity of microorganisms is implicit in every discussion of biogeochemistry.

Just as rivers provide microorganisms with a wide array of substrates, nutrients and energy sources, rivers contain within their corridors a diverse set of physicochemical environments within which nearly all biochemical transformations can occur. Most rivers in the Amazon are dominated by heterotrophic respiration over photosynthesis (R/P ratio > 3) due to low light penetration in turbid rivers and in canopy-covered streams (Quay et al. 1995). Community respiration rates in the Amazon and major tributaries show a wide range, from 0.2-2 μmol C L^{-1} hr^{-1} (Richey et al. 1990; Benner et al. 1995; Devol et al. 1995), with no consistent seasonal or river-type patterns. These rates appear to be substrate limited rather than nutrient limited (Benner et al. 1995), further evidence that the bulk of dissolved and particulate OM in rivers is of limited bioavailability but that a small pool of labile compounds fuels the majority of respiration (Amon and Benner 1996a). Water flow in and out of suboxic and anoxic hyporheic zones in river beds is a likely source of labile fermentation products to the river. Methane gradients from banks to the main river channel can be quite large (Richey et al. 1988; Devol et al. 1994), but quantification of fluxes for other associated fermentation products has not yet been attempted. Lastly, in less turbid waters photochemical reactions can be important in both oxidizing DOM and in releasing VLMW organic compounds from more recalcitrant material for bacterial consumption (Amon and Benner 1996b; Moran and Zepp 1997). As light penetration increases, so does photosynthesis. In floodplain lakes, grassland streams, clearwater rivers and to some extent blackwater rivers, respiration to photosynthesis ratios approach one (Quay et al. 1995). Depth integrated gross photosynthesis in these waters is comparable to the more productive regions of the oceans, with rates as high as 160 mmol C m^{-2} d^{-1} (Wissmar et al. 1981;

Quay et al. 1995). All of these various biological process are cumulatively important. Concentrations of CO_2 over the Amazon surface exhibit a diurnal cycle with amplitudes of 70 to 150 ppm (Quay et al. 1989). Thus, to say that large rivers "breath" is not simply metaphorical.

OVERVIEW

The Amazon River Basin – from the Andean Cordillera to the Atlantic Ocean – contains within its border a large variety of river and basin types. Nevertheless, these rivers exhibit remarkable consistencies in the processes that control the fate and transport of bioactive elements. River-borne material resides in three compositionally distinct size fractions that have contrasting transport properties and reaction histories. Coarse particulates are the freshest, degrading to form the fine particulate and dissolved fractions, which continually interact with each other via sorption processes. Organic matter in these fractions contains most of the bioactive material in the river, yet inorganic material is of critical importance due to its ability to complex and protect organic matter from degradation.

Variability in the composition and dynamics of river-borne material from one river (or season) to another is often much less than differences between size fractions within a single river (or season). However, it is often this variability that potentially offers the most insight regarding important processes. Furthermore, understanding how these processes scale with basin size is of critical importance. The watersheds of streams and small rivers most often represent a single geologic and climatic zone. Each small river thus exhibits the narrow range of characteristics typical of its limited basin, yet these rivers respond to episodic forcing (storms, landslides, fires,

development) quite quickly and strongly. Large rivers can contain high sub-basin heterogeneity with respect to ecosystems, geology, climate, and timing of weather events. Material carried by these large rivers integrates this heterogeneity, yet the relative influence of each sub-basin is continually changing with time and with distance downstream. It may thus be possible to take advantage of these inherent spatial and temporal variations to advance our understanding of the processing of organic matter in large river systems.

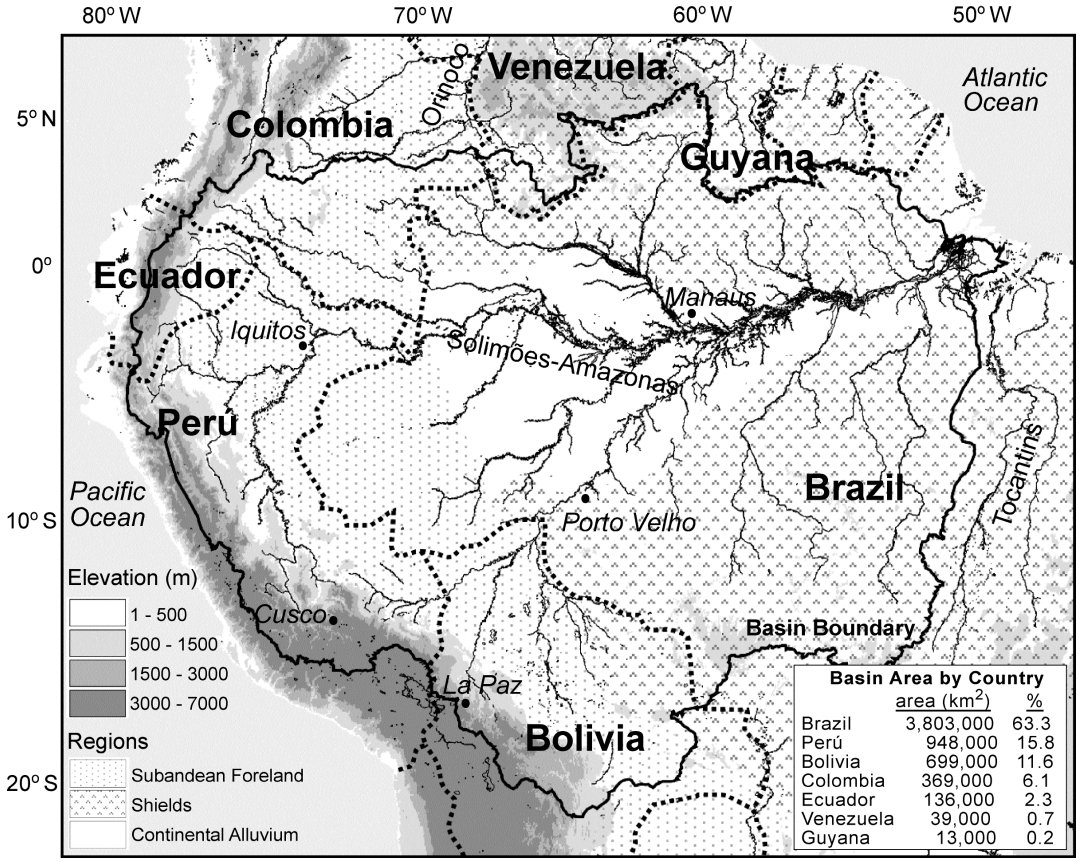

Figure 2.1. General physiographic features of the Amazon basin. The basin boundary is shown as a thick black line. National boundaries are shown as thick dotted lines. Major cities in the basin are included. The portion of the the total basin area encompassed in each country is listed in the inset table; total basin area is 6,007,000 km2. Also shown are elevation and the main morphostructural regions.

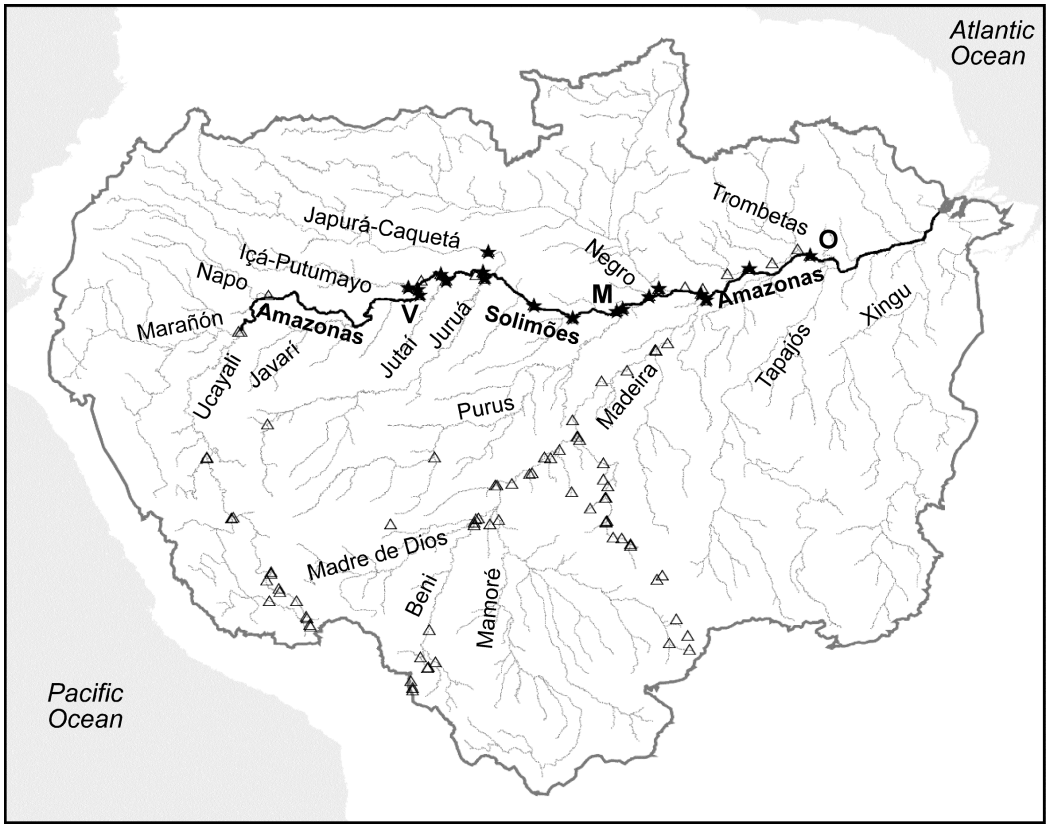

Figure 2.2. Amazon river network and CAMREX river sampling sites. The names of the mainstem and major tributaries are shown. The Amazon mainstem (thick black line) first begins under the name of "Amazonas" in the confluence of the Ucayali and Marañón in Perú. As it enters Brazil, its name changes to "Solimões", and becomes the "Amazonas" again after the confluence of the Rio Negro. The total length of the river is about 6,500 km, from its mouth to its source in the Ucayali headwaters south of Cusco. CAMREX mainstem sampling stations are shown as solid stars, from Vargem Grande (V) to Óbidos (O). 11 mainstem sites and the mouths of the 7 major tributaries were sampled through cross-sectional composites during 12 cruises between 1982 and 1991.All other CAMREX sampling sites are shown as open triangles. The site of the Marchantaria-Manacapurú time series is labelled "M".

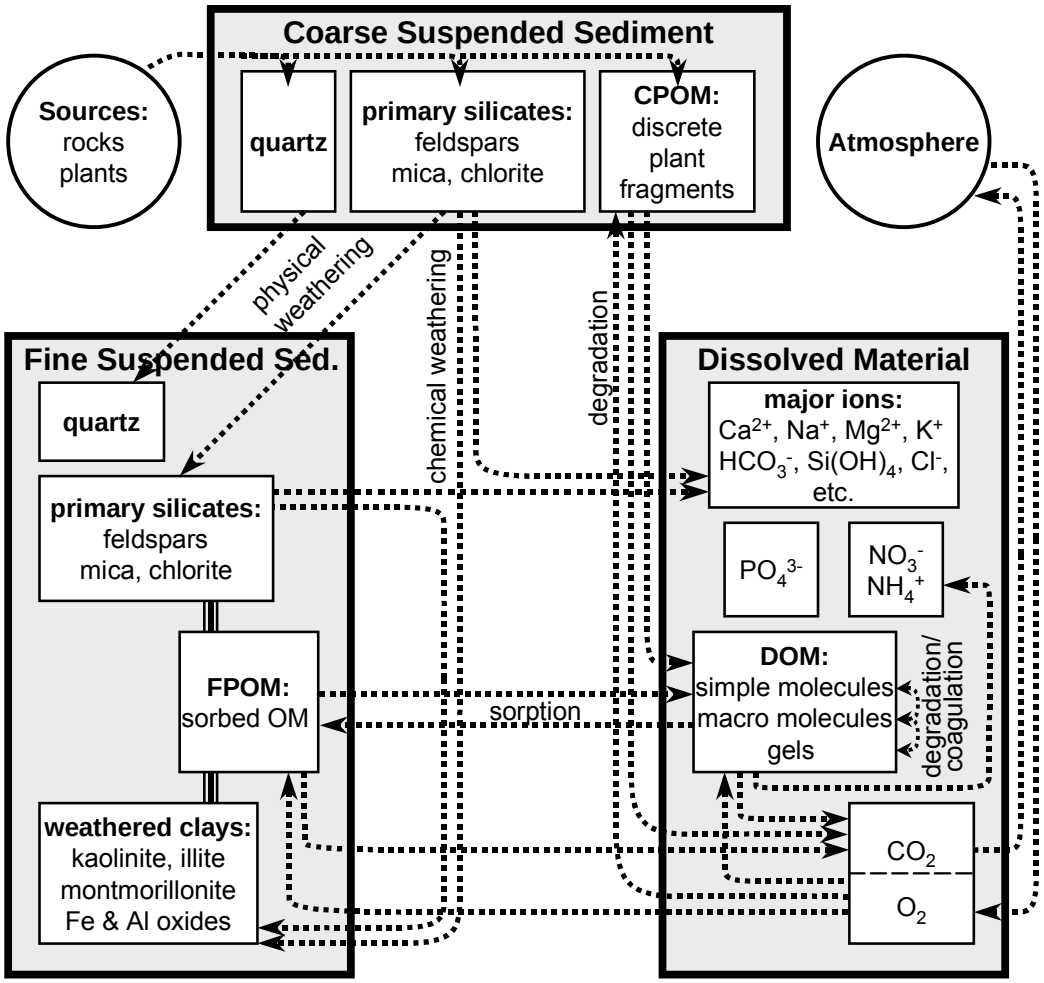

Figure 2.3. Conceptual model for the composition of the three principal size fractions carried by rivers, and the processes that are responsible for continuous interactions between them. Microbial mediation of these processes is implicit for many of these arrows. Bars connecting boxes within the fine particulate fraction represent the physical associations between mineral and organic components.

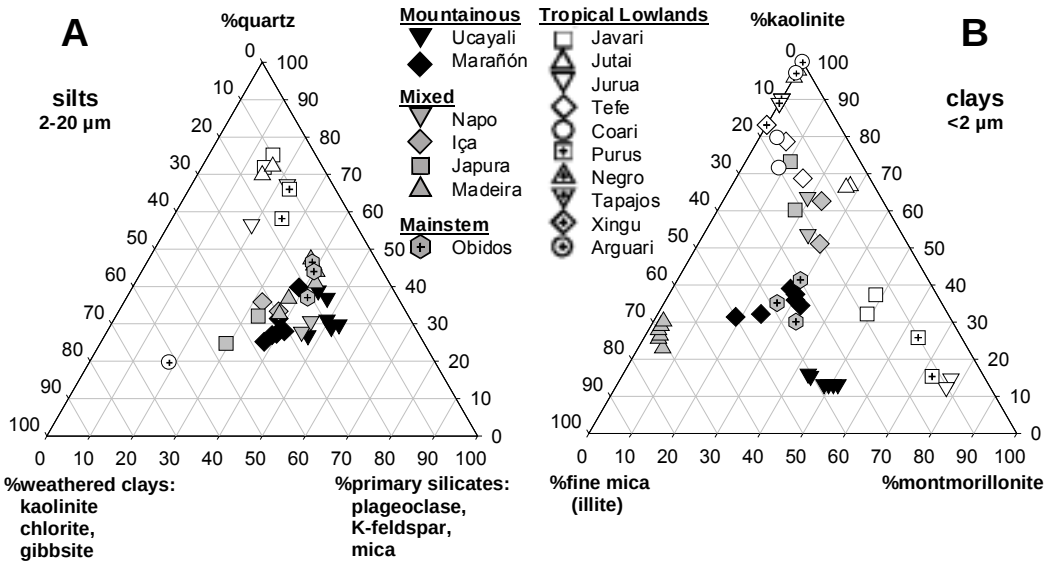

Figure 2.4. Major mineralogical composition of A) silt sized sediments (2-20 µm) and B) clay sized sediments (<2 µm) within the Amazon Basin. "Mixed" refers to river basins that drain both mountainous and lowland environments. Data from Gibbs (1967).

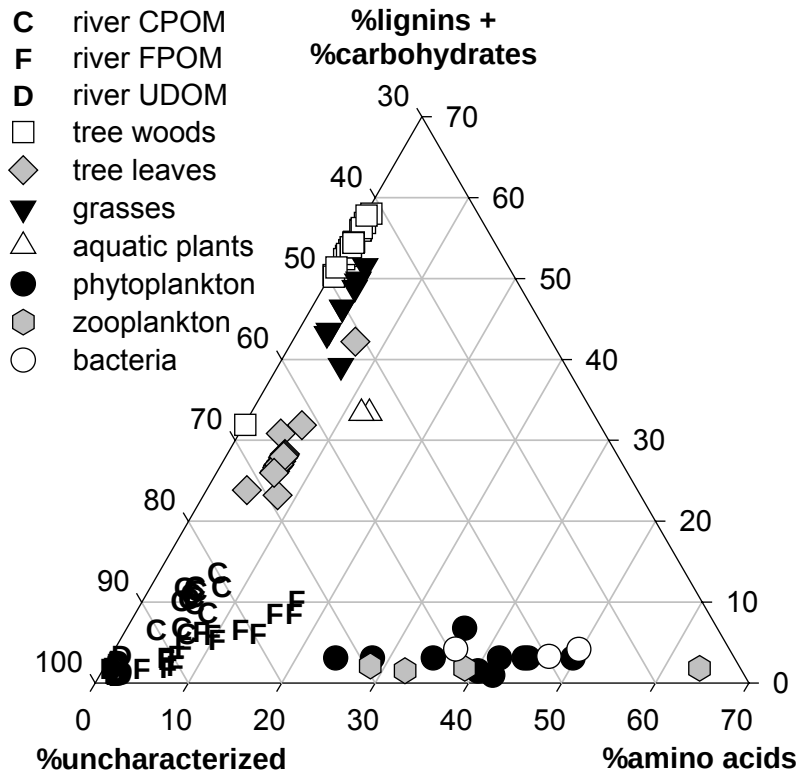

Figure 2.5. Major biochemical composition of coarse and fine particulate organic matter (OM) and ultrafiltered dissolved OM carried by rivers of the Amazon Basin, relative to the composition of source materials. River data from Ertel et al. (1986), Hedges et al. (1986), Hedges et al. (1994), Hedges et al. (2000) and source data from these papers and from Cowie and Hedges (1984; 1992b), Goni and Hedges (1992) and unpublished data. Notice that upper and right axes terminate at 70% of the respective biochemicals, due to all samples containing at least 30% of OM not identifiable in these biochemical classes. All DOM compositions fall in the grouping at >95% uncharacterized.

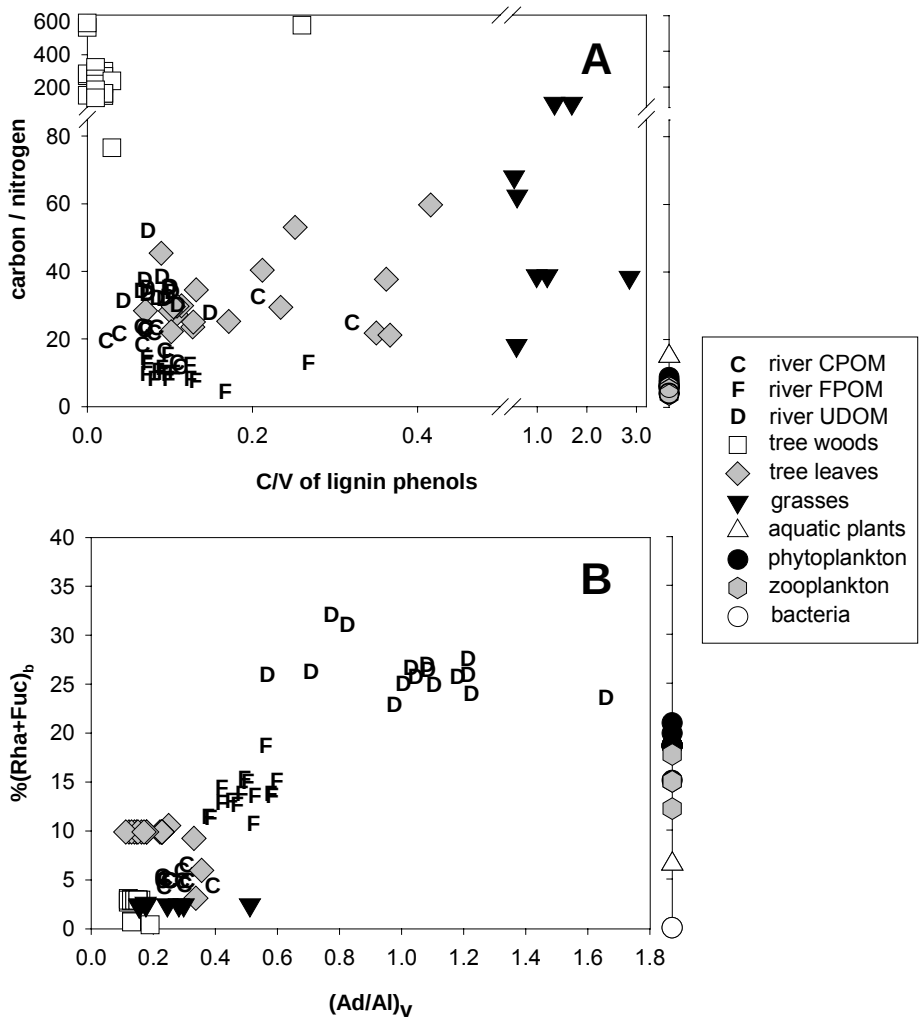

Figure 2.6. Biochemical parameters commonly used to interpret A) organic matter sources and B) organic matter degradation. Riverine coarse and fine particulate OM and ultrafiltered dissolved OM are again presented relative to common source materials. In A, the ratio of cinamyl to vanilyl lignin phenols (C/V) clearly distinguishes between woods, leaves, grasses and all aquatic organisms (which contain no lignin and are thus plotted to the right). In B, FPOM and UDOM are outside the range of plant sources with respect to both the acid to aldehyde ratio of lignin phenols, (Ad/Al)v, and the percent contribution of sugars rhamnose and fucose to total carbohydrates, $\%(Rha+Fuc)_b$ -- two parameters that increase with increasing degradation within sediments. Data obtained from the references listed for Figure 5. Average $\%(Rha+Fuc)_b$ values were used for some woods and leaves for which no measurements were made.

CHAPTER 3: SORPTIVE FRACTIONATION OF DISSOLVED ORGANIC NITROGEN AND AMINO ACIDS ONTO FINE SEDIMENTS WITHIN THE AMAZON BASIN

INTRODUCTION

Riverine transport of organic matter (OM) from land to sea represents a major link in the global cycles of bioactive elements, which modulates the biosphere over geological time (Meybeck 1982). These terrestrial OM losses support significant heterotrophic activity within rivers, estuaries and marine systems alike (Kaplan and Newbold 1993; Mayer et al. 1998). Where and when this river-borne OM is finally respired is of consequence to global carbon models (Stallard 1998). Thus, understanding the processes that control the pathways from initial source to final mineralization of riverine organic matter is important on both regional and global scales.

Three dominant and competing processes of OM cycling are advective transport, degradation, and sorption. Of these, the importance of sorption has only recently been appreciated. Most mineral surfaces in the biosphere maintain strong physicochemical associations with organic molecules, gels and micro-aggregates (Oades 1989; Mayer 1994a; Christensen 1996) at relatively consistent organic carbon (OC) to surface area (SA) ratios of 0.5 – 1.1 mg OC m^{-2} SA (Mayer 1994a; Hedges and Keil 1995; Keil et al. 1997). Sorption – defined for this paper as all processes by which organo-mineral associations are formed – is found to be fast with respect to biodegradation (McKnight et al. 1992; Qualls and Haines 1992; Day et al. 1994) and sparingly reversible (Zhou et al. 1994; Gu et al. 1995). Most importantly, the intimate association of OM with mineral surfaces significantly decreases its

bioavailability (Keil et al. 1994a; Nelson et al. 1994; Baldock and Skjemstad 2000). Whether an organic molecule sorbs or remains dissolved determines in large part its transport potential and susceptibility to degradation.

In the Amazon and other major rivers of the world, about 90% of transported organic matter is either sorbed to fine minerals or has remained dissolved (Meybeck 1982; Keil et al. 1997). Worldwide, the compositions of these two fractions are quite distinct, whereas differences within a fraction from one river to another are generally subtle. Relative to co-existing dissolved organic matter (DOM), fine particulate organic matter (FPOM, 0.45 - 63 μm) is generally enriched in ^{13}C and ^{15}N (Quay et al. 1992; Hedges et al. 2000) and depleted in ^{14}C (Hedges et al. 1986a; Raymond and Bauer 2001), suggesting different sources and pathways. Biochemically, FPOM consistently has lower carbon to nitrogen ratios (Williams 1968; Meybeck 1982; Lewis et al. 1995, and many others), higher hydrolyzable amino acid and carbohydrate concentrations (Ittekkot et al. 1986; McKnight et al. 1992; Hedges et al. 1994; Mannino and Harvey 2000), less non-protein amino acids (Hedges et al. 1994; Mannino and Harvey 2000), higher ratios of glucose relative to fucose and rhamnose (Hedges et al. 1994; Hedges et al. 2000) and lower acid to aldehyde ratios in lignin phenols (Ertel et al. 1986; Hedges et al. 2000; Lobbes et al. 2000). Previous interpretation of these biochemical differences, largely based relative to compositions of aquatic primary producers, suggests that riverine FPOM is substantially less degraded than DOM. On the other hand, the biochemical signature of riverine FPOM closely resembles OM in tropical mineral soils.

One biochemical signature, that basic amino acids are enriched in riverine FPOM relative to DOM, has its most plausible explanation in preferential sorption of

these amino acids over others (Hedges et al. 1994; Hedges et al. 2000). At natural pH, the nitrogenous amine side chain of basic amino acids provides a net positive charge that is attracted to the net negative charge of aluminosilicate clay minerals comprising the bulk of fine riverine sediments (Gibbs 1967). This type of preferential sorption has been observed for mixtures of dissolved free amino acids (Dashman and Stotzky 1982; Hedges and Hare 1987; Henrichs and Sugai 1993; Wang and Lee 1993), and for melanoidin polymers synthesized from the condensation of glucose with acidic, neutral and basic amino acids (Hedges 1978). These arguments could be extended to observations of total nitrogen and amino acid enrichment on FPOM as well – two compositional patterns that are commonly interpreted as signs that FPOM is less degraded.

The idea that organic matter biochemically fractionates during sorption is far from new. Evidence for preferential sorption of higher molecular weight, more aromatic and carboxyl rich, and more hydrophobic fractions of natural OM (Davis and Gloor 1981; Jardine et al. 1989; McKnight et al. 1992; Day et al. 1994) has long suggested such fractionation. More recent evidence confirms that sorptive fractionation of natural OM occurs as a result of competition for mineral binding sites (Gu et al. 1995; Gu et al. 1996; Kaiser and Zech 1997). However, no study has specifically tested whether the same biochemical signatures that are used to infer differences in sources or degradation history might also be affected by sorptive fractionation. This study takes a first step in that direction.

The goal of this study is to examine which, if any, of the nitrogen and amino acid compositional signatures of riverine DOM and FPOM directly result from sorptive fractionation. To test this hypothesis, changes in DOM and POM

compositions during sorption were directly observed in a set of nine laboratory experiments, in which natural suspended river sediments and organic-free kaolinite were mixed with various natural DOM samples from the Peruvian Amazon. Incubation conditions were consciously chosen to best mimic those found in rivers, including inoculation with native microbial consortia. The Amazon Basin in Peru is an ideal site to test these hypotheses. This region contains both tropical lowland and montane river types, which happen to be well characterized with respect to their dissolved and particulate amino acid patterns (Hedges et al. 1994; Hedges et al. 2000).

METHODS

Sample Collection

All samples were collected during the October 1996 CAMREX (Carbon in the Amazon River Experiment) expedition to Amazon River source basins in Peru (Table 3.1). Samples spanned most major environments found in the Amazon watershed – from Andean "Altiplano" grasslands at 4000+ m elevation, to cobbled "mesoscale" rivers in the 200-500 m foothills, and finally to the typical lowland Amazon mainstem at ~100 m elevation near Iquitos.

Natural DOM and suspended sediments were collected from rivers by gentle pumping (ShurFlo DC submersible diaphragm pump) to avoid excessive shear stresses on particles. The pump was submerged to 6/10 the total river depth (4/10 from bottom) in the thalweg (main flow) in order to sample suspended sediment size distributions where water velocities are most representative of depth-integrated fluxes. Wetland waters were collected by submerging bottles 50 cm below the

surface. Coarse, sand-sized suspended material was removed in the field from river and wetland waters with a 63 μm sieve. All samples were processed for sorption experiments within several hours of collection.

Sorptive Partitioning Experiment

Individual partitioning experiments (Fig. 3.1) were conducted in field labs by mixing 1-2 L of natural pre-filtered DOM (using precombusted Whatman® GF/F filters, nominal pore size of 0.7 μm) with suspended minerals at concentrations representative of rivers sampled during the field expedition (~300 mg sediment L^{-1}). DOM samples were collected from two rivers and one wetland (Table 3.1). In addition, two leaf litter leachates were created by immersing litter from dominant grass communities in distilled water for 24 hours. These five DOM samples were mixed individually with either naturally suspended fine particles from two rivers (added as whole water suspensions) or with an organic-free kaolinite (Ward's kaolinite API#5 from Bath, South Carolina) as a control sorbent. Organic carbon had been removed from the kaolinite earlier by pre-treatment with 30% hydrogen peroxide for 2.5 hours at 50-60°C – a process which reduced organic carbon concentrations from 0.38% to 0.040% (final molar C/N = 15.5). These dissolved and particulate sample sets each represent a continuum of increasing freshness: the DOM suite follows a history of decreasing exposure to mineral surfaces and to bacterial degradation (Table 3.2), and the suspended sediments represent end-members of equilibration with ambient natural organic substances.

In all, nine different combinations of DOM and sediments were mixed in batch sorption type experiments (Table 3.2). In order to mimic conditions within rivers, mixtures were incubated for 24 hours under live conditions (i.e. with native

microbial communities) at ambient temperatures of 20-32°C (Fig. 3.1). During each 24 hour experiment, gentle agitation by flipping sample bottles every 1-5 hours maintained sediments in suspension as best as possible while not disturbing particle aggregates. Sorption experiments were terminated by filtration, taking care to homogeneously subsample suspended sediments using a churn sample splitter (Bel-Art). Fine suspended sediment (FSS) concentrations were determined gravimetrically by filtration of a known water volume onto pre-weighed membrane filters (Millipore HAWP, 0.45 μm pore size), with FSS replicates confirming the ability to consistently and homogeneously subsample a suspension. Samples for organic analysis were filtered through two stacked glass fiber filters (Whatman® GF/F, 0.7 μm pore size, pre-combusted at 500°C for 4 hours), with the lower of each filter pair serving as a DOM filter blank for all POM analyses. The quantity of water passed through each filter was chosen to maximize filter sediment loading; excessive particle clogging stopped filtration at 25-150 ml for 25 mm filters and 60-250 ml for 47 mm filters. Immediately after filtration, the resulting DOM sample was preserved with $HgCl_2$ to a final concentration of 100 μM, and filtered POM subsamples were air dried in a dehydrating oven (50° – 70°C). Sub-samples of both the DOM and the POM, before and after mixing, were analyzed for total organic carbon and nitrogen and hydrolyzable amino acids. After analysis, sorbed components were calculated as the difference between the initial and final concentrations.

Mineral Surface Characterization

Surface areas were measure by one-point BET (Brauner-Emmett-Teller) isotherms of N_2 adsorption using a Quantachrome Monosorb surface area analyzer, and normalized to a certified standard (Mayer 1994a). Uncertainties for this method

are <5% of measured values. Surface area was quantified for the two natural riverine suspended mineral samples from material isolated by tangential flow microfiltration with an Amicon H5MP01-43 hollow fiber filter (0.1 μm pore size). Prior to SA analyses, organic carbon was removed from these natural particle assemblages by combustion at 300°C for 12 hours. Preliminary diffuse reflectance infrared Fourier-transform (DRIFT) spectra (Janik et al. 1995) of these natural suspended sediment samples suggested appreciable quantities of smectites in addition to kaolinite, which is characteristic of the sampled basins of Peru (Gibbs 1967).

Organic Analyses

Particulate carbon and nitrogen were analyzed directly on whole 25 mm Whatman® GF/F filters (0.7 μm pore size) with a Leeman Labs CE440 elemental analyzer. For each sample, individual blanks (obtained by analysis of the lower of each filter pair) were subtracted from the total C and N measured. This individual filter blank approach was necessary because during filtration non-trivial and highly variable quantities of DOC and DON (2-70 μg C $filter^{-1}$) sorbed onto the filter versus procedural blanks in which ultra-low DOC Milli-Q water was passed through identical pre-combusted GF/F filters. Consistent with the findings of Moran et al. (1999), the amount of DOM sorbed into our blank filters was found through multiple linear regression analysis (MLR) to be positively correlated to DOC concentrations, total POC or PON on sample filter, and the total volume filtered (multiple $R^2 = 0.78$ for C and 0.64 for N, n = 65). However, because a lower filter blank was analyzed for every sample in my experiments, these MLR results were not used for blank estimation in my study. All POC analyses were run in duplicate on identically filtered subsamples. The combined analytical and experimental uncertainty

(including errors propagated through subtraction of lower filter blanks) averaged ±5%, with a maximum of ±14%.

Dissolved organic carbon (DOC) concentrations were measured after acidification and sparging with a modified high temperature combustion MQ Scientific 1001 DOC analyzer (M. L. Peterson et al., manuscript in preparation). The standard error of three injections per sample vial was generally 2-5%, however analytical reproducibility from day to day was closer to ±10%. Dissolved organic nitrogen was measured as the difference in nitrate concentrations before and after high intensity UV oxidation as per the method of Abell et al. (2000). In seawater this method exhibits essentially 100% oxidation efficiency and ±2% variability for replicates (Abell et al. 2000), however the $HgCl_2$ preservative in my samples necessitated use of a less precise nitrate analyzer and complicated calibration due to reduction column poisoning. Standard deviations of replicate analyses thus ranged from 3% to 10%, with propagated uncertainties of 6-17%

Amino acid analysis was performed with reverse-phase HPLC of hydrolysates versus charged-matched recovery standards based on the method of Cowie and Hedges (1992a). Sample quantities corresponding to 10-30 μg N were measured into 4 ml reaction vials via evaporation of whole water for DOM and via portions of 47 mm filters (punched out with cork bores to reproducibly cut out exact filter areas) for POM. The vial was then spiked with a mixture of acidic, basic, and neutral non-protein amino acids (α-aminoadipic acid, γ-methylleucine, and δ-hydroxylysine, respectively) as recovery standards for the corresponding charge classes of protein amino acids. All samples were hydrolyzed with 6 N HCl under N_2 in a sealed vial for 60-65 minutes at 150°C. Reaction mixtures were immediately neutralized by

repeated evaporation (Jouan RC1022 centrifugal vacuum evaporator) and borate buffer addition until reaching a pH of 8.5-9.5, pipetted into a clean vial (discarding the mineral matrix) and dried for frozen storage. Just prior to HPLC analysis, samples were redissolved in 1.0 ml Milli-Q water, filtered (Gelman A/E glass fiber filter), and spiked with *o*-methylthreonine as an analytical recovery standard. Amino acids in standards and samples were derivatized on-line immediately prior to injection (Gilson Model 231 sample injector) with *o*-phthaldialdehyde (OPA) and resolved on a 15 cm x 4.6 mm ID C_{18} analytical column (Beckman ODS ultrasphere, 5 μm pore size) using a binary solvent gradient of methanol versus aqueous sodium acetate (adjusted to pH 6.0). Fluorescent OPA derivatives were detected with a Waters Model 420 fluorescent detector (set to 328 nm excitation and monitoring >450 nm emissions) and quantified using EZ-Chrom Data System v. 6.5 (Scientific Software). Of the 20 amino acids found in protein, 16 can be quantified by this OPA method along with four natural non-protein amino acids. However, because of poor reproducibility of ornithine due to hydrolytic degradation (Cowie and Hedges 1992a), only 19 amino acids are presented here. The detection limits of this method with the Waters 420 fluorometer vary from amino acid to amino acid, ranging from 100 to 300 pmol injection^{-1}. Duplicate analyses were run on most samples, with variation <5% for all amino acids from POM samples and generally <15% for DOM samples (excepting a few cases of larger relative uncertainty for trace amino acids in a few samples).

RESULTS

Carbon and nitrogen sorption

Appreciable sorption of DOM to sediments occurred in all nine mixing sets (Table 3.2), with newly sorbed organic matter ranging from 0.1 to 3.0 weight percent POC (mg OC 100 mg^{-1} sediment). By analyzing both initial and final DOC and FPOC, mass balances could be calculated for each sorption experiment. Because mineral concentrations remained constant during each experiment, mass balance of organic carbon can be assessed from sediment mass normalized values (as in Table 3.2) or from volume or surface area normalized values (which can be calculated from Table 3.2). In general, carbon lost from the DOM pool was gained by the FPOM pool, with additional DOM losses likely due to respiration during the experiment. Small changes relative to total concentration for the dissolved fractions make calculations of lost DOC much less sensitive than for gained FPOC. Thus, for experiment numbers 1, 4 and 9 much less DOC disappeared than is reasonable (Table 3.2). Excluding these samples, respiration losses (estimated from OC loss) ranged from 22-25% of sorbed carbon for the natural river and wetland waters (or ~1% of initial DOC) and 15-60% of sorbed carbon for the leachates (or 2-20% of initial DOC).

Surface area (SA) loadings of all nine sorption experiments fell within the full range of values commonly observed in the natural environment (Table 3.2) (Hedges and Keil 1995). River and wetland DOM sorbed within the range of 0.1-0.2 mg OC m^{-2} SA, diluted leachates sorbed at 0.7-1.2 mg OC m^{-2} SA, and undiluted leachates sorbed at the highest levels of 2.4-2.7 mg OC m^{-2} SA. The extent of sorption generally increased with increasing DOM freshness.

Results of batch sorption experiments such as these are commonly expressed in terms of a partitioning coefficient (K_d), calculated as the ratio of final POC (mg OC

g^{-1} particle) to final DOC (mg OC L^{-1} water). Values determined for these nine experiments ranged from 0.07 to 1.8 L g^{-1} (Table 3.2). Plots of final sorbed versus dissolved concentrations, or adsorption isotherms, illustrate systematic changes in sorptive partitioning with changes in OC concentrations within a system (Fig. 3.2). Such a treatment of all of my data collectively is not conventional, because of the diverse sources of DOM and sediments used. Experiment numbers 1, 2, 3, 4 and 6 are strictly one-point isotherms and pairs 5, 7 and 8, 9 are two-point isotherms. Despite this caveat, it appears that a composite isotherm of surface-area normalized particulate concentrations for all nine experiments (Fig. 3.2) follows the classic hyperbolic form of the site-limited Langmuir isotherm ($r^2 = 0.84$), as is commonly observed for natural DOM sorption (Day et al. 1994; Gu et al. 1995). Natural suspended sediments from two different rivers both fall on the Langmuir isotherm line after equilibration with new DOM (experiments 4 and 6), despite containing appreciable quantities of smectite clays. Even the original river particles from these two experiments fall on the model line when compared to DOC concentrations in their respective rivers at the time of collection (Fig. 3.2). The asymptotic surface loading of the Langmuir model fit (2.3 ±1.1 mg OC m^{-2} SA) approached maximal surface loadings found in the environment (Hedges and Keil 1995).

Relative to carbon, dissolved organic nitrogen was preferentially partitioned onto mineral particles in all nine experiments (Table 3.2). Atomic carbon to nitrogen ratios of initial "parent" DOM and final FPOM ranged from 10-32 and from 4.3 to 9.1 respectively. Sorbed FPOM had atomic C/N ratios (calculated as the ratio of final minus initial carbon over final minus initial nitrogen) of 3.3 to 6.5 (Figure 3). Regressions of OC as a function of N for the initial DOM show a highly linear fit (r^2

= 0.997) with a slope of 19.6 ±0.6 (mol C mol^{-1} N) and an intercept of –1.1 ±4.5 mg C L^{-1}. A similar regression for the final FPOM associated with the kaolinite gave r^2 = 0.999, slope = 5.2 ±0.09 mol C mol^{-1} N and y-intercept = 0.00 ±0.02 mg C L^{-1}. The zero intercepts, especially for the FPOM fractions, are strong evidence that inorganic nitrogen, such as sorbed NH_4^+, did not contribute appreciably to C/N ratios.

Amino acid composition

The percent of total organic carbon measurable as amino acids ($\%T_{AA}C$) in natural river and wetland DOM (experiments 1-4) ranged from 0.6% to 3.5% (Table 3.3). Before sorption, amino acids comprised 4.4% to 5.2% of DOC in leachates and 8.0% and 9.5% of FPOC on the two natural river sediments. Amino acids accounted for 5.9% to 46% of FPOC for all sediments after sorption. In all nine cases, the organic material that sorbed was clearly enriched in amino acids relative to its parent DOM (Fig. 3.4A). Whereas sorption of natural waters produced FPOM with $\%T_{AA}C$ values characteristic of natural river sediments, the $\%T_{AA}C$ of FPOM sorbed from leachates greatly exceeded values of previously measured river sediments (Ittekkot et al. 1986; Hedges et al. 1994). As seen for OM surface loading, the degree of amino acid enrichment during sorption seemed to increase with increasing DOM freshness (Fig. 3.4A).

The preferential sorption of amino acids over other compounds was even apparent when normalized to total organic nitrogen ($\%T_{AA}N$) (Fig. 3.4B). Generally about twice the fraction of the sorbed nitrogen pool could be identified as occurring in amino acids when compared to the corresponding DON pool. In these experiments, $\%T_{AA}N$ values of both dissolved and particulate fractions were roughly comparable to those found for natural samples (Hedges et al. 1994; Hedges et al. 2000). Similar to

$\%T_{AA}C$ trends, preferential enrichment of amino acids relative to bulk nitrogen appeared to increase with increasing DOM freshness.

Analysis of the relative abundance of individual amino acids in each sample revealed distinct compositional trends between DOM and sorbed FPOM (Table 3.3). As is commonly done, amino acid compositions are presented and discussed here on a mole percent (mol%) basis, in which molar concentrations of each amino acid for a sample were normalized to the total concentration of all amino acids, such that their sum equals 100%. Amino acid compositions of DOM and FPOM were comparable to previously published data obtained using similar analytical methods (Keil et al. 2000). Glycine and alanine dominate, followed by glutamic acid/glutamine, valine and threonine. Mole percentages of methionine, tyrosine and histidine are all generally less than one.

Changes in amino acid compositions during sorption can be visualized in two ways (Fig. 3.5). First, direct changes in the contribution of an amino acid to the total pool can be calculated by subtracting mol% values of each initial DOM sample from the respective sorbed FPOM values. The resulting "difference" spectra (Fig. 3.5A) have units of Δmol%, such that positive values indicate enrichment in FPOM relative to DOM. The sum of these mol% differences for each sample equals zero. Visualizing enrichment in this way, the pattern of amino acid fractionation was remarkably consistent from one sample to another. These patterns could be generally grouped by the side-chain functionality of individual amino acids. Basic amino acids, with positively charged nitrogenous side chains, were strongly enriched in the sorbed FPOM relative to the initial DOM. The summed contribution of basic amino acids as a group increased by 3-11 mol%. Amino acids with more hydrophobic side chains –

with the exception of valine – were also enriched in the FPOM, generally by 2-4% each. Concentrations of non-protein amino acids (NPAA) as a group approached the detection limit in FPOM, whereas NPAAs comprised 8-12 mol% in dissolved samples. Glycine and alanine showed large, negative Δmol% values for a few of the experiments. However, as dominant amino acids these depletions in the FPOM were relatively minor compared to their overall concentrations. In fact, much of this depletion may simply result from mathematical artifacts introduced by presenting compositions on a mol% basis. Because the sum of mol% values of all amino acids in a sample must equal 100%, a change in the absolute concentration of only one amino acid will change the mol% values of all other amino acids. Furthermore, this change is not uniformly distributed. For each amino acid, the change is directly proportional to the new mol% value of that amino acid. Therefore, the depiction of compositional differences in Figure 5A may misrepresent sorptive fractionation for certain of the more abundant amino acids.

An alternate way to visualize fractionation patterns that does not present these biases is through an enrichment factor (Fig. 3.5B), in which proportional changes in the contribution of each amino acid in the initial fraction are compared relative to the final fraction. The enrichment factor is calculated as the mol% value found in FPOM divided by the mol% in DOM, yielding values >1 for amino acids enriched in FPOM. To ease graphical comparison with amino acids depleted in FPOM, the negative inverse, $-\text{mol\%}_{DOM}/\text{mol\%}_{FPOM}$, was used to calculate DOM enrichment factors in lieu of values between 0 and 1. This visualization highlights the large fractionation of basic and non-protein amino acids. Basic amino acids were enriched in FPOM by a factor of 2-10 over their original contributions in DOM. NPAAs on the other hand

were highly depleted in the FPOM by factors generally ranging from 3 to 60. Hydrophobic amino acids (excepting valine) were enriched in FPOM by factors of 1.5-2.2. Alanine and glycine, due to their high relative abundance in DOM, were relatively depleted by generally less than a factor of 1.5. Methionine is perhaps the one amino acid misrepresented by this presentation. As a result of its trace levels in DOM, it showed large relative enrichment factors for six sorption experiments.

Following previous convention (Cowie and Hedges 1994; Hedges et al. 1994; Keil et al. 1998), the most striking of these dissolved versus particulate amino acid patterns can be summarized by two parameters, a sorption proxy B/(B+A) and a degradation proxy %(βAla+γAba). B/(B+A) represents the ratio of basic amino acids, arginine and lysine, to the sum of these basic plus the two acidic amino acids, aspartic and glutamic acid. Values for sorbed FPOM in these experiments are 0.15-0.20 larger than those for DOM (Fig. 3.6A). %(βAla+γAba) is the total mol% of β-alanine and γ-aminobutyric acid, the two most abundant non-protein amino acids. Values of this parameter ranged from 5.4% to 10.7% for initial DOM in these nine experiments, whereas sorbed FPOM never exceeded 2.2% (Fig. 3.6B). With the exception of river 1, dissolved %(βAla+γAba) increased with increasing DOM freshness.

DISCUSSION

Patterns of sorptive fractionation

The elemental and amino acid compositions of dissolved and particulate organic matter in these nine experiments – including those directly resulting from sorption – closely mimic compositional patterns of coexisting DOM and FPOM in the

Amazon (Fig. 3.7) and other rivers of the world. Experimental carbon-to-nitrogen ratios are substantially lower in all FPOM samples relative to the corresponding DOM (Fig. 3.3). Such nitrogen enrichment on particles is a dominant characteristic of organic matter in the Amazon River (Williams 1968; Hedges et al. 1994; Hedges et al. 2000) and other rivers around the world (Meybeck 1982; Lewis et al. 1995; Lobbes et al. 2000). The amino acid content of all DOM samples and of FPOM sorbed from natural river and wetland waters matched the range of $\%T_{AA}C$ and $\%T_{AA}N$ values observed previously at 15 sites within the Amazon (Fig. 3.4) (Hedges et al. 1994; Hedges et al. 2000), reproducing the typically strong pattern seen in rivers of amino acid enrichment on particles versus the dissolved phase (Ittekkot et al. 1986; McKnight et al. 1992; Mannino and Harvey 2000). Differences in mol% contributions of individual amino acids between DOM and FPOM in the experiments (Table 3.3 and Fig. 3.5) also closely mirrored patterns observed between naturally co-occurring DOM and FPOM fractions collected in the Amazon (Hedges et al. 1994; Hedges et al. 2000). Plots similar to those in Fig. 3.5 for these natural samples (not shown) reveal few exceptions to the trends shown here. Lastly, FPOM compositions in these experiments are all directly the result of sorbing DOM to particles with surface loadings within the typical range (0.1 to 2.0 mg OC m^{-2} SA) found for most riverine suspended sediments (Keil et al. 1997; Mayer et al. 1998).

This study thus presents substantial evidence that sorptive processes play a significant role in determining the organic nitrogen compositions of particulate material in river systems. Although the contrasting compositions of co-existing DOM and FPOM in rivers have long been noticed, substantial differences between the two phases with respect to likely sources, ages, and diagenetic histories have obscured the

role of sorption. By using well-characterized DOM sources in sorption experiments conducted under natural conditions, I clearly demonstrate that the contrasting nitrogen and amino acid patterns of DOM and aluminosilicate bound FPOM are primarily determined by preferential sorption of nitrogenous OM components.

The importance of sorptive fractionation to FPOM, and possibly DOM, compositions is likely not limited to riverine environments. Clear interpretation of published marine and soil data is hampered by the fact that few studies provide elemental and biochemical compositions of both DOM and coexisting mineral-associated FPOM. Many studies also use classic humic extraction methods (i.e. XAD resins) that preferentially exclude nitrogen and proteinaceous OM. Nevertheless, the pattern of enrichment of nitrogen and hydrolyzable amino acids in FPOM versus DOM does seem to extend to marine and soil environments. Molar carbon-to-nitrogen ratios of fine-grained marine sediments generally exhibit C/N ratios of 6 to 12 (Carter and Mitterer 1978; Cowie and Hedges 1992b; Keil et al. 1998, and many others), yet the few dissolved organic C/N ratios measured in pore waters range from 8 to 25 (Burdige and Zheng 1998; Lomstein et al. 1998) and coastal and oceanic DOM exhibits C/N values from 9 to 23 (McCarthy et al. 1996; Benner in press). Likewise, amino acids comprise 7% to 25% of organic carbon in coastal sediments (Carter and Mitterer 1978; Keil et al. 1998; Keil et al. 2000), yet $\%T_{AA}C$ values are ~9% for pore water DOM (Lomstein et al. 1998) and 2-6% for coastal and oceanic DOM (McCarthy et al. 1996; Benner in press). Even compositional patterns for basic, acidic and non-protein amino acids in marine environments show trends similar to those in rivers (McCarthy et al. 1996; Keil et al. 1998; Lomstein et al. 1998). In soils, mineral-associated FPOM exhibits C/N ratios of 7-14 (Oades 1989; Amelung et

al. 1998), whereas water-extracted soil DOM has C/N ratios of 26-55 (Qualls and Haines 1992; Gu et al. 1995; Kaiser and Zech 1997). Although these compositional patterns in marine and soil environments are consistent with the results of these experiments, the mechanisms causing the observed differences between phases could be quite diverse and include microbial mediated processes.

Mechanisms for fractionation

Investigations of dissolved organic matter association with sediments have identified a wide variety of mechanisms that contribute to total sorption. These are: surface complexation or ligand exchange by carboxyl groups (Gu et al. 1995; Kaiser and Zech 1997; Arnarson and Keil 2000), electrostatic anion exchange (Jardine et al. 1989), hydrophobic and other entropy driven physical interactions (Jardine et al. 1989; Gu et al. 1996; Kaiser et al. 1997) and cation bridging (Day et al. 1994; Arnarson and Keil 2000). In addition, recent applications of theory from polymer gel physics have been quite successful in unifying these various mechanisms to describe natural OM sorption behavior over wide ranges of conditions (van de Weerd et al. 1999; Filius et al. 2000). Essentially all of these mechanisms and conceptualizations exhibit the potential to drive the selective sorption of certain functional groups (and thus molecules) over others – this competitive sorption has been observed in numerous studies (Gu et al. 1996; Kaiser and Zech 1997).

Electrostatic mechanisms are a logical choice to explain the observed nitrogen and amino acid fractionation patterns. Most primary amines and many nitrogenous functional groups, including the side chains of basic amino acids, have a net positive charge at pH < 8 (histidine is an exception, with $pK_A = 6.0$ for the side chain). Aluminosilicate clay minerals, including kaolinite and smectite, have a net negative

surface charge at natural pH. For small molecules (<200 daltons) electrostatic attractions and repulsions are well known to produce patterns of selective sorption similar to those found here (Dashman and Stotzky 1982; Henrichs and Sugai 1993; Wang and Lee 1993). In nature, however, the fact that most OM is sorbed as macromolecules adds a level of complication in using these electrostatic arguments to explain the enrichment of certain amino acids over others. From a geochemical perspective, bulk amino acid compositions of OM are rather uniform, with only subtle variability from source to source and sample to sample (Cowie and Hedges 1992b; Keil et al. 2000). However, individual proteins within organisms are well known to exhibit much larger ranges in the compositions of constituent amino acids (National Center for Biotechnology Information, http://www.ncbi.nlm.nih.gov/). That polypeptides might sort themselves during sorption, based on the cumulative effects of differences in side-chain abundances rather than from relatively minor differences in net macromolecular charge (Henrichs 1995), is not only plausible but also consistent with results from polymer gel physics (van de Weerd et al. 1999).

If electrostatic interactions do indeed control the fractionation pattern of amino acids, then one might expect very different amino acid distributions in organic matter sorbed to minerals exhibiting a positive net surface charge. Two previous studies show this to be the case. Carter (1978) conducted OM sorption experiments similar to those presented here, in which he found substantial enrichment of acidic amino acids on positively charged carbonate minerals – patterns that matched those in natural marine carbonate sands (Carter and Mitterer 1978). On the other hand, he found that sorption of the same DOM to quartz sand resulted in relative depletion of acidic amino acids accompanied by strong enrichment of basic amino acids, similar to

my results with aluminosilicates. McKnight et al. (1992) studied sorption *in situ* at the confluence of a blackwater stream with a stream dominated by hydrous iron and aluminum oxide precipitates. Among other findings, metal oxide minerals below the confluence sorbed OM that was enriched in total organic nitrogen, in total amino acids and notably in acidic amino acids relative to the DOM of the blackwater stream. Thus, electrostatic mechanisms do appear to drive fractionation of polypeptides based on subtle differences in amino acid composition. Furthermore, the range of functional group types (basics, acidics, hydrophobics, etc.) available for peptide binding can explain why nitrogen in general and proteinaceous material in particular appear to be preferentially sorbed to diverse mineral types exhibiting either positive or negative net surface charge.

Another striking observation from these experiments was that the total amount of OM sorbed (Fig. 3.2), and the fractionation of that OM (Figs. 4, 5, 6A), seemed to be a function of the freshness of the initial DOM. Experiment numbers 1 through 9 used initial DOM of increasing freshness with respect to previous exposure to mineral surfaces and with respect to bacterial degradation. There are thus two families of possible explanations for the observed trends.

Considering that DOM fractionates during sorption, it is clear that successive interactions with minerals will leave a "parcel" of DOM more and more depleted in its surface-active components. For each interaction with minerals, bulk DOM should exhibit decreasing average partition coefficients, K_d. Thus, on average the DOM that is freshest with respect to previous contact with mineral surfaces should sorb most. Given the results of this study with aluminosilicate minerals, the most surface-active DOM components (highest K_d) are likely those exhibiting lower C/N ratios, higher

amino acid contents, and greater proportions of basic and hydrophobic functional groups. Whether sorption in other systems would result in the observed patterns seen here depends largely on the solid-to-solution ratio. Systems with excess surface relative to DOM (such as highly erosive streams or soil B horizons) might exhibit the highest fractionation at lower surface loadings. Increased sorption would deplete the pool of available high-K_d compounds and sorption of DOM components with more average compositions would mask the initial fractionation. The fact that most minerals also show surface-site heterogeneity (Mayer 1999) would enhance these effects as the "best" sites fill first. The residual DOM in those systems with excess surface area would tend to show strong patterns of depletion of surface-active components. Conversely, in systems where DOM is in relative excess to available surfaces (such as these experiments, wetlands or organic-rich soil horizons), the pool of high K_d compounds might not be measurably depleted, even at the highest surface coverages. Thus, biochemical fractionation in surface-limited systems would be most apparent on minerals, whereas fractionation of residual DOM might be undetectable. Likewise, DOM with little history of mineral contact will yield sorbed FPOM with a strong fractionation signature, whereas DOM with an extensive history of previous mineral interactions will sorb FPOM that has a less distinct fractionation signature.

These ideas have been codified by van de Weerd et al. (1999), who have developed a set of competitive Langmuir-type equations to explicitly address the kinetics and thermodynamics of interacting species within a heterogeneous DOM mixture. Their application of this model to the experimental data of Gu et al. (1994) shows excellent agreement with measured sorption and desorption behavior of bulk OM. The ability of this treatment to simulate all the data without changing model

parameters, including desorption hystereses, supports the concept of cumulative sorptive fractionation. Modeled fractionation increases with increasing surface loading, just as observed in my experiments, and evolves with increased interaction time. While these authors use polymer gel theory to independently estimate most model parameters, the concept of increasing fractionation with increasing surface loading is valid for any suite of reversible association mechanisms in a surface-limited system.

The second family of mechanistic explanations stems from the observation that the sequence of experiment numbers 1 to 9 also corresponds to a likely history of decreasing diagenesis and increasing bioavailability of the initial DOM. In general, hydrolyzable amino acids are preferentially utilized by bacteria and become depleted relative to bulk OM during diagenesis (Cowie and Hedges 1992b; Wakeham et al. 1997). Evidence is also accumulating in support of the size-reactivity-continuum model of Amon and Benner (1996a), suggesting that the size of remnant DOM will decrease with degradation (Burdige and Gardner 1998). Both of these trends could result in decreasing average surface affinity of DOM with advancing degradation regardless of mineral type (Davis and Gloor 1981; McKnight et al. 1992; van de Weerd et al. 1999), without requiring prior sorption of high K_d components. However, increasing degradation will also tend to increase in OM the relative abundance of carboxyl and hydroxyl groups (Sun et al. 1997), which are known to be important in the complexation of OM onto positively charged minerals (McKnight et al. 1992; Gu et al. 1995; Kaiser et al. 1997). How these opposing diagenetic trends might combine to enhance or reduce sorption for various mineral types is open to speculation. It is worth noting that the surface loadings obtained in these experiments

matched closely those observed along the continuum of increasing oxygen exposure time in marine systems (Hedges et al. 1999). Sorption of river and wetland DOM occurred within the 0.1-0.5 mg OC m^{-2} range that is observed in deep sea and deltaic sediments (Hedges and Keil 1995; Keil et al. 1997). Diluted leachates sorbed within the range of 0.5-1.1 mg OC m^{-2} that is typical of coastal margin sediments. Undiluted leachates sorbed at higher levels, within the range of 1.5-3.0 mg OC m^{-2} commonly found in sediments under anoxic bottom waters (Hedges and Keil 1995). A question that certainly deserves to be tested is whether degradation alone can substantially change the K_d distribution in DOM.

Another possible explanation for observed increases in fractionation with increasing freshness is that microorganisms might mediate these sorptive patterns indirectly through growth on the minerals. Given typical bacterial abundances ($< 10^7$ ml^{-1}) (Benner et al. 1995) and typical bacterial amino acid compositions (Cowie and Hedges 1992b), it is unlikely that microbial biomass alone could account for observed concentrations of C, N and amino acids in these experiments. However, even where bacterial biomass contributes insignificantly to total OC, the cumulative remains of bacterial cell walls and exopolymers might be quantitatively important (Oades 1989). My batch sorption incubations lasted 24 hours at 20°-32°C, allowing numerous generations of microbial colonies to leave behind their biofilms and necromass. Given crudely estimated respiration losses of 15-60% of sorbed carbon and possible growth efficiencies of 10-50% (Amon and Benner 1996a), microbial residues could account for as little as 1.5% or as high as 30% of FPOM analyzed in these experiments. Regardless, the quantity of material produced should be a function of growth rate, growth efficiency and thus the bioavailability of the DOM substrate.

That this experiment was conducted with living microbial assemblages distinguishes it from otherwise similar studies (Day et al. 1994; Gu et al. 1995; Filius et al. 2000). It is thus interesting to note that these same studies all find sorptive loadings below 0.4 mg OC m^{-2} SA despite using highly surface-active goethite. Could the much greater surfaces loadings observed here on kaolinite and natural mineral assemblages be due to microbial remains? One count against this argument is the moderate enrichment of glycine in the DOM of natural waters (experiments 1-4) and alanine in leachates (experiments 5-9) relative to FPOM in those experiments (Fig. 3.5). Both amino acids are generally highly enriched in peptidoglycan of bacterial cell walls (Keil et al. 2000), suggesting that DOM might contain the larger fraction of bacterial necromass. However, little is known regarding the amino acid composition of bacterial biofilms, and it is conceivable that bacteria could employ peptide adhesives with compositions dominated by surface-active basic and hydrophobic amino acids.

Non-protein amino acids

In addition to reproducing natural patterns of nitrogen, total amino acid, and basic amino acid enrichment on particles, these sorption experiments also generated the lower mol% non-protein amino acids that is typical of riverine FPOM relative to DOM (Fig. 3.5-7). This result was not entirely expected. Because non-protein amino acids are thought to be products of bacterial alteration (Lee and Cronin 1982), the observed pattern in rivers had been interpreted as evidence that DOM was significantly more degraded than FPOM. In studies of sedimentary organic matter, the parameter %(βAla+γAba) is a clear indicator of diagenetic alteration (Cowie and Hedges 1994; Dauwe et al. 1999). In contrast, my partitioning experiments clearly

demonstrate that peptides containing NPAAs have very low surface affinity and are thus preferentially retained in solution.

A plausible explanation for this result is that NPAAs are likely to reside in degraded peptides that are considerably smaller than peptides without NPAAs. Because β-alanine and γ-aminobutyric acid are produced by decarboxylation of the peptide-forming carboxyl group of aspartic acid and glutamic acid respectively, they must exist on the C-terminus of peptide cleavage products or as free amino acids (Keil et al. 2000). These ideas are supported by findings in sedimentary pore waters of substantially higher contributions of NPAAs to the dissolved free amino acid (DFAA) pool relative to total (free and combined) dissolved amino acids (Burdige and Martens 1990; Lomstein et al. 1998). My study, in which whole water DOM was analyzed, evidenced higher NPAA concentrations than studies of similar rivers in which only high molecular weight (>1000 daltons) DOM was analyzed (Hedges et al. 1994; Hedges et al. 2000). If NPAAs are indeed predominantly in smaller peptides, they could easily be out-competed for surface sites by larger molecules with greater numbers of surface-active functional groups (Henrichs 1995). Furthermore, the observation that experimentally sorbed FPOM contained less NPAA than is typical of riverine and marine sediments (Hedges et al. 1994; Hedges et al. 2000; Keil et al. 2000) suggests that the accumulation of sedimentary NPAA may require degradation of peptides that are already associated with minerals. Regardless of mechanism, non-protein amino acids can no longer be interpreted solely as a diagenetic parameter when comparing between dissolved and particulate phases.

Implications for interpreting OM compositional patterns

The results of this study, especially those for NPAAs, imply that sorption could be responsible for other compositional signatures that might otherwise be attributed to diagenetic processes or varying source. An example of a diagenetic parameter exhibiting sensitivity to sorptive fractionation is the amino acid degradation index of Dauwe et al. (1999). Although being developed from (and for) diagenetic sequences in marine sediments, it might be tempting to apply the index to infer differences in diagenetic history between DOM and FPOM samples. The wide separation of index values between DOM and FPOM samples in these experiments (Fig. 3.8) clearly demonstrates the complications that sorptive processes introduce to comparisons between dissolved and particulate organic matter. For each sorption experiment, organic matter in the final dissolved and particulate fractions both have essentially the same age and gross diagenetic history, yet DOM fractions consistently give lower index values suggesting that they are more degraded. Interestingly enough, the index does seem appropriate for distinguishing differences between FPOM samples. Natural river FPOM has lower values indicative of more degraded material, sorbed riverine and wetland DOM have intermediate values, and sorbed leachates give the highest values (Fig. 3.8) – suggesting increasing freshness as one would expect. One might thus argue that for these experiments the Dauwe index reflects increasing average partition coefficients for a sample.

These observations highlight a number of important questions regarding linkages between the roles of sorption and degradation in determining OM compositions. As previously discussed, more degraded (smaller, N-poor) molecules should exhibit lower surface affinity relative to fresher (larger, N-rich) OM. If this is so, sorptive fractionation cannot be viewed independently from diagenetic OM

alteration. Separating the effects of these two processes may prove to be quite difficult. In natural systems, does sorption serve primarily to separate more degraded OM from less degraded OM, or does sorption serve primarily as a means of protecting mineral-associated molecules from degradation? The answer will likely depend on environmental conditions and may change over short temporal and spatial scales. In addition to sorption's role in determining nitrogen and amino acid compositional patterns, the possibility exists that some of the other commonly used OM diagenetic or source parameters might also be affected by sorptive fractionation. For instance, Guggenberger et al. (1994) found distinct lignin and carbohydrate compositions in the hydrophilic acid fraction of soil DOM relative to the much more easily sorbed hydrophobic fractions or soil horizons. Comparisons of clay-bound soil OM versus soil DOM support the possibility that these compound classes may also fractionate during sorption (Kaiser and Guggenberger 2000). Overall, diagenetic processes can no longer be considered alone when interpreting OM compositions between dissolved and particulate phases. It is clearly important to first understand sorptive fractionation patterns within a biochemical class prior to interpreting compositional differences between its dissolved and particulate fractions.

Where in a river basin does sorptive fractionation occur?

The specific goal of this study has been to examine whether sorption can explain the compositional patterns of co-occurring DOM and FPOM within rivers of the Amazon. Although tested in the context of sediments suspended within a river, it is likely that sorptive signatures are imprinted anywhere that "fresh," surface-active DOM contacts mineral surfaces. Therefore, surface soil horizons are likely to be important for initial imprinting, followed by confluences of sediment-rich streams

with “blackwaters”. However, rivers are active systems with continuous inputs, degradation and exchange. That >60% of FPOM in the lower Amazon is derived from lowlands (based on stable isotope mass balance) (Hedges et al. 2000), despite ~85% of associated minerals originating in the Andes (Gibbs 1967), is a strong indication that mineral-associated OM actively repartitions on time scales less than its transit time to the sea. Continuous re-equilibration of riverine sediments with surface-active DOM components thus likely occurs over the entire length of the river corridor.

OVERVIEW

This study demonstrates that all the published organic nitrogen compositional patterns of the Amazon Basin can be recreated in a beaker by sorbing natural dissolved organic matter to aluminosilicate mineral surfaces under natural conditions. Furthermore, because nitrogen and amino-acid rich OM is preferentially sorbed, the availability of mineral surfaces provides ecosystems with a mechanism for retaining fresher, more reactive organic matter. Additional studies are underway to investigate the relative importance of abiotic, physicochemical mechanisms versus microbially mediated processes in determining these compositional patterns. Regardless of mechanism, the process of associating organic molecules with mineral surfaces is clearly of prime importance in determining the compositions of dissolved and fine particulate organic matter in river basins.

Table 3.1. Sources for dissolved and particulate samples used in mixing experiments

Sample	Location	Elevation (m)	Lat. (deg min)	Long. (deg min)	Description
river 1	Rio Ucayali	110	04° 28.29' S	73° 25.96' W	Amazon River mainstem in lowlands near Iquitos
river 2	Rio Urubamba	290	10° 41.95' S	73° 44.73' W	Mesoscale tributary (57,000 km^2) in depositional zone
wetland	altiplano wetland	3930	14° 21.79' S	71° 19.11' W	Wetland typical of high-altitude Andean plains
leachate 1	gramalote grass	110	04° 28.29' S	73° 25.96' W	Leached from the dominant lowland riverbank grass
leachate 2	altiplano grasses	3930	14° 21.79' S	71° 19.11' W	Leached from a mixture of typical altiplano grasses

Table 3.2. Sorption carbon mass balance. Except for the first DOC column, all organic carbon concentrations are normalized to 100 mg sediment mineral particles for ease of comparison.

			Initial						Final				Change			Partition
Experiment	DOM	Particle	DOC	DOC	DON	FPOC	FPON	SA	DOC	FPOC	FPON	OC/SA	Δ DOC	Δ FPOC	Δ FPON	K_d
Number	Source	Source	(mg L^{-1})	(mg OC 100 mg^{-1} sed.)				(m^2 g^{-1})	(mg OC 100 mg^{-1} sed.)			(mg OC m^{-2})	(mg OC 100 mg^{-1} sed.)			(L g^{-1})
1	river 1	kaolinite	3.87	1.26	0.14	0.040	0.0030	12.5	1.24	0.135	0.036	0.11	-0.02	0.095	0.033	0.36
2	river 2	kaolinite	7.72	2.47	0.09	0.040	0.0030	12.5	2.35	0.133	0.028	0.11	-0.12	0.093	0.024	0.18
3	wetland	kaolinite	11.0	3.68	0.42	0.040	0.0030	12.5	3.44	0.23	0.038	0.18	-0.24	0.19	0.035	0.22
4	wetland	river 2	9.60	7.33	0.65	1.55	0.190	15.5	7.38	1.72	0.221	1.11	0.05	0.17	0.031	1.8
5	leachate 1	kaolinite	381	64.6	3.98	0.040	0.0030	12.5	59.6	2.53	0.566	2.03	-4.9	2.5	0.563	0.07
6	leachate 1	river 1	79.4	29.4	1.86	0.85	0.117	22.7	25.9	3.82	0.861	1.68	-3.5	3.0	0.744	0.55
7	dil. leach. 1	kaolinite	8.09	2.87	0.17	0.040	0.0030	12.5	1.77	0.75	0.165	0.60	-1.1	0.71	0.162	1.5
8	dil. leach. 2	kaolinite	24.2	8.34	0.45	0.040	0.0030	12.5	5.45	1.29	0.308	1.03	-2.9	1.2	0.305	0.82
9	leachate 2	kaolinite	268	72.5	3.95	0.040	0.0030	12.5	70.5	2.88	0.635	2.31	-2.0	2.8	0.632	0.11

Table 3.3. Amino acid compostitions of DOM and POM before and after mixing. THAA, total hydrolyzable amino acids; %TAAC and %TAAN, percent of total organic carbon (or nitrogen) measurable as amino acids. ASP, aspartic acid (includes asparagine, which converts to aspartic acid during hydrolysis); GLU, glutamic acid (includes glutamine which converts to glutamic acid during hydrolysis); SER, serine; GLY, glycine; THR, threonine; ALA, alanine; TYR, tyrosine; MET, methionine; VAL, valine; PHE, phenylalanine; ILE, isoleucine; LEU, leucine; HIS, histidine; ARG, arginine; LYS, lysine; bALA, b-alanine; gABA, g-amino butyric acid; aABA, a-amino butyric acid.

Experiment number	Fraction	THAA (mg 100 mg-1 OC)	$\%T_{AA}C$	$\%T_{AA}N$	ASP (mol%)	GLU (mol%)	SER (mol%)	GLY (mol%)	THR (mol%)	ALA (mol%)	TYR (mol%)	MET (mol%)	VAL (mol%)	PHE (mol%)	ILE (mol%)	LEU (mol%)	HIS (mol%)	ARG (mol%)	LYS (mol%)	βALA (mol%)	γABA (mol%)	αABA (mol%)
1	$DOM_{initial}$	3.2	1.4	3.9	6.4	11.4	5.5	19.6	7.9	13.9	0.9	0.0	7.8	3.3	4.0	4.6	0.0	0.6	2.5	8.2	2.1	1.3
2	$DOM_{initial}$	1.3	0.6	4.7	6.7	13.6	8.5	17.9	8.2	13.6	0.0	0.5	7.6	4.5	3.8	5.1	0.0	0.0	2.4	4.2	1.3	2.2
3	$DOM_{initial}$	8.4	3.5	10.0	6.0	8.9	13.3	18.7	8.1	14.0	0.9	0.0	9.2	2.5	2.8	3.9	0.7	0.8	1.8	6.0	0.8	1.6
4	$DOM_{initial}$	6.0	2.5	9.3	6.0	9.2	13.0	18.7	8.1	14.0	0.8	0.04	9.1	2.6	2.9	4.0	0.6	0.8	1.9	5.9	0.8	1.7
5	$DOM_{initial}$	10.4	4.6	22.4	5.5	10.5	6.7	12.8	6.5	22.7	1.0	0.03	10.6	2.2	4.1	4.4	0.7	0.5	0.5	1.8	7.6	1.8
6	$DOM_{initial}$	10.2	4.4	21.2	5.5	10.5	6.7	12.9	6.6	22.6	1.0	0.03	10.6	2.2	4.1	4.4	0.7	0.5	0.6	1.9	7.5	1.8
7	$DOM_{initial}$	10.3	4.5	22.7	5.5	10.5	6.7	12.8	6.5	22.7	1.0	0.03	10.6	2.2	4.1	4.4	0.7	0.5	0.5	1.8	7.6	1.8
8	$DOM_{initial}$	11.9	5.2	29.4	3.3	10.5	5.6	12.6	5.1	29.1	1.2	0.4	8.2	2.1	4.2	4.5	0.4	0.5	1.4	2.3	8.4	0.4
9	$DOM_{initial}$	10.6	4.6	26.1	3.3	10.5	5.6	12.6	5.1	29.1	1.2	0.4	8.2	2.1	4.2	4.5	0.4	0.5	1.4	2.3	8.4	0.4
4	$FPOM_{initial}$	18.1	8.0	21.5	6.4	9.2	8.9	16.3	8.0	15.0	1.6	0.2	7.9	4.3	5.1	6.1	1.7	3.8	4.7	0.4	0.5	0.1
6	$FPOM_{initial}$	21.5	9.5	23.0	6.6	9.6	11.1	14.6	7.8	14.1	1.6	0.0	7.9	4.0	4.4	5.7	2.2	3.7	3.8	1.3	1.4	0.2
1	DOM_{final}	3.0	1.3	3.6	6.5	12.6	7.0	19.2	7.6	11.5	1.0	0.0	7.0	3.5	3.9	6.3	0.0	0.6	2.7	5.8	3.1	1.7
2	DOM_{final}	1.2	0.5	3.6	6.5	10.5	7.6	17.2	10.3	13.6	0.7	0.7	6.5	2.9	3.8	4.0	0.0	0.9	5.4	5.8	2.5	1.3
3	DOM_{final}	7.4	3.2	8.0	5.9	8.9	11.8	17.5	8.4	14.0	1.0	0.0	10.4	2.3	2.8	3.5	0.0	0.0	3.4	7.5	0.5	2.1
4	DOM_{final}	3.8	1.6	6.8	6.7	10.1	7.1	16.6	9.0	16.8	1.0	0.2	7.8	2.8	3.8	5.4	0.0	0.2	1.4	9.1	1.3	0.7
5	DOM_{final}	10.6	4.6	24.4	6.2	9.4	8.0	14.2	8.0	20.5	1.2	0.0	11.6	2.1	4.0	4.8	1.1	0.6	0.5	2.6	3.4	1.8
6	DOM_{final}	7.9	3.4	34.9	7.3	11.0	10.1	14.5	10.7	15.3	0.7	0.0	9.1	2.8	3.9	4.8	1.3	0.6	1.0	4.3	0.9	1.7
7	DOM_{final}	not determined (sample lost)																				
8	DOM_{final}	7.7	3.4	25.6	6.7	12.1	5.0	16.0	5.9	16.6	1.1	0.0	9.3	2.9	4.5	5.5	0.0	0.0	1.9	8.7	2.2	1.6
9	DOM_{final}	7.9	3.5	26.7	3.8	9.3	5.1	13.5	5.4	26.5	1.2	0.1	10.0	2.2	4.1	5.2	0.5	0.5	1.0	2.9	8.0	0.7
1	$FPOM_{final}$	13.3	5.9	7.6	7.3	10.3	9.9	11.4	7.1	16.5	3.1	0.0	8.2	4.0	4.5	6.5	1.9	4.0	4.2	0.5	0.4	0.4
2	$FPOM_{final}$	20.3	9.1	14.4	6.2	10.2	7.5	15.0	7.7	15.9	2.4	0.0	9.1	4.4	5.5	6.7	1.1	3.7	3.8	0.0	0.2	0.4
3	$FPOM_{final}$	19.2	8.5	15.6	7.2	12.0	9.5	14.5	9.1	12.7	2.0	0.0	8.0	4.3	5.0	8.2	0.7	2.6	3.0	0.9	0.1	0.2
4	$FPOM_{final}$	21.2	9.4	23.7	6.4	10.1	9.4	14.4	8.4	14.3	1.7	0.4	7.9	4.4	5.1	6.6	1.5	3.9	4.5	0.4	0.4	0.1
5	$FPOM_{final}$	46.8	21.1	30.1	6.4	12.5	7.1	11.1	7.1	16.2	2.4	0.8	7.7	4.4	5.3	7.6	1.7	4.6	4.6	0.0	0.4	0.1
6	$FPOM_{final}$	75.0	33.8	48.8	5.9	11.1	6.7	11.8	6.5	16.8	2.4	1.1	7.8	4.4	5.5	7.2	1.5	4.9	5.7	0.2	0.4	0.1
7	$FPOM_{final}$	81.3	36.6	53.2	6.3	10.6	6.7	11.4	7.3	17.7	2.4	0.3	7.6	4.5	5.3	7.2	1.6	3.8	4.9	2.2	0.0	0.1
8	$FPOM_{final}$	83.2	37.2	51.8	5.3	11.8	5.5	16.2	6.0	15.6	2.0	0.9	7.5	3.9	5.4	7.1	1.6	4.8	5.9	0.2	0.1	0.1
9	$FPOM_{final}$	103.3	46.6	70.9	6.2	11.2	5.8	13.5	6.7	14.5	2.3	1.7	8.0	4.3	6.0	7.4	1.8	4.6	6.0	0.1	0.1	0.0

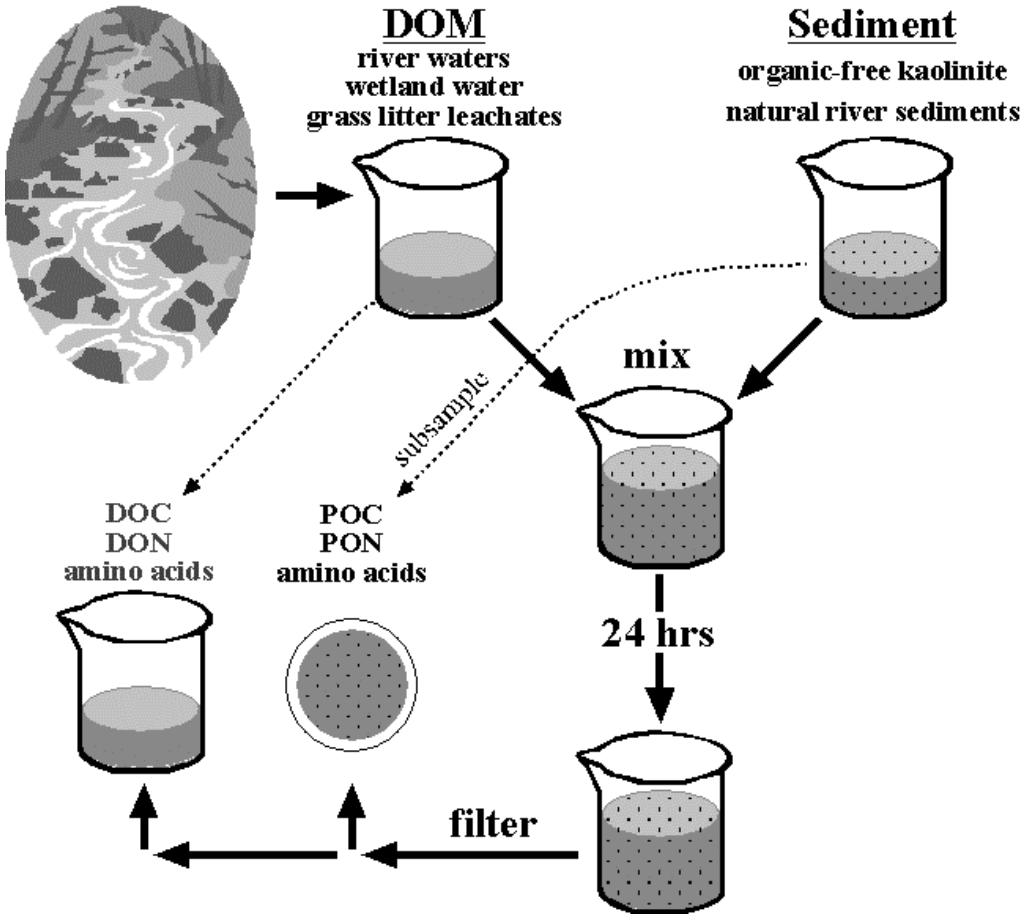

Figure 3.1. Schematic of experimental method for batch sorption type incubations. Dissolved organic matter (DOM) was isolated from five natural sources (see Table 3.1) and mixed with slurries of either natural river suspended sediments or commercially obtained kaolinite. Analyses were performed on both dissolved and particulate fractions before and after mixing.

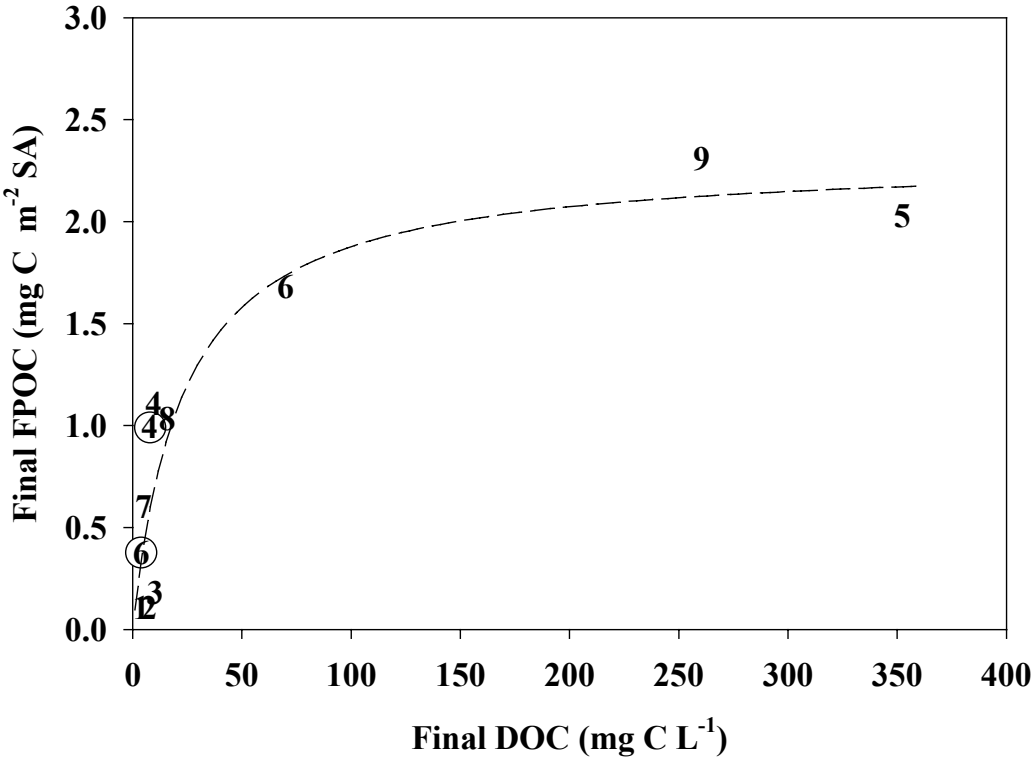

Figure 3.2. Sorption isotherms of the nine respective mixing experiments given in Table 3.2, plotted as surface area (SA) normalized fine particulate organic carbon (FPOC) as a function of dissolved organic carbon (DOC). Experiments numbers 1, 2, 3, 4 and 6 are strictly one-point isotherms and pairs 5, 7 and 8, 9 are two-point isotherms. However, these points, including the original riverine FPOC from experiments 4 and 6 relative to riverine DOC (circled values), give a reasonable fit to a Langmuir isotherm model (dashed line, r2 = 0.84, n = 11, qmax = 2.3 ±1.1 mg OC m-2 SA, K = 0.043 ±0.015 L mg-1 C).

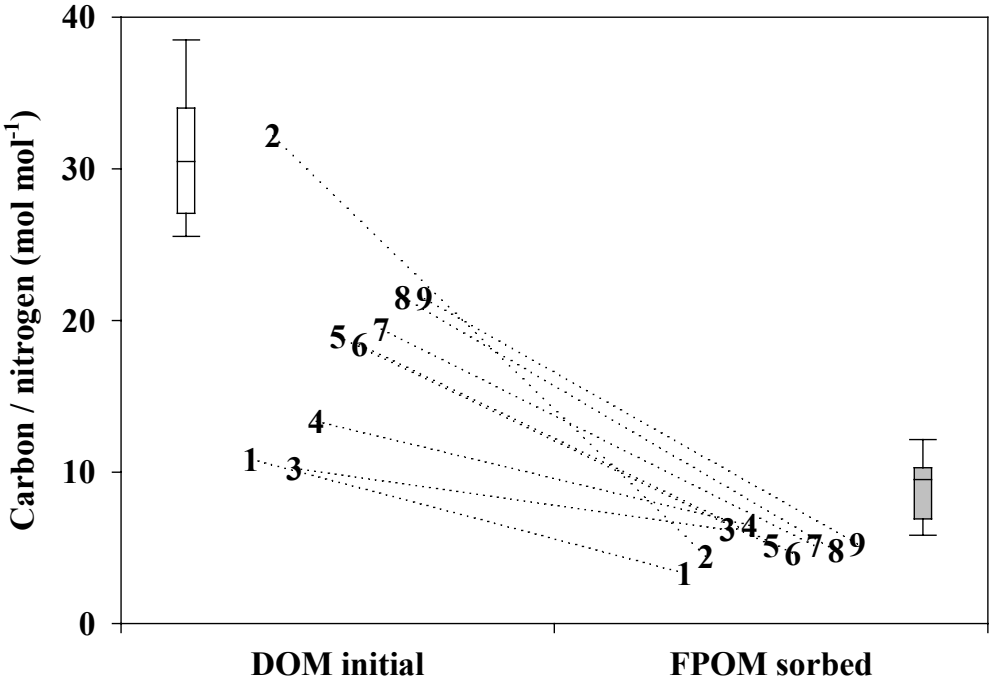

Figure 3.3. Molar carbon-to-nitrogen ratios of sorbed FPOM (calculated from the difference between initial and final FPOC and FPON) relative to the "parent" DOM for the nine respective mixing experiments given in Table 3.2. As a reference, box plots present the distribution of values measured in 15 natural river samples from the Amazon Basin (Hedges et al. 1994; Hedges et al. 2000). The median value is framed by boxes showing the 25th and 75th percentile of values and by "whiskers" showing the 10th and 90th percentile.

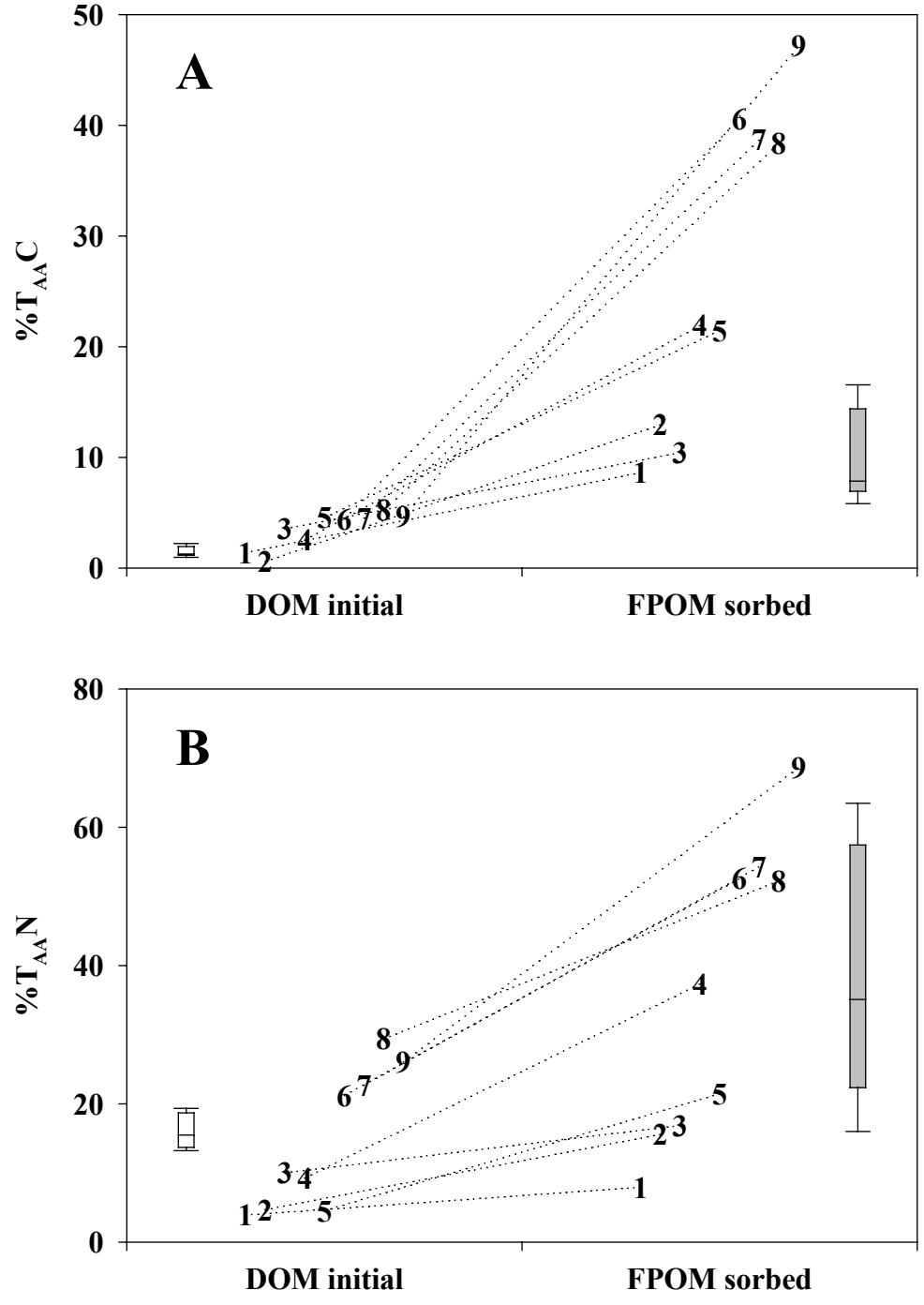

Figure 3.4. Total amino acid content, normalized to **A)** carbon and **B)** nitrogen, of sorbed FPOM relative to the "parent" DOM. Amazon compositions illustrated as in Fig. 3.3.

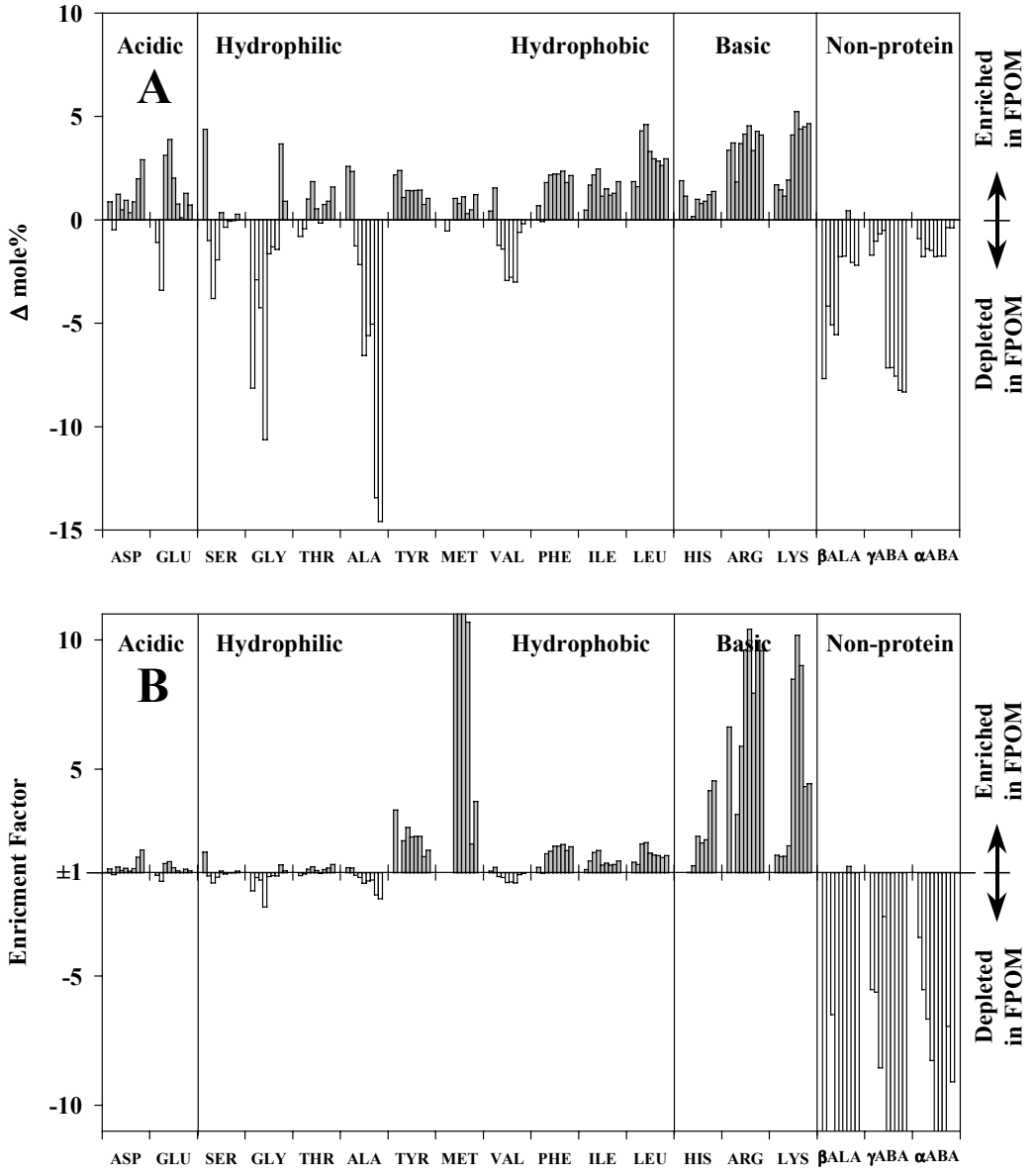

Figure 3.5. Patterns of amino acid enrichment on sorbed FPOM relative to initial DOM, plotted **A)** as the difference between the mol% amino acid composition of FPOM and DOM and **B)** as the factor by which an amino acid is enriched or depleted in FPOM relative to its mol% in DOM. Positive values in both A and B correspond to enrichment of that amino acid in the FPOM relative its parent DOM. Off-scale values in B are < +40 and > −60. For each individual amino acid, the bars are presented in order from left to right for experiments number 1 to 9 respectively. Amino acids are presented within each functional grouping in chromatographic elution order. Although neutral amino acids are given in this relative order of hydrophobicity, only serine, threonine and tyrosine actually have polar side-chains.

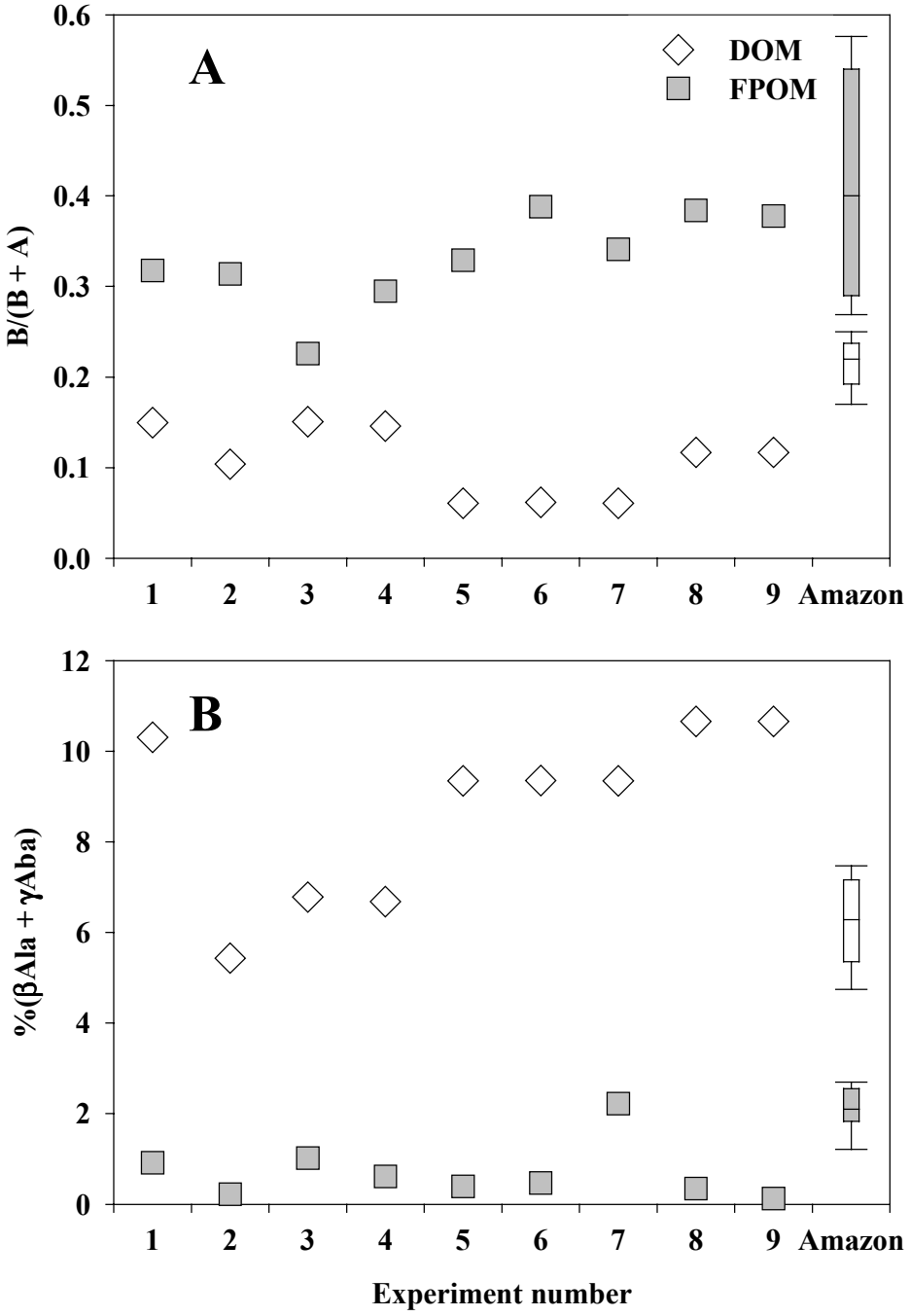

Figure 3.6. Amino acid parameters of initial DOM and sorbed FPOM for each mixing experiment. Subplots compare **A)** B/(B+A) as an indicator for sorption, and **B)** %(βAla+γAba) as an indicator for microbial degradation. Amazon compositions illustrated as in Fig. 3.3.

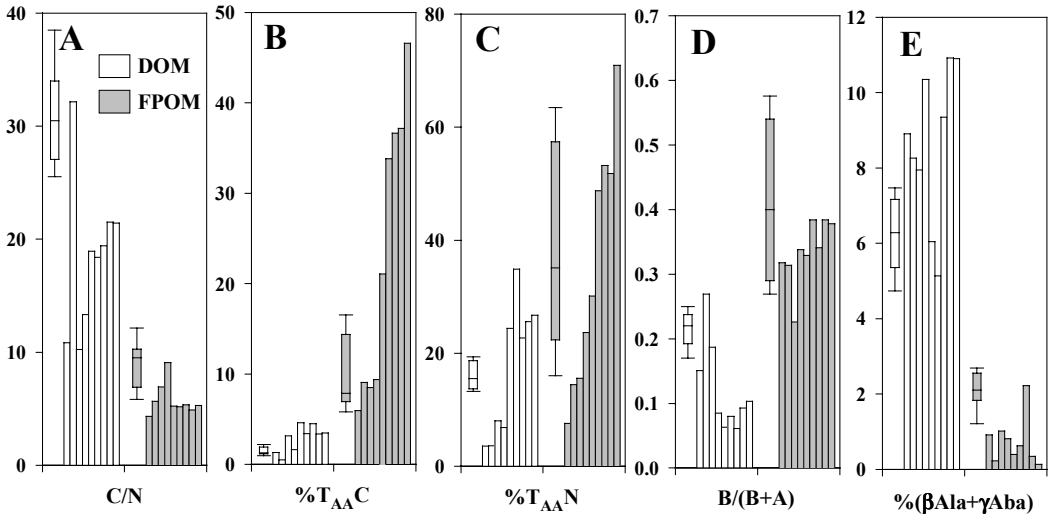

Figure 3.7. Final composition of dissolved and fine particulate organic matter (DOM and FPOM) for the nine sorption experiments in this study, as shown by **A)** molar carbon to nitrogen ratio, **B)** percent total carbon as amino acids, **C)** percent total nitrogen as amino acids, **D)** ratio of basic to basic plus acidic amino acids, and **E)** sum of mol% βAla and γAba. Initial DOM values are used in lieu of final values for experiment number 7. Amazon compositions illustrated as in Fig. 3.3.

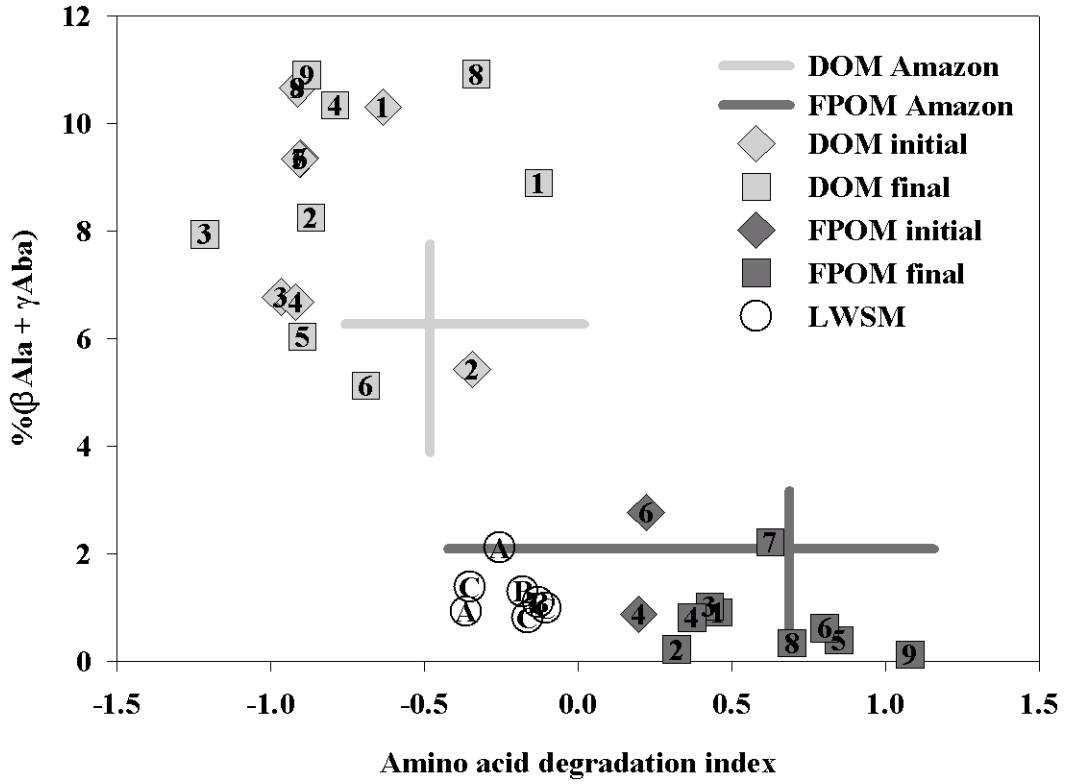

Figure 3.8. The Dauwe et al. (1999) degradation index for samples used (or produced in) my mixing experiments. Crosses represent the median and range of values from rivers in the Amazon Basin. Replicate analyses of Lake Washington Standard Mud (LWSM) demonstrates potential analytical variability in these indices, with letters distinguishing different analysts. Values inside other symbols represent mixing experiment number.

CHAPTER 4: THE ROLE OF MICROBES IN BIOCHEMICAL AND ISOTOPIC FRACTIONATION OF ORGANIC MATTER DURING ASSOCIATION WITH CLAY MINERALS

INTRODUCTION

The importance of organo-mineral associations in stabilizing organic carbon and nitrogen in soils, sediments and the marine water column have become increasingly appreciated over the last decade (Keil et al. 1994a; Mayer 1994a; Baldock and Skjemstad 2000; Kaiser and Guggenberger 2000; Kennedy et al. 2002; Armstrong et al. in press). It is now clear that most organic matter in soils and sediments is physically associated with minerals (Keil et al. 1994b; Hedges and Oades 1997) and is at least partially protected by that contact (Keil et al. 1994a; Nelson et al. 1994; Baldock and Skjemstad 2000). Despite this attention, there is still considerable debate over the mechanisms by which organic matter (OM) becomes associated with minerals. Many studies have investigated chemo-sorption reactions of dissolved organic matter (DOM) with minerals (Davis 1982; Jardine et al. 1989; Day et al. 1994; Gu et al. 1995), whereas others, typically in soil sciences, have focused on microbial immobilization and particle aggregation processes (Oades 1988; Christensen 1996; Baldock and Skjemstad 2000). These perspectives are not entirely inconsistent. Although organic carbon concentrations in soils and sediments are strongly related to mineral surface area (SA) – with OC:SA ratios typically 0.5 – 1.1 mg m^{-2} (Hedges and Keil 1995; Keil et al. 1997; Mayer and Xing 2001) – organic matter appears to be associated to minerals heterogeneously as microaggregates rather than as a uniform surface film (Ransom et al. 1997; Mayer 1999; Mayer and Xing 2001). Recently the sorption behavior of mineral-associated OM has been

successfully modeled after gels and tangled polymer networks (van de Weerd et al. 1999; Filius et al. 2000). However, in addition to being formed via physico-chemical mechanisms, gels are also commonly formed by particle-attached bacteria as biofilms (Costerton et al. 1987). Furthermore, although attached bacteria represent a small fraction of particulate carbon (<5%), they are generally more active and have much shorter doubling times than free-living bacteria (Crump et al. 1998; Crump and Baross 2000). An important question then is: what is the relative importance of abiotic versus microbially mediated processes in the formation of organo-mineral aggregates in natural systems?

The biochemical composition of mineral-associated organic matter from all environments is quite distinct relative to either coexisting dissolved organic matter or local plant sources. In terrestrial environments, mineral-associated OM found in the fine particulate (0.1-63 μm) and high density ($\rho > 1.5$ g/cm^3) fractions of sediments and soils is consistently enriched in nitrogen and total amino acids relative to both DOM and coarse (>63 μm) or low density ($\rho < 1.5$ g/cm^3) terrestrial organic matter (POM) (Meybeck 1982; Oades 1989; Hedges et al. 1994). Biochemical signatures – such as relative proportions of individual amino acids, neutral sugars and lignin phenols – of mineral-associated OM is likewise distinct with respect to coexisting DOM (Hedges et al. 1994; Hedges et al. 2000). Mineral-associated OM in marine environments closely resembles that from terrestrial environments, with similar C/N ratios and amino acid and neutral sugar distributions (Wakeham et al. 1997; Keil et al. 1998; Lomstein et al. 1998). However, planktonic organic matter sources are typically even more enriched in N, amino acids and neutral sugars (Wakeham et al. 1997). Why is it that these compositionally very different organic matter sources

converge to form mineral-associated OM fractions that are so similar? In addition to exhibiting distinct biochemical compositional signatures, mineral-associated OM is also generally enriched in ^{13}C and ^{15}N and depleted in ^{14}C relative to DOM and POM that is not associated with minerals (Hedges et al. 1986b; Trumbore et al. 1995; Ehlreringer et al. 2000; Hedges et al. 2000; Raymond and Bauer 2001). Most of these isotopic and biochemical signatures are commonly used to infer differences in sources and diagenesis between OM fractions or to constrain bulk carbon cycling processes in sediments and soils. However, few studies consider the role of sorption and related processes in determining these same signatures.

Recently, I conducted a set of sorption experiments in order to test whether organo-mineral association processes could be responsible for observed OM compositional trends in the Amazon Basin (Aufdenkampe et al. 2001). In these experiments, natural suspended river sediments and organic-free kaolinite were mixed with various natural DOM samples. In every case, relative to the parent DOM the newly formed mineral-associated OM fraction was enriched in nitrogen (normalized to organic carbon), in total hydrolyzable amino acids (THAA, normalized to total organic carbon and nitrogen), and in basic and hydrophobic amino acids (normalized to THAA). These compositional differences between dissolved and mineral-associated fractions closely matched compositional patterns observed in the Amazon Basin, thus providing direct evidence that the contrasting nitrogen and amino acid patterns of DOM and aluminosilicate-bound OM are primarily determined by preferential sorption of nitrogenous OM components. Furthermore, the extent of compositional differences between DOM and mineral-bound OM appeared to increase with increasing DOM freshness, suggesting that the native microbial

communities present in these incubations might play an important role in mediating these patterns.

My previous study also offered the suggestion that stable carbon isotopes might also be fractionated during sorptive processes (Aufdenkampe et al. 2001). While attempting to use ^{13}C as a tracer of gross exchanges between DOM and natural river particles, I discovered that newly sorbed carbon was enriched by up to 3 ‰ in ^{13}C relative to DOC (unpublished data). Furthermore, these enrichments appeared to be a function of the amino acid content of the new mineral-bound OM (Fig. 4.1). If such an isotopic fractionation is common during the formation of mineral-bound OM, understanding this process would be critical to a wide range of organic carbon studies (Ehlreringer et al. 2000).

The broad goal of this study is to further understand the processes that control compositional signatures of natural organic matter, such that observed signatures can then be better used to constrain organic carbon cycling in environmental systems. To this end, I performed a set of experiments to study the kinetics and extents of natural DOM "sorption" to organic-free kaolinite, under both sterile and microbially active conditions. The two objectives of the study were 1) to test the role of the microbial community in forming organo-mineral associations and their compositions, and 2) to test whether "sorption" is responsible for other characteristic compositional patterns, such as $\delta^{13}C$ signatures, between samples.

METHODS

Partitioning Experiment Protocols

A leaf litter leachate was diluted to eight different concentrations, filter sterilized, subdivided into 150 bottles and incubated with organic-free kaolinite minerals and with native bacteria (for half the bottles) for various lengths of time. This protocol thus allowed for direct comparisons of both kinetics and extents of organo-mineral associations between sterile versus microbially active conditions. Incubation protocols were in many ways similar to those used in a previous study (Aufdenkampe et al. 2001). Leaf litter was collected from the forest floor near Barro Branco stream in Reserva Ducke, Brazil (McClain et al. 1997) and air-dried for transport and storage at 4°C. To revive microbial populations after cold storage, the litter was placed in a humid incubator for six days, then immersed in Nanopure water (Barnstead) at 30°C while bubbling air to maintain oxic conditions. After 60 hours native microbial populations reached 10^8 cells ml^{-1} in log-phase growth, and the leachate was seived and filtered (using 0.2 μm pore size Gelman VacuCaps). The leachate was diluted with Nanopure water (Barnstead) to dissolved organic carbon (DOC) concentrations of approximately 2, 5, 10, 20, 40, 100, 300 and 600 mg C L^{-1}. These dilutions were then filter sterilized (using 0.1 μm Gelman VacuCaps) and transferred into autoclaved bottles using sterile technique, such that each bottle contained 125 ml leachate and 50 ml headspace. Autoclaved, organic-free kaolinite (Ward's kaolinite API#5 from Bath, South Carolina; pre-treated with 30% hydrogen peroxide for 2.5 hours at 50-60°C) was added to each bottle to give a final mineral concentration of 300 ±4 mg L^{-1}. The surface area of the organic-free kaolinite (12.1 ±0.1 m^2 g^{-1}) was determined from five-point Brauner-Emmett-Teller isotherms of N_2 adsorption using a Micromeritics Gemini SA analyzer.

Immediately after adding the kaolinite, half the bottles were inoculated with the native microbial community from the leachate such that the initial concentration of each bottle would be ~10^6 cells ml^{-1}. As a control for bacterial growth alone, four bottles containing 20 mg C L^{-1} DOM were inoculated and incubated for 75 hours without any addition of kaolinite. During course of the experiment bottles were maintained at ~30°C. Gentle agitation by flipping bottles every 1-4 hours maintained sediments in suspension as best as possible while not disturbing particle aggregates. Furthermore, the ~50 ml headspace in each bottle assured that oxic conditions were maintained. Consumption of the 0.45 mmol of oxygen gas within each incubation would have required remineralization equivalent to more than 43 mg OC L^{-1}, far larger than any observed changes in DOC concentrations.

For the kinetic experiments, bottles starting with ~20 mg L^{-1} of DOC were terminated by filtration in triplicate or quadruplicate at increasing intervals over a 75 hour period. In addition, three sterile bottles were incubated for 360 hours. For the isotherm experiments, all samples (four per each of seven DOC concentrations) were terminated after 30-33 hours. Each bottle destined for chemical analysis was filtered through a stack of two fiber filters, quartz on top (~3.0 μm Whatman® QMA) and glass on bottom (~0.7 μm Whatman® GF/F), both pre-combusted at 500°C for 4 hours. The quartz filter, which only trapped particle attached organic matter and bacteria, was used in all subsequent chemical analyses whereas the glass fiber filter served to remove most remaining particles from the dissolved phase. Immediately after filtration, the resulting DOM sample was frozen and filtered POM samples were air dried in a dehydrating oven (50° - 70°C) as preservation for subsequent chemical analyses.

Microbiological Methods

Bottles terminated for biological measurements (approximately one in four) were subsampled for microbial counts and for thymidine uptake experiments while taking care to maintain a homogeneous suspension of particles (via pipet "pumping"). A 3.0 μm pore size membrane filter (25 mm Nucleopore PC), attached to the end of a syringe, was then gently lowered through the remaining sample to remove particles. Thus, a subsample containing only free-living bacteria (i.e. not particle attached) was obtained for microbial counts and thymidine uptake experiments. Counts and rates of particle-attached bacteria were calculated by difference.

Microbial populations were quantified with epifluorescence microscopy of dual dyed (acridine orange and DAPI) samples. Rates of bacterial growth were determined from [^{3}H]thymidine uptake rates into total macromolecules (i.e. the cold trichloroacetic acid (TCA) insoluable fraction) from triplicate incubations per sample (Bell 1993). Growth rates were calculated using a thymidine conversion factor (TCF) of $6.1 \pm 3.4 \times 10^{18}$ cells mol^{-1} as was previously observed in the Amazon River (Benner et al. 1995) and a carbon conversion factor (CCF) of 25 fg $cell^{-1}$ as is commonly used in eutrophic marine and fresh waters (Bell 1993). The CCF is an average for bacterial biomass and does not include extracellular exudates or non-living cell remains.

Organic Analyses

Concentrations and isotopic signatures of particulate carbon and nitrogen were simultaneously analyzed on a Carlo Erba NC 2500 Elemental Analyzer (EA) interfaced with a Finnigan DeltaPlus XL Isotope Ratio Mass Spectrometer (IRMS). Samples on quartz fiber filters were subsampled precisely by punching out uniform

circles with a cork bore. Elemental compositions were quantified via a thermal conductivity detector (TCD). Analytical uncertainties of each measurement were calculated as the 67% confidence limits of the inverse prediction from the calibration regression (Sokal and Rohlf 1995). These uncertainties were relatively large due to small sample sizes, averaging 4.0% ± 2.4% of carbon values (range of 0.5% to 10.5%) and 8.2% ± 5.0% of nitrogen values (range of 0.9% to 27.1%). Analytical uncertainties of isotopic compositions were ±0.2‰ for carbon and ±0.3‰ for nitrogen.

The organic-free kaolinite was measured to have carbon and nitrogen concentrations of 0.035% ±0.002% OC and 0.0014% ±0.0002% N and a $\delta^{13}C$ signature of -28.6 ±0.5‰. These values were used to blank correct calculated C/N and $\delta^{13}C$ values for the new mineral-associated OM at the end of each incubation (Table 4.1). Given OC/SA values are not blank-corrected, as such a calculation simply involves taking a difference (because mineral surface area is constant) (Table 4.1). Nitrogen concentrations were too low to measure $\delta^{15}N$ for the organic-free kaolinite.

Dissolved organic carbon (DOC) concentrations were measured after acidification and sparging with a modified high temperature combustion MQ Scientific 1001 DOC analyzer (M. L. Peterson et al., manuscript in preparation). Although the standard deviation of four injections per sample vial was generally <1.5% of the mean, the 67% confidence limits of the of the inverse prediction from the calibration regression yielded analytical uncertainties of 1-5% of measured values (Sokal and Rohlf 1995). The C:N ratio and isotopic compositions of the initial dissolved organic matter in these experiments was analyzed by evaporating the

leachate into tin boats filled with precombusted (450°C for 4 hours) diatomaceous earth (available as Chromosorb W from Costech).

Uncertainties

Best estimates of values in this paper are given where possible along with their associated standard errors (±SE), representing 67% confidence limits. Original measurement uncertainties were propagated through to all calculated values, such as C:N ratios, by addition in quadrature (Taylor 1997). Weighted averages were used to combine values having a wide range of individual uncertainties (i.e. C/N); arithmetic means are used where not explicitly stated (Taylor 1997).

RESULTS

Organic carbon dynamics

Within 10-20 minutes of adding the organic-free kaolinite to the filtered leachate, substantial dissolved organic matter had associated with the mineral surfaces. For the sterile kinetic experiment (~20 mg DOC L^{-1}), surface area normalized concentrations of mineral-associated OC jumped from an initial 0.03 mg OC m^{-2} SA to 0.13 ± 0.02 mg OC m^{-2} SA within the first 25 minutes (Fig. 4.2A) (Table 4.1). Within 8 hours, concentrations stabilized at a plateau of 0.18 ± 0.04 mg OC m^{-2} SA for the remainder of the sterile experiment. The inoculated kinetic experiment produced organic carbon loadings of 0.154 ± 0.005 mg OC m^{-2} SA in the first half hour that then continued to increase linearly by 0.26 ± 0.02 µg C m^{-2} h^{-1}, or 10 ± 3 µg C L^{-1} h^{-1} (r^2 = 0.88, n = 24), to a maximum of 0.41 ± 0.03 mg OC m^{-2} SA at 75 hours (Fig. 4.2A).

Organic carbon loadings onto kaolinite showed a similar pattern when examined as a function of DOC concentration (Fig. 4.2B) (Table 4.2). Even at DOC concentrations of ~1.6 mg C L^{-1}, sorption was appreciable in the sterile experiment (0.11 ± 0.02 mg OC m^{-2} SA). These surface loadings increased with increasing DOC concentration to a clear plateau at the highest DOC values, following the classic hyperbolic form of the site-limited Langmuir isotherm (r^2 = 0.74, n = 15, q_{max} = 0.37 ± 0.14 mg OC m^{-2} SA, K = 0.050 ± 0.015 L mg^{-1} C) as is commonly observed with DOM sorption (Day et al. 1994; Gu et al. 1995). In contrast, organic carbon loading in the microbially active experiment appeared to increase linearly as a function of final DOC concentration (r^2 = 0.85, n = 14) in the range from 3.9 to 290 mg DOC L^{-1}, from 0.16 ± 0.02 to 1.7 ± 0.6 mg OC m^{-2} SA. However, the one data point at 560 mg DOC L^{-1} does suggest a plateau and a Langmuir isotherm fits all the data reasonably well (r^2 = 0.87, n = 15, q_{max} = 3.3 ± 1.9 mg OC m^{-2} SA, K = 0.0035 ± 0.0018 L mg^{-1} C).

Decreases in dissolved organic carbon concentration that roughly balanced the amount of organic carbon removed by mineral association were observable in the sterile experiments. However, because DOC was generally in large excess to mineral-associated POC, even 1-5% analytical uncertainties in dissolved concentrations precluded rigorous mass balance. In inoculated experiments DOC was sequestered not only by sorption to minerals but also by assimilation into the active biomass of the microbial community. DOC concentrations decreased on average by 19 ± 3 μg C L^{-1} h^{-1} (r^2 = 0.53, n = 29) during the 75-hour inoculated kinetic experiment, whereas concentrations were constant over the same time for the sterile experiment (Fig. 4.3).

Microbial dynamics

The microbiological community was active during inoculated experiments. After an initial lag of ~24 hours in the kinetic experiment, total bacterial populations increased linearly in the last 48 hours at a rate of $7.6 \pm 0.1 \times 10^6$ cells L^{-1} h^{-1} (r^2 = 0.999, n = 3) from 0.9×10^9 cells L^{-1} to 4.6×10^9 cells L^{-1} (Fig. 4.4A). Initially, the population was dominated by free-living bacteria (in aggregates <3.0 μm), but after 75 hours the free-living population appeared to be stabilizing near 2.5×10^9 cells L^{-1}. During the following 48 hours, the particle-attached bacterial population exhibited exponential growth, reaching nearly equal numbers to the free-living population (Fig. 4.4A). At higher DOC concentrations microbes did not exhibit a lag in growth (Fig. 4.4B). Populations of both free-living and particle-attached bacteria reached ~5×10^9 cells L^{-1} in 100 and 300 mg DOC L^{-1} after ~33 hours of incubation (Fig. 4.4B). In contrast, populations did not increase in the 2, 5 and 10 mg DOC L^{-1} incubations over the same time period. Translated into carbon units (assuming 25 fg $cell^{-1}$) and normalized to the available mineral surface area in incubations, total bacterial biomass represented ~0.007 mg OC m^{-2} SA for all incubations containing < 25 mg DOC L^{-1} lasting less than 33 hours (Fig. 4.3). With increasing time and DOC concentration, biomass represented as much as 0.03 and 0.08 mg OC m^{-2} SA respectively. Total bacterial biomass was thus equivalent to 2-12% of mineral-associated organic matter, and particle-attached bacteria equivalent to 0.2-6%. In terms of carbon, total biomass increased by 1.90 ± 0.02 μg C L^{-1} h^{-1} (r^2 = 0.99, n = 3) over the last 48 hours of the kinetic experiment.

Thymidine uptake rates increased from about 0.5 pmol L^{-1} h^{-1} to 4.7 pmol L^{-1} h^{-1} over the 75-hour inoculated experiment. Although fewer in number, the particle-

attached community drove most of this increase; thymidine uptake by free-living bacteria remained at 0.5 ± 0.3 pmol L^{-1} h^{-1} for the entire experiment. Cell specific uptake rates clearly show the disproportionate activity of the particle-attached community (Fig. 4.4C). However, the metabolic advantage of particle-attached bacteria appeared to maximize at both intermediate incubation time and also at intermediate DOC concentrations (Fig. 4.4C, D). Translated into units of carbon production (assuming 25 fg $cell^{-1}$), the microbial community assimilated ~0.1 to 1.2 µg C L^{-1} h^{-1} (Fig. 4.4E, F).

Compositional selectivity of organo-mineral associations

In all experiments, nitrogen-rich organic matter was preferentially sequestered from DOM onto minerals (Fig. 4.5). Although the molar C:N ratio of the initial DOM was 23.9 ± 1.6 for all incubations, mineral-associated POM never exceeded 15 mol C mol^{-1} N. For the sterile and inoculated kinetic experiments, organic matter that associated with minerals within the first hour had statistically indistinguishable weighted average C:N ratios of 6.3 ± 0.6 and 5.7 ± 0.3 respectively (Fig. 4.5) (Tables 1, 2). C:N ratios of mineral-associated OM increased rapidly to 8.7 ± 0.6 by 8.5 hours and 8.1 ± 0.4 by 10 hours in the sterile and inoculated experiments respectively. From there, C/N for sterile incubations exhibited substantial variability yet appeared to increase slightly as a function of time ($p = 0.04$ for all points; $p = 0.12$ if excluding the two high points at 48 and 360 hours) (Table 4.1). For inoculated incubations, the weighted mean C/N decreased to 7.0 ± 0.5 at 50-75 hours (Table 4.2). As a function of DOC concentration, C:N ratios increased from 6-7 at the lowest DOC to >8 for intermediate concentrations (~20 mg DOC L^{-1}) (Fig. 4.5B). Despite, higher analytical uncertainty due to smaller sample size and also substantial variability

between replicates, sterile incubations exhibited higher C/N ratios that continued to increase with increasing DOC. Weighted mean ratios increased from 12.0 ± 0.3 to 14.9 ± 1.8 at 100 and 560 mg DOC L^{-1} respectively (Table 4.1). In contrast, C:N ratios of mineral-associated OM decreased with increasing DOC in inoculated experiments having greater than ~20 mg DOC L^{-1} (Fig. 4.5B). Weighted mean values decreased from 8.7 ± 0.4 to 6.2 ± 0.2 at 24 and 560 mg DOC L^{-1} respectively. Filtered bacteria from the kaolinite-free controls exhibited a C:N of 6.0 ± 0.5 (n = 7).

Mineral-associated OM exhibited more positive $\delta^{13}C$ values relative to initial DOM in 95 of the 97 bottles analyzed (Tables 1 & 2, Fig. 4.6). The DOM used for all incubations had an initial $\delta^{13}C$ signature of –29.8 ± 0.1 ‰ (n = 5). Initially, minerals in the sterile kinetic experiment sorbed OM that was only slightly enriched, but $\delta^{13}C$ increased with time, reaching –28.3 ± 0.4 ‰ at 18 hours (Fig. 4.6A & Table 4.1). However, $\delta^{13}C$ signatures subsequently decreased to –29.0 ± 0.4 ‰ at 75 hours and later. The inoculated kinetic experiment showed a similar pattern in the $\delta^{13}C$ of mineral-associated OM as a function of time. Values were on average 1.1 ‰ enriched relative to the sterile experiment and 1.5 to 2.4 ‰ enriched relative to the initial DOM. In the isotherm experiment, mineral-associated OM was enriched at all DOC concentrations (Fig. 4.6B & Table 4.2). Minerals in sterile incubations sequestered OM that was on average 1.4 ‰ enriched relative to the initial DOM, whereas inoculated incubations exhibited 1.6 to 3.0 ‰ enrichments that increased with increasing DOC concentration. . Filtered bacteria from the kaolinite-free controls were characterized by a $\delta^{13}C$ of –26.8 ± 0.5 ‰ (n = 4).

Stable nitrogen isotope signatures exhibited complex patterns, in part due to the large analytical uncertainties associated with small sample sizes (Fig. 4.7; Table1

1-2). The DOM for all incubations had a $\delta^{15}N$ signature of 8.2 ± 0.6 ‰ (*n* = 9). Within the first three hours, mineral-associated OM was depleted in ^{15}N relative to DOM in both sterile and inoculated experiments. Values increased in the sterile experiment to a mean $\delta^{15}N$ of 10.3 ± 2.2 ‰ for the five samples collected between 25 to 75 hours (Fig. 4.7A). POM in inoculated incubations also became enriched with time, but only to a mean of –0.4 ± 1.5 ‰ after 27 hours. At the lowest DOC concentrations (1.6 - 7.0 mg L^{-1}), both sterile and inoculated treatments resulted in POM with $\delta^{15}N$ of 2.5 to 4.9 ‰. However, the two treatments diverged with increasing DOC. POM in the sterile systems became more enriched, with six of seven subsequent values being more enriched than the DOM (Fig. 4.7B). On the other hand, mineral-associated OM in the inoculated systems decreased following a hyperbolic function to an asymptote of –7.7 ± 1.1 ‰ at 290 to 660 mg DOC L^{-1}. Bacteria obtained from kaolinite-free controls had $\delta^{15}N$ signatures of –6.5 ± 1.9 ‰ (n = 6).

DISCUSSION

Abiotic versus microbially-mediated sorption

The suite of physico-chemical sorption reactions at play in the sterile experiments produced surface loadings of 0.1 to 0.4 mg OC m^{-2} SA (Tables 1 & 2, Fig. 4.2), closely matching the range observed in other studies of natural OM sorption (Gu et al. 1996). This range is similar to surface loadings observed for deltaic and oxidized deep sea sediments (Keil et al. 1997; Hedges et al. 1999) and some deeper soil horizons (Mayer and Xing 2001). In contrast, fine suspended river particles, coastal marine sediments and soil A horizons typically exhibit 0.5 to 1.1 mg OC m^{-2}

SA (Mayer 1994a; Hedges and Keil 1995; Keil et al. 1997; Mayer 1999). Sediments under anoxic bottom waters and organic soil O horizons have the highest surface loadings, generally 1.5 to 3.0 mg OC m^{-2} SA. In comparison, minerals exposed to inoculated DOM in this study developed surface loadings that were 1.5 to 6 times larger than sterile controls. Evidently, to reproduce these more typical OC:SA ratios in the laboratory, bacteria are an essential component; the only other study I know of to conduct sorption experiments with substantial native bacteria populations produced a similar result (Aufdenkampe et al. 2001).

Clearly both abiotic sorption and microbially-mediated organo-mineral associations are important in natural systems. As reported previously, physico-chemical sorption reactions occur very rapidly. I measured near steady-state loadings within minutes of mixing kaolinite with DOM. Therefore, organo-mineral associations that are mediated by bacteria literally occur on top of abioticly sorbed OM. These first organo-mineral associations form the biochemical environment that bacteria subsequently attach to and grow upon. However, bacterial attachment and growth can not directly account for the additional carbon that associates to minerals. Measured attached biomass was a small fraction (0.2% to 6%) of the differences between the sterile and inoculated experiments (Fig. 4.2) and bacterial biomass-carbon production rates (calculated from thymidine uptake, which does not consider production of non-cell organic matter such as exudates) are an order of magnitude less than the rate of increase in mineral-associated OM in the live kinetic experiment. Therefore, most of the mineral-associated carbon must either be produced by the bacteria as exudates (extracellular polysaccharides and peptides) or the attached bacteria and their exudates must serve as new sites for additional sorption of DOM.

Sorptive fractionation

A striking finding of this study is that both abiotic and microbially-mediated processes lead to preferential mineral association of OM that is enriched in both nitrogen and ^{13}C relative to the initial, parent DOM (Fig. 4.5 & 6). Yet, it appears that bacteria enhance these biochemical and isotopic fractionations. Mass balance constraints show in fact that the additional sorbed carbon in inoculated experiments must very closely match the N/C and $\delta^{13}C$ signatures of the free-living bacterial biomass isolated from the kaolinite-free controls. This suggests that additional "sorption" in live experiments is likely formed from bacterial exudates and other products.

Why is the abiotically sorbed carbon enriched in nitrogen and ^{13}C? Previous findings show preferential sorption of natural organic matter enriched in positively charged amino acids onto negatively charged minerals, and preferential sorption of OM enriched with negatively charged amino acids onto positively charged minerals (Carter 1978; McKnight et al. 1992; Aufdenkampe et al. 2001). These observations suggest that electrostatic mechanisms might be responsible for the preferential sequestration of nitrogen, and peptides in particular, onto minerals. Furthermore, peptides and proteins are remarkable as much for the wide range of functional groups available to interact with surfaces as for their ability to refold themselves to best minimize their energy in a particular chemical environment. Thus, peptide enrichment on surfaces is likely to be a ubiquitous feature in all natural systems, leading to enrichment of nitrogen and perhaps also ^{13}C in mineral-associated organic matter.

This study presents, for the first time, conclusive evidence that sorption and related processes are responsible for an enrichment of ^{13}C in mineral-associated OM. This enrichment is not likely due to a classical isotopic fractionation driven by thermodynamic or kinetic mechanisms (Hayes in press). Instead, the enrichment could be due to the preferential sorption of proteins. Its well known that bulk protein is generally 0.5-4 ‰ enriched in ^{13}C and 3-4‰ enriched in ^{15}N relative to total OM (Abelson and Hoering 1961; Macko et al. 1987; Hayes in press). Given that sorptive processes are known to enrich peptides onto mineral surfaces (McKnight et al. 1992; Aufdenkampe et al. 2001), it is likely that this biochemical fractionation would result in an apparent isotopic fractionation. In fact, unpublished results from my earlier study (Aufdenkampe et al. 2001) showed a ^{13}C fractionation from during sorption that increased as the percent of total particulate carbon contained in hydrolyzable amino acids ($\%T_{aa}C$) increased (Fig. 4.1). For the present study, I calculate for each sample the fraction of total mineral-associated organic carbon that is proteinaceous material by assuming all nitrogen is contained as protein, which has a average C/N = 3.8. Furthermore, by mass balance, I can calculate the $\delta^{13}C$ of that proteinaceous material, by assuming that the remainder has a isotopic signature similar to the initial DOM used in experiments. I thus find that 49 ±11% of mineral-associated OC is likely to be proteinaceous material, and it is 1.8 ±1.1‰ enriched in $\delta^{13}C$ relative to the initial DOM. These calculated carbon isotope differences between protein and bulk OM agree quite closely with values obtained from direct measurement (Abelson and Hoering 1961; Macko et al. 1987; Hayes in press), thus lending strong support to the hypothesis that observed carbon isotope fractionations during OM association with minerals are due to peptide enrichments onto minerals.

Stable nitrogen signatures from incubations in the present study tell a more complicated story. For all data collected after 24 hours, abiotically sorbed OM generally was enriched in ^{15}N, by on average 3.7 ± 5.5 ‰, relative to DOM (Fig. 4.7). This fractionation could be also explainable by the preferential sorption of proteinaceous OM, because proteins generally exhibit $\delta^{15}N$ values that are 3-4‰ higher than bulk OM (Macko et al. 1987). On the other hand, my inoculated experiments produced mineral-associated OM with low $\delta^{15}N$ signatures relative to DOM. These depletions appeared be a strong function of DOC concentration and also appeared to fluctuate over the first 24 hours before stabilizing (Fig. 4.7b). A clue to the cause of these patterns was found in concentrations of dissolved inorganic nitrogen species in the studied incubations. Although nitrate and nitrite were only found at concentrations <1 μM, ammonium ranged from 4.9 to 1200 μM as a function of initial DOM dilutions (data not shown) and net loss during inoculated incubations ranged from 0.5 to 75 μM. Sterile incubations showed no net loss of ammonium, suggesting that lost ammonium was incorportated by microbial biomass.

Ammonium uptake by bacteria is known to be accompanied by strong negative nitrogen isotope fractionation that changes as a function of ammonium concentration, from approximately –12 ‰ at 10 μM to –21‰ at 70-400 μM to –14‰ at >5 mM (Hoch et al. 1992). A plot of $\delta^{15}N$ of mineral-associated OM from my experiments – as a function of the fraction of that OM that appears to have originated as ammonium (Fig. 4.8) – suggests that isotopic fractionation during ammonium uptake was important to final mineral-associated $\delta^{15}N$ signatures. Although errors in mass balance calculations were high as a result of subtracting similar ammonium concentrations from before and after the experiments, regression of this data can offer

a few insights. Extrapolating to zero ammonium uptake suggests that the remaining mineral-associated material had $\delta^{15}N$ signatures of 3.0 ± 2.4 ‰ and 3.9 ± 1.3 ‰ for the kinetic and isotherm experiments respectively. Likewise, extrapolating to 100% of PON from ammonium uptake and by assuming that ammonification of the original leachate was not fractionating (i.e. $\delta^{15}NH4 \approx \delta^{15}N\text{-}DON = 8.2 \pm 0.7$ ‰), I calculate average isotopic fractionations of –24.0 ± 5.8‰ and –15.0 ± 1.5‰ for the kinetic and isotherm experiments respectively. Mass balance calculations for individual samples generally give similar results, but with large error bars and scatter. Rayleigh distillation considerations were not necessary, as the dissolved organic and inorganic nitrogen pools were never reduced by more than 20% from initial values.

Consequences for biogeochemical studies of carbon and nitrogen

The finding that sorption and other processes of organo-mineral association are responsible for carbon isotope fractionations of 1-3 ‰ is of substantial consequence to a wide range of biogeochemical applications. First, the enrichment in isotopic signatures between mineral-associated OM relative to DOM and plant sources appears to be universal. Measurements of $\delta^{13}C$ of coexisting coarse particulate OM (i.e. low density), fine particulate OM (i.e. mineral-associated OM) and DOM in 160 samples from rivers throughout the Amazon Basin show a very consistent pattern (Fig. 4.9). FPOM is consistently enriched by 1.5 to 2.5 ‰ over DOM and 0.5 to 1.5 ‰ over CPOM, which is largely composed of detrital plant fragments (Hedges et al. 1986a; Quay et al. 1992; Hedges et al. 1994; Hedges et al. 2000). An explanation that is consistent with my experimental results is that when CPOM leaches, components that are enriched in ^{13}C associate with minerals, leaving behind a DOM that is depleted in ^{13}C relative to the plant source. However, the

enriched $\delta^{13}C$ signatures of FPOM might have previously been ascribed to the fact that 85% of sediment carried by the Amazon main channel originates in the Andes, where OM is typically enriched with elevation (Fig. 4.9). However, relative $\delta^{13}C$ differences between OM fractions are maintained throughout the basin, including in lowland tributaries that have no high elevation headwaters. Therefore, sorptive fractionation appears to be the most plausible explanation for observed differences between $\delta^{13}C$ signatures of FPOM and DOM throughout the basin, and exchange between the two phases must occur on short time scales relative to transit times within the river system. These insights have played a key role in evaluating the rate at which a tropical streams receive new organic matter inputs after conversion of forest to pasture (Bernardes et al. in preparation).

The finding that sorption and related processes are responsible for stable carbon isotope fractionations may have its most significant impact on soil carbon studies. A very common observation in pristine soils is a 2-3 ‰ increase in $\delta^{13}C$ with soil depth, yet possible explanations continue to be hotly debated in the literature (Ehlreringer et al. 2000). Each proposed mechanism for the observed down-core increases has different implications for soil carbon models that depend on isotopic data to constrain results. That these trends covary with increasing proportions with depth of high density, mineral-associated OM versus low density detrital material has not yet entered the debate. It appears that the results from this study could help resolve the mechanisms for observed $\delta^{13}C$ profiles, which is critical to efforts to model carbon turnover rates in soils.

Table 4.1. Final values for the kinetic experiment, means ± standard errors (nd = not detected).

Incubation Time (h)	DOC (mg L^{-1})	OC/SA (mg m^{-2})	C/N *† (molar)	$\delta^{13}C$ * (‰)	$\delta^{15}N$ (‰)
Initial Kaolinite	--	0.035 ± 0.002	30.0 ± 4.3	-28.6 ± 0.5	nd
Initial DOM	571 ± 8	--	23.9 ± 1.6	-29.8 ± 0.1	8.2 ± 0.7
			Sterile		
0 - 0.3	20.7 ± 0.4	0.14 ± 0.02	6.3 ± 0.7	-29.1 ± 1.1	-3.5 ± 1.7
0.3 - 1	21.3 ± 1.5	0.12 ± 0.01	6.5 ± 1.1	-29.3 ± 0.1	nd
1 - 3	20.5 ± 0.0	0.11 ± 0.01	6.3 ± 0.4	#REF! ± 0.0	nd
3 - 6	21.8 ± 1.2	0.10 ± 0.01	6.4 ± 0.4	-29.6 ± 0.1	nd
8 - 11	20.5 ± 0.7	0.14 ± 0.03	8.7 ± 0.6	-29.3 ± 0.1	-9.0
18 - 20	21.2 ± 0.9	0.16 ± 0.00	8.0 ± 0.5	-28.3 ± 0.4	nd
25 - 28	21.1 ± 0.8	0.17 ± 0.02	7.4 ± 0.8	-28.5 ± 0.2	13.9
48 - 51	20.6 ± 0.6	0.18 ± 0.08	11.3 ± 1.1	-28.7 ± 0.2	9.3 ± 1.2
74 - 75	20.4 ± 0.2	0.16 ± 0.01	8.8 ± 0.8	-29.0 ± 0.6	9.7
359	20.6 ± 0.4	0.21 ± 0.01	10.0 ± 1.3	-28.9 ± 0.2	-0.5
			Inoculated		
0 - 0.3	nd	nd	nd	nd	nd
0.3 - 1	21.0 ± 7.5	0.17 ± 0.01	5.7 ± 0.3	-28.3 ± 0.5	-5.7 ± 5.6
1 - 3	16.9 ± 11.2	0.19 ± 0.02	6.4 ± 0.4	-28.1 ± 0.4	-12.4
3 - 6	15.7 ± 10.7	0.19 ± 0.02	6.2 ± 0.8	-28.6 ± 0.4	-3.6 ± 13.1
8 - 11	18.6 ± 9.8	0.19 ± 0.03	8.1 ± 0.4	-27.7 ± 0.7	-3.7
18 - 20	16.9 ± 11.2	0.26 ± 0.04	7.9 ± 0.3	-27.9 ± 0.1	-4.4
25 - 28	10.4 ± 11.2	0.26 ± 0.02	8.7 ± 0.3	-27.4 ± 0.1	-0.7 ± 1.8
48 - 51	16.4 ± 10.8	0.29 ± 0.01	6.9 ± 0.7	-27.6 ± 0.5	1.1
74 - 75	16.0 ± 10.4	0.41 ± 0.03	7.1 ± 0.3	-27.9 ± 0.3	-1.3
359	nd	nd	nd	nd	nd

* blank corrected to remove the effects of the initial kaolinite composition

† weighted average

Table 4.2. Final values for the isotherm experiment, means ± standard errors (nd = not detected).

Incubation Time (h)	DOC (mg L^{-1})	OC/SA (mg m^{-2})	C/N *† (molar)	$\delta^{13}C$ * (‰)	$\delta^{15}N$ (‰)
			Sterile		
30	1.6 ± 0.1	0.11 ± 0.02	5.9 ± 0.2	-28.2 ± 0.3	4.9
30	4.7 ± 0.3	0.14 ± 0.02	12.4 ± 1.5	-28.2 ± 0.3	nd
31	10.6 ± 0.3	0.15 ± 0.00	7.0 ± 1.2	-28.7 ± 0.4	21.0
32	21.5 ± 0.3	0.15 ± 0.01	11.7 ± 1.4	-28.2 ± 0.4	6.3
32	43.7 ± 0.7	0.22 ± 0.02	13.6 ± 1.5	-28.2 ± 0.2	11.0
33	99 ± 1.1	0.31 ± 0.02	12.0 ± 0.3	-28.2 ± 0.8	19.6 ± 5.6
32	279 ± 15	0.38 ± 0.04	14.5 ± 0.2	-28.7 ± 0.3	8.5
32	561 ± 26	0.35 ± 0.004	14.9 ± 1.8	-28.9	nd
			Inoculated		
30	3.9 ± 0.1	0.16 ± 0.02	6.9 ± 0.2	-27.8 ± 0.4	2.5
30	6.8 ± 0.2	0.19 ± 0.01	7.2 ± 0.4	-28.2 ± 0.7	3.0 ± 0.7
31	12.7 ± 0.4	0.24 ± 0.02	7.9 ± 0.3	-28.1 ± 0.4	-0.2 ± 0.8
31	24.2 ± 0.3	0.28 ± 0.02	8.7 ± 0.4	-27.7 ± 0.3	-0.4 ± 2.1
32	43.4 ± 0.1	0.38 ± 0.03	7.7 ± 0.2	-27.6 ± 0.3	-1.1 ± 1.6
33	100 ± 1.0	0.69 ± 0.05	8.0 ± 0.5	-27.2 ± 0.2	-4.1 ± 1.6
33	287 ± 11	1.74 ± 0.62	6.3 ± 0.05	-27.1	-7.9 ± 1.3
32	558 ± 26	2.07 ± 0.03	6.2 ± 0.2	-26.8	-7.2

* blank corrected to remove the effects of the initial kaolinite composition

† weighted average

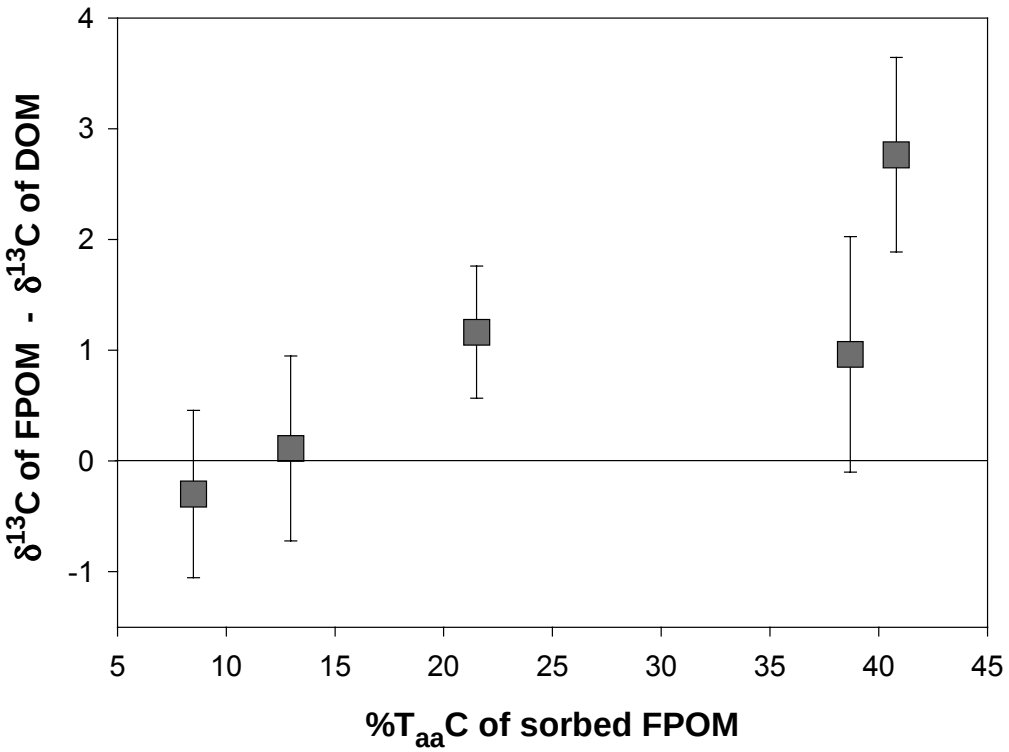

Figure 4.1. Stable carbon isotopic fractionation during sorption as a function of enrichment of amino acids in sorbed organic matter, for five sorption experiments from a previous study (Aufdenkampe *et al.*, 2001) (unpublished data). Error bars are calculated by least-squares error propagation of analytical uncertainties.

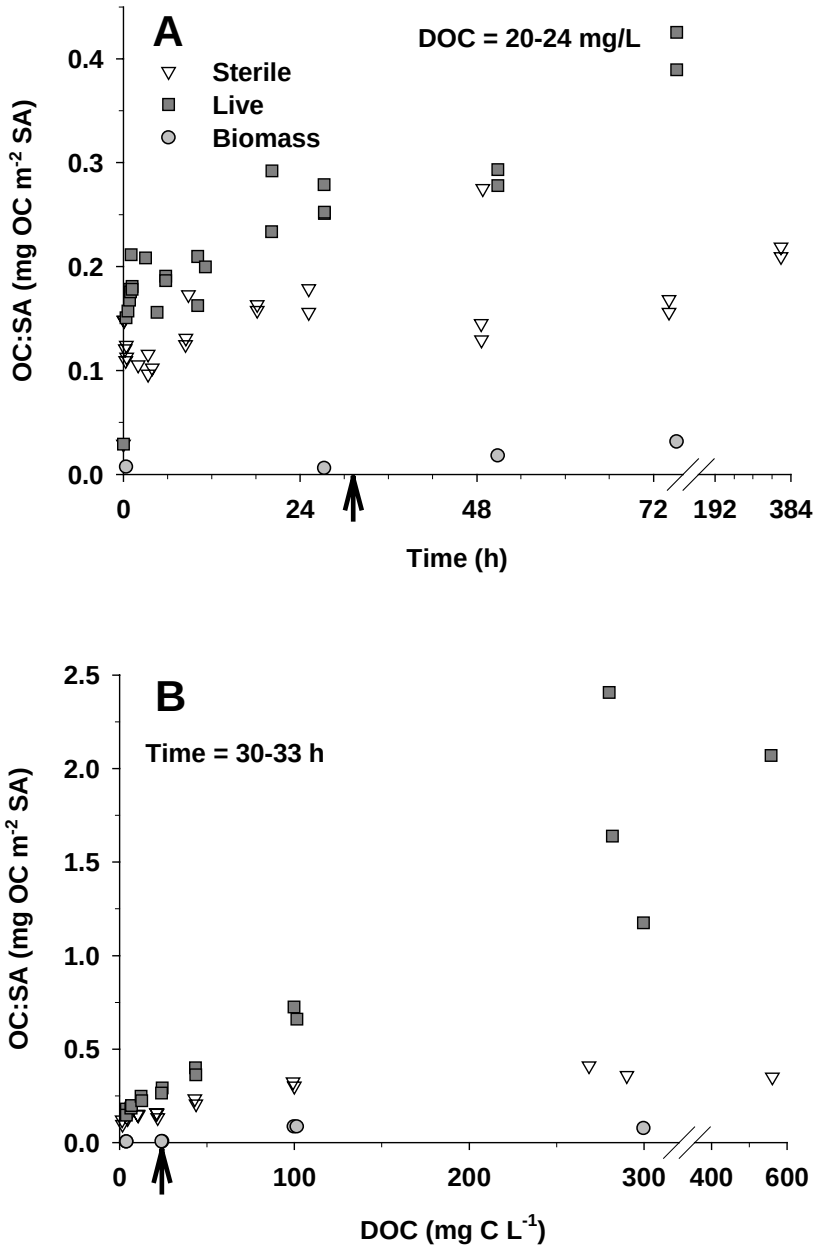

Figure 4.2. Organic carbon to surface area ratios (OC:SA) of kaolinite after incubations for the A) kinetic experiment, in which minerals were mixed with dissolved organic matter (DOM) at 20-24 mg C L^{-1} for various lengths of time, and for the B) isotherm experiment, in which minerals were mixed with various concentrations of DOM for 30-33 hours. For each experiment set, a samples inoculated with native microbial consortia were compared to sterile controls. Final DOC concentrations are plotted in B. In each panel, bold arrows point to the location on the x-axis that corresponds to final conditions in the other panel. Triangles show values from sterile incubations, squares from live incubations, and circles show biomass as calculated from assuming 25 fg $cell^{-1}$.

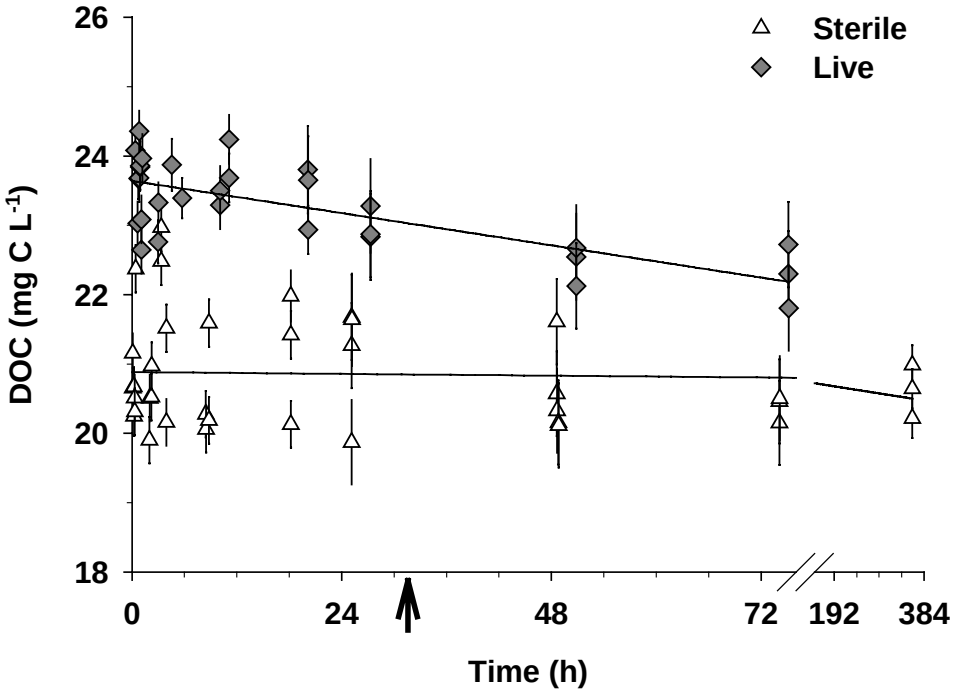

Figure 4.3. Changes in dissolved organic matter (OM) concentration as a function of time. Lines represent linear regressions of the data. Concentration in the live kinetic experiment decreased by 19 ± 3 μg C L^{-1} h^{-1} (r^2 = 0.53, n = 29), whereas the regression of DOC in the sterile gave a slope that was not significantly different than zero.

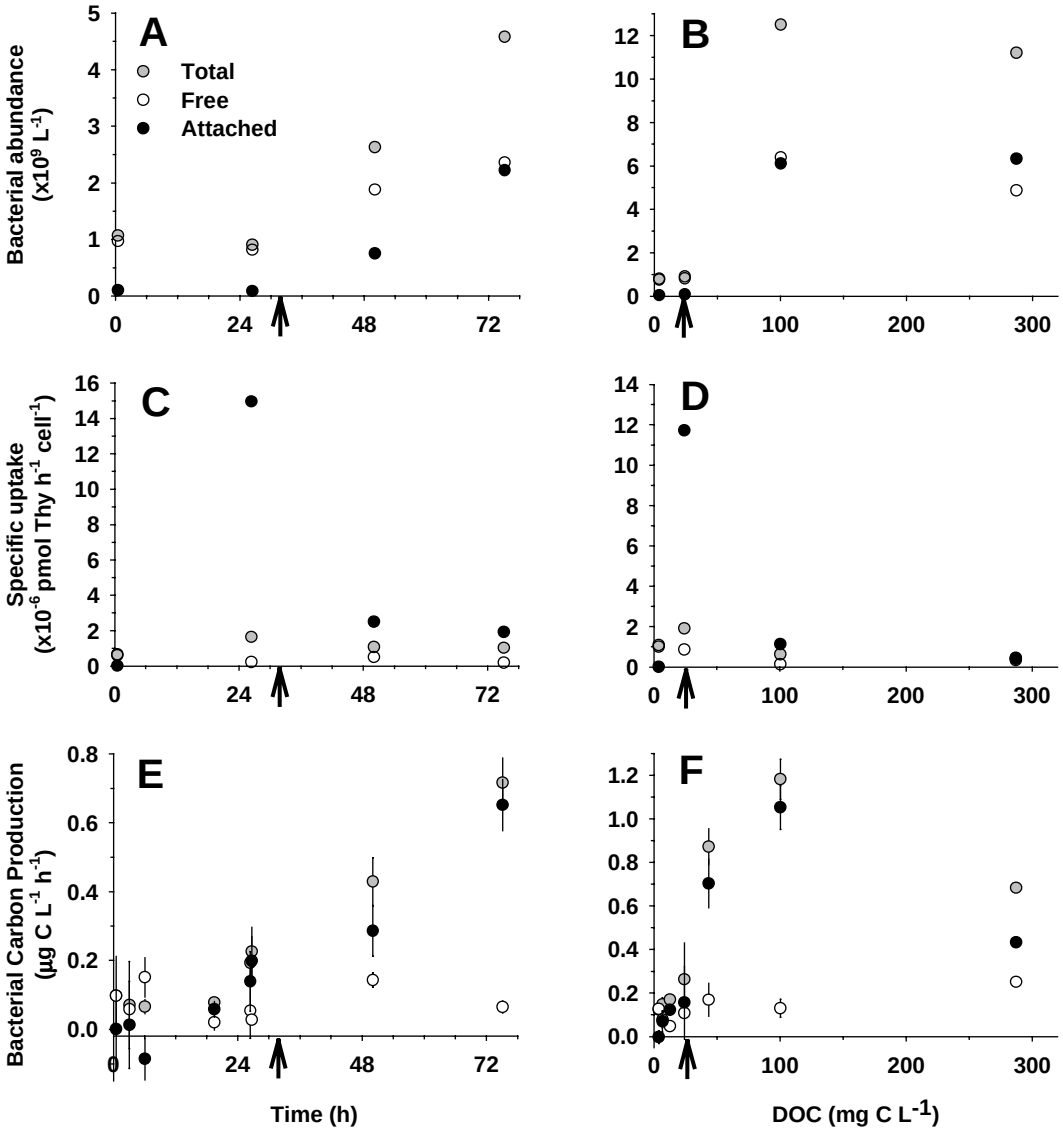

Figure 4.4. Microbial dynamics within incubations of the kinetic and isotherm experiments, as shown by bacterial abundance (A, B), cell specific thymidine uptake rates (C, D), and bacterial carbon production (E, F). Free-living bacteria were separated from the total population with a 3.0 µm nucleopore filter; the abundance and thymidine uptake rates of particle-attached bacteria were calculated by difference. However, because rates are normalized to cell abundances in C & D, they do not appear as differences. Data for total, free and attached overlap at 0 hours in C and at 2 and 290 mg C L^{-1} in D.

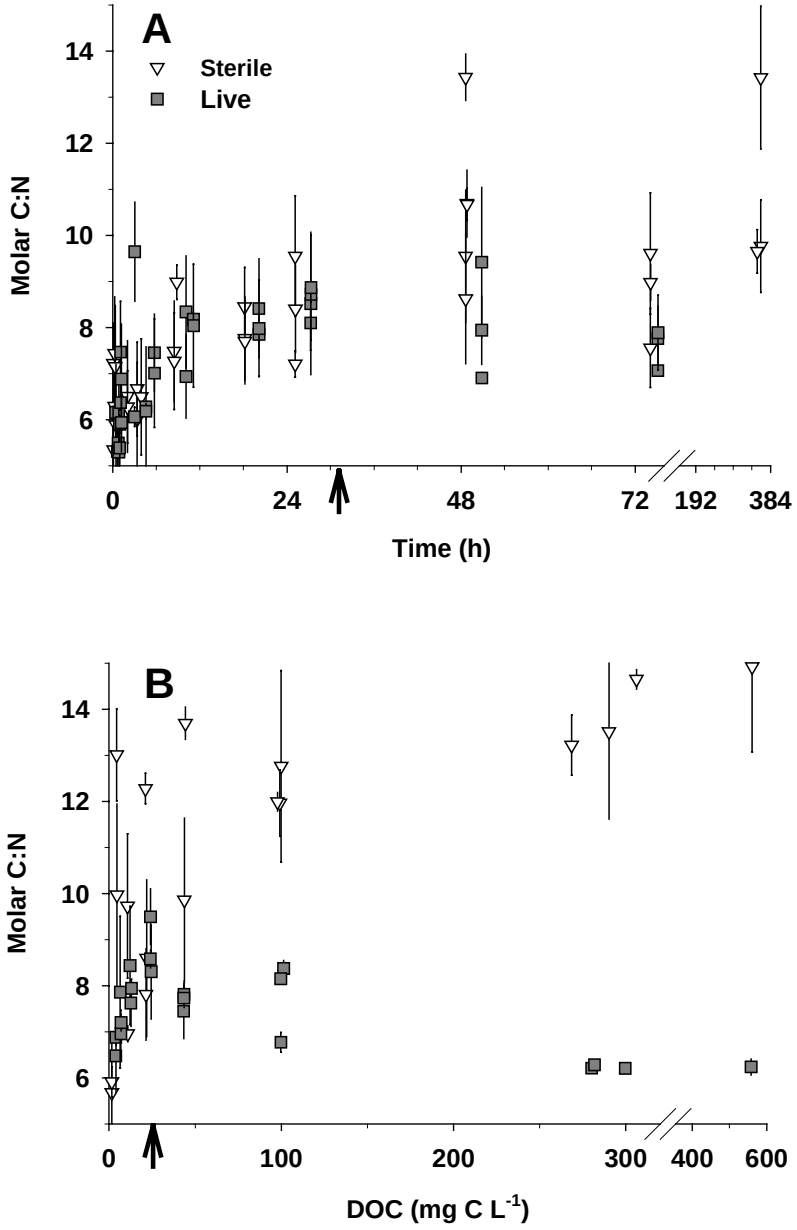

Figure 4.5. Molar carbon to nitrogen ratios of mineral-associated OM at the end of the A) kinetic, and B) isotherm incubations. Error bars are propagated from uncertainties in the elemental analysis of C and N. Errors are large where sample quantities were small. The C:N of the added DOM was 23.9 ± 1.6 for all incubations.

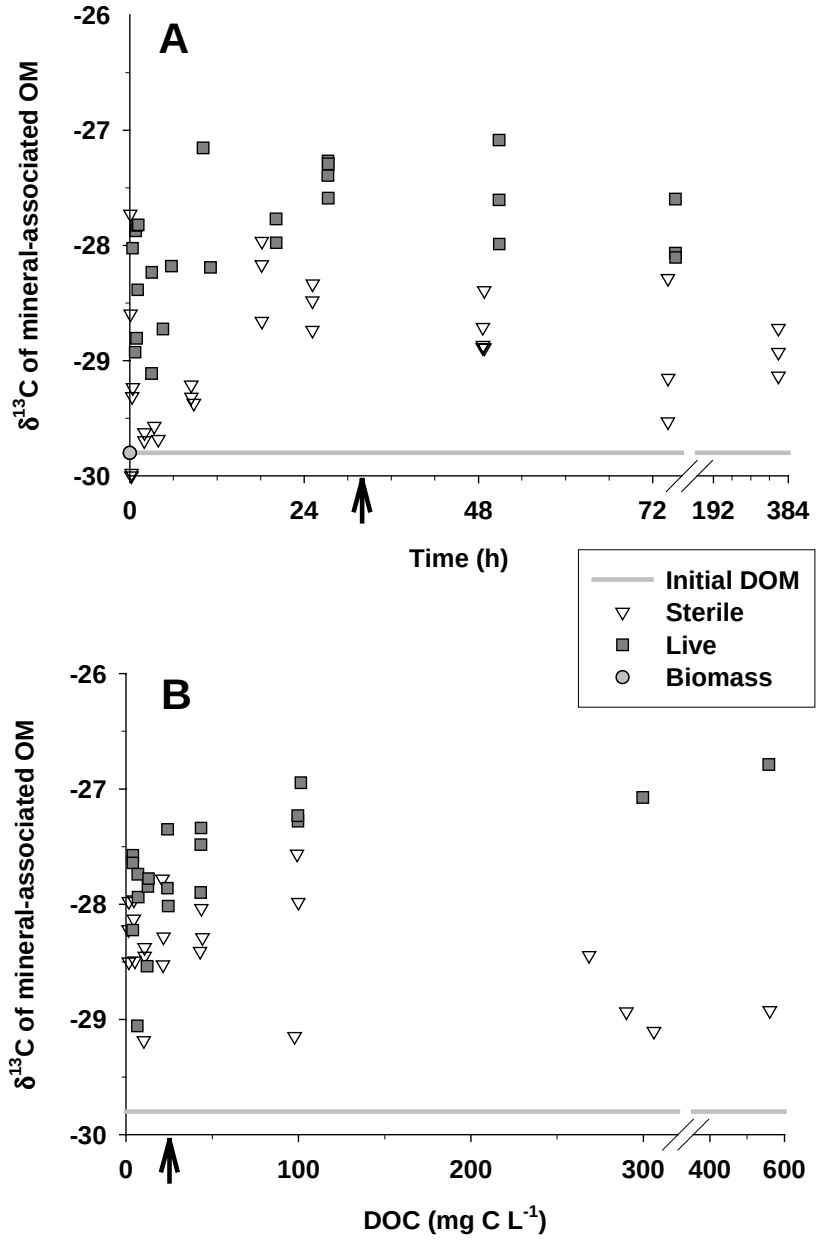

Figure 4.6. Stable carbon isotope signatures of mineral-associated OM at the end of the A) kinetic, and B) isotherm incubations. The line in each plot indicates the initial $\delta^{13}C$ value of the incubated DOM (–29.8 ± 0.1 ‰). All $\delta^{13}C$ values are per mil (‰) deviations relative to the PDB standard.

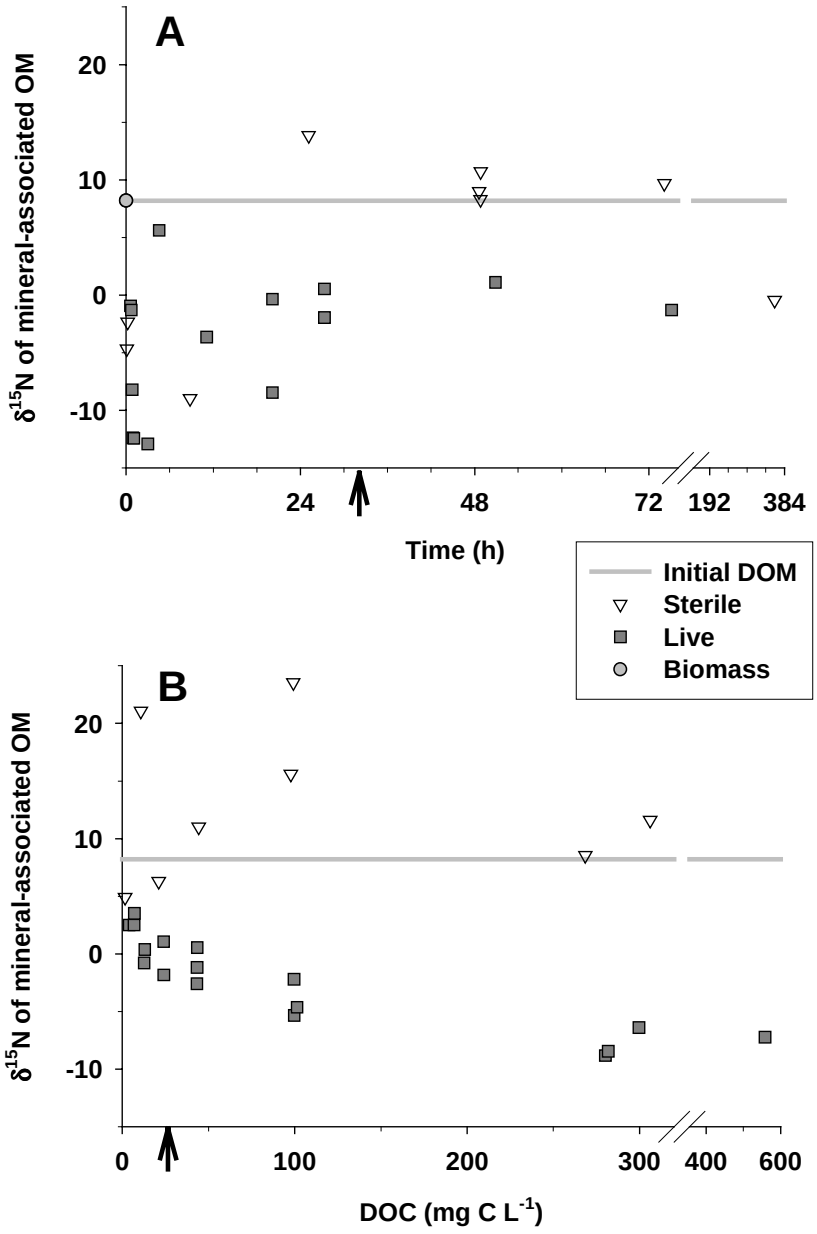

Figure 4.7. Stable nitrogen isotope signatures of mineral-associated OM at the end of the A) kinetic, and B) isotherm incubations. The line in each plot indicates the initial $\delta^{15}N$ value of the incubated DOM (8.2 ± 0.1 ‰). All $\delta^{15}N$ values are per mil (‰) deviations relative to air.

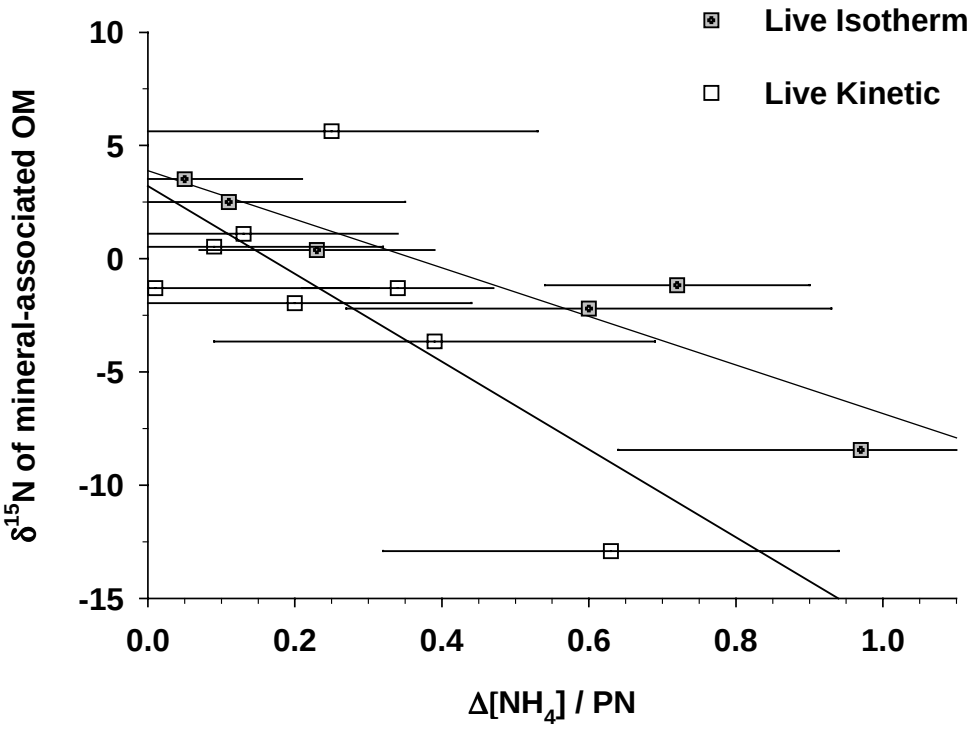

Figure 4.8. Stable nitrogen isotope signatures of mineral-associated OM as a function of the fraction of particulate nitrogen (PN) that could have resulted from ammonium uptake by the microbial community ($\Delta[NH_4]/PN$). Large horizontal error bars result from the taking the difference of similar $[NH_4]$ values from before and after the experiment. Data from both live kinetic and live isotherm experiments are presented.

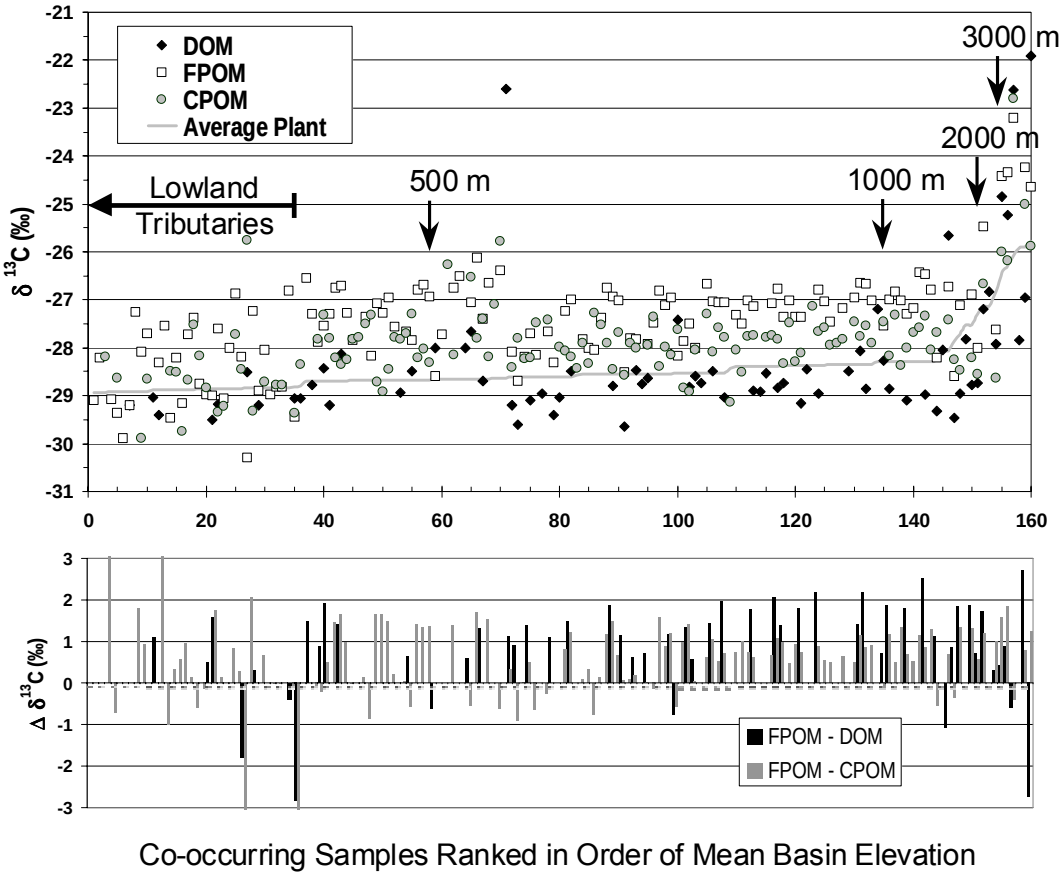

Figure 4.9. Stable carbon isotope signatures in OM from rivers of the Amazon Basin, presented as A) absolute $\delta^{13}C$ values and as B) the difference between co-occurring fractions. Data from (Hedges et al. 1986a; Quay et al. 1992; Hedges et al. 1994; Hedges et al. 2000) and unpublished sources. Average plant values as a function of elevation are taken from regressions in Korner et al. (1992).

CHAPTER 5: ORGANIC MATTER IN THE PERUVIAN HEADWATERS OF THE AMAZON: A COMPARISON TO BOLIVIAN TRIBUTARIES AND THE LOWLAND AMAZON MAINSTEM

INTRODUCTION

The Amazon River system is unique for both its geographic extent and the magnitude of hydrologic and biogeochemical fluxes within its channels. Since the physical and biogeochemical processes that take place within the Amazon's waters and watersheds follow the same laws that govern other large tropical river systems, studies of organic matter cycling within the Amazon's diverse and largely pristine rivers have broad applicability to carbon cycle issues at both local and global scales. For these reasons, the Amazon River system has spawned a extensive number of important studies on the mechanisms that control the fate and transport of organic matter (OM) in aquatic systems (Hedges et al. 1986b; Amon and Benner 1996a; Keil et al. 1997; Mayer et al. 1998; Richey et al. In Press). These studies, however, have largely focused on the lowland reaches of the Amazon main channel and its largest tributaries. Relatively little is known about the Andean headwaters where over 85% of the river system's sediment load (Gibbs 1967) and 30-60% of its water originates.

The CArbon in the AMazon River EXperiment (CAMREX) project has studied the fluxes, transformations and composition of organic matter along a 1,800-km reach of the lower Amazon for over twenty years (recently reviewed by Devol and Hedges 2001). One of the more striking findings from these studies is that the three principal size fractions of riverine organic matter – coarse particulate OM (CPOM, > 63 μm), fine particulate OM (FPOM, 0.1-63 μm), and dissolved OM (DOM, < 0.1 μm) – exhibit distinct compositional characteristics from one another.

Furthermore, within each size fraction elemental (C, N), isotopic (^{13}C, ^{14}C) and biochemical (amino acid, carbohydrate, lignin) compositions vary little in space or time along the 1,800-km reach of the lower Amazon or between major tributaries (sampled at their mouths). The compositional distinctions between CPOM, FPOM and DOM suggest that these size fractions play functional roles in OM dynamics within the river system.

In brief, CPOM biochemically and microscopically resembles partially degraded tree leaves and other non-woody C3 vascular plant tissues (Hedges et al. 1994). Largely unassociated with minerals and composed of discrete organic particles (Keil et al. 1997), CPOM is equivalent to the low-density (<1.6 g/cm^3) fraction of soils. Organic molecules in FPOM are intimately associated with weathered aluminosilicate minerals, with OC/surface-area loadings of 0.5-1.0 mg OC/m^2 (Keil et al. 1997), as are often observed in soils and sediments (Mayer 1994a). FPOM is nitrogen-rich and biochemically less degraded than DOM; these patterns appear to result in part from biochemical "fractionation" of DOM as it sorbs to mineral surfaces (Aufdenkampe et al. 2001). Once sorbed, studies in other systems show that organic molecules are apparently protected and cycle at much slower rates as long as they remain sorbed (Keil et al. 1994a; Nelson et al. 1994). DOM is highly degraded and nitrogen-poor (Hedges et al. 1994). In the lowlands, about 60-85% of the DOM is of high molecular weight (HMW >1000 Daltons), but decreases in size and bioavailability with degradation to form the low molecular weight (LMW) fraction (Amon and Benner 1996a). Living phytoplankton and bacteria comprise a small fraction of TOC in the river system (Wissmar et al. 1981; Benner et al. 1995).

By showing no downstream evolution of OM these findings could be interpreted as evidence that large river systems act primarily as conduits from land to sea. On the other hand, relatively large microbial respiration fluxes of OM within river waters suggests rather that these large rivers that are in dynamic equilibrium with respect to OM sources and losses. Resolving this question – to what extent do large tropical river systems serve as a pipe versus as a processor of terrestrial OM – has substantial implications to our understanding of carbon export losses from terrestrial ecosystems and therefore of the global carbon cycle (Schimel et al. 2001; Richey et al. In Press).

One test of the pipe versus processor question is to explore whether compositional evolution of riverine organic matter is apparent further upstream. Recently, the CAMREX project has initiated a number of field expeditions to various headwater regions of the Amazon River Basin to employ similar techniques that had been used to study the lower reaches of the river system. Hedges *et al.* (2000) presented the results from the first of those field studies – describing OM compositions along a transect from the Bolivian Andes to the Madeira and eventually to the Amazon mainstem. As members of CAMREX, here I present results from the second major field initiative – from a diverse set of Andean environments near the source of the Amazon in Peru, down through a range of depositional reaches in the foreland basin, to the confluence of major lowland rivers that form the Rio Amazonas proper (Fig. 5.1). The objective of this paper is to evaluate the extent to which compositions of the three primary OM fractions evolve downsteam, with the overall goal of assessing the extent to which these rivers simply act as downstream conveyors

of OM versus serving to dynamically process OM inputs that are continuous in space and time.

Study Area

The headwaters of the Amazon River originate in the Andean Cordillera of southern Peru, just north and west of Lake Titicaca. Here in the high altitude grassland steeps, or altiplano, the Rios Vilcanota and Apurimac begin there long descent to the Atlantic Ocean, a journey of approximately 6000 km (Table 5.1, Fig. 5.1). The Rio Vilcanota begins at Lake Langui-Layo (U1) at 3,970 m elevation and is augmented by effluents from the many wetlands similar to the one sampled (U2), which are scattered across the altiplano. Shortly after descending into the Vilcanota-Urubamba valley, the Vilcanota (U4) is joined by the larger Rio Salcca (U5), which drains one of the most heavily glaciated massifs in the region. The now muddy Rio Vilcanota continues to flow down the moderately populated valley through several villages and towns, and is joined by small streams draining the ancient Inca city of Cuzco. Approximately 210 km after leaving Laguna Langui-Layo, the river begins to drop (at site U7) down a deeply incised and humid valley by more than 2000 m in less than 100 km to the city of Quillabamba (U8) (Table 5.1, Fig. 5.2). The river, now named Rio Urubamba, flows out of the Andean foothills though cobbled and braided channels (U9) where it is joined by the smaller Rio Yanatili (U10), which was sampled just downstream of the town of Quellouno.

Parallel to the Vilcanota-Urubamba river system flows the larger and longer Rio Apurimac – Rio Tambo river system, which is considered the true headwater of the Amazon River. However, being much less populated and accessible, I were only

able to sample the Apurimac in one location (T1) before it descends from the Andes and is renamed the Rio Tambo. The next accessible sampling location was located 550 km downstream in the Andean forelands, at the confluence of the Rio Tambo (T2) with the Rio Urubamba (U11) at the town of Atalaya. At this point the Rio Tambo watershed is nearly twice as large as the Rio Urubamba basin (Table 5.2). Below their confluence, the river is known as the Rio Ucayali. We next sampled the Ucayali (U12) upstream of its confluence with the Rio Pachitea (P), which increases the watershed area by 12% (Table 5.2). Below this, near the city of Pulcalpa, the river channel is highly sinuous and rapidly migrating (Salo et al. 1986; Puhakka et al. 1992; Räsänen et al. 1992). Over 1000 km downstream, the equally large Rio Marañón (M) joins the Rio Ucayali (U13) near the city of Iquitos. 200 km further, at the confluence with the Rio Napo (N), the river becomes knows as the Rio Amazonas. Although still 3300 km from the Atlantic, the river is approximately 1 km wide and has fully evolved from Andean streams into a large, lowland tropical river.

The watersheds of the Tambo and Urubamba experience a pronounced seasonality in precipitation as might be expected at 10-15° S latitude due to seasonality in the location of the intertropical convergence. June-August is typically the driest time of year, receiving only ~25 mm rainfall per month, whereas 150 to 225 mm/month is typical for January and February. In general, there is a gradient of decreasing precipitation from the eastern slopes of the Andes to the west that is noticeable in the studied watersheds (Table 5.2). The annual pattern in rainfall is matched by a cycle in temperature. June and July are typically 5°C colder than October-April. Because of their proximity to the equator, the Rio Marañón and especially the Rio Napo exhibit much different patterns of seaonality. Low and high

water are respectively in August and March in the Marañón. The Napo has two annual peaks in rainfall in April-May and October-November. Average basin temperatures are also much more constant in these watersheds.

At the time of sampling in late October and early November 1996, the rainy season had not quite arrived as it typically does in September. Thus, the high elevation rivers (which we sampled first) were sampled at the lowest water stage of the hydrograph. All rivers were sampled just upstream of major confluences. Spatially averaged characteristics of the watershed upstream of each sampling station as calculated from geographic data (more below) are given in Table 5.2

METHODS

Sampling

At most Andean sites, sampling was performed from bridges. A weighted submersible pump (ShurFlo DC diaphragm pump) was hung from each bridge into the thalweg (main flow) to 6/10 the total river depth (4/10 from bottom), in order to sample suspended sediment size distributions where water velocities are most representative of depth-integrated fluxes {ref}. At lowland sites, the pump was suspended from a drifting boat. Wetland waters were collected by submerging bottles 50 cm, and Lake Langui-Layo was sampled from 2-3 meters depth at the dam. River depths were monitored with a standard digital fishfinder/sonar (Hummingbird, available at marine supply stores), in which the transducer was mounted on a floating plywood surfboard that could be deployed from bridge or boat. With this method, it was possible to monitor the depth of the pump and the river bottom simultaneously.

At all sites, small and large volume water samples (10 and 60 liters respectively) were collected via the submersible pump for dissolved and fine suspended material. A 63 μm Nitex screen was used to sieve out coarse material. A plankton net constructed from the same 63 μm Nitex screen was used to collect larger amounts of coarse material for chemical analyses. Large volume water samples and coarse suspended sediment (CSS) samples were immediately preserved in the field with $HgCl_2$, to a final concentration of 100 μM. Each evening after sample collection, small volume samples were filtered and processed for various dissolved and particulate analyses for eventual analysis in the laboratory. Care was taken to homogeneously subsample suspended sediments by use of a churn sample splitter (Bel-Art). Dissolved subsamples were preserved with $HgCl_2$ (also to 100 μM) and particulate samples on filters were immediately dried in a dehydrating oven. Fine suspended sediment (FSS) concentrations were determined gravimetrically, in triplicate, by filtration of a known water volume onto preweighed membrane filters (Millipore HAWP, 0.45 μm pore size).

After being shipped back to the laboratory, fine particulate and high molecular-weight dissolved materials were isolated from large volume samples with a Amicon DC-10 tangential flow ultrafiltration system using methods described previously (Benner 1991; Hedges et al. 2000). Briefly, samples were passed through an Amicon H5MP01-43 hollow fiber cartridge (0.1 μm nominal cutoff) to concentrate fine particles in a ~1 L volume. The permeate was then processed a second time, using a S10N1 spiral-wound cartridge (1,000 atomic mass unit (amu) nominal cutoff) to concentrate the ultrafiltered dissolved fraction. A freeze drier and a centrifugal

evaporator (Jouan) were used to isolate the particulate and dissolved materials respectively from these concentrates.

Chemical analyses – Coarse particulate, fine particulate and ultrafiltered dissolved organic matter (CPOM, FPOM and UDOM respectively) were analyzed for total carbon, organic carbon and total nitrogen on a Carlo Erba model 1108 CHN analyzer. Organic carbon was determined after vapor phase acidification (Hedges and Stern 1984), and inorganic carbon determined by difference between acidified and non-acidified samples. Dissolved organic carbon (DOC) concentrations were measured after acidification and sparging with a modified high temperature combustion MQ Scientific 1001 DOC analyzer (Peterson et al. submitted). Mineral surface areas (SA) of suspended fine and coarse particulates were determined from five-point Brauner-Emmett-Teller isotherms of N_2 adsorption using a Micromeritics Gemini SA analyzer. Prior to SA analysis, organic matter was removed from each sample by multiple treatments with 50% hydrogen peroxide at 50-60°C for several hours until all bubbling had ceased.

Lignin phenols were measured using the method of Hedges and Ertel (1982) as described by Hedges et al. (1986a; 2000). Samples were reacted with a suspension of CuO in 8 wt% NaOH within a high-pressure bomb at 155°C. Reaction products were converted to trimethylsilyl derivatives and analyzed on a Hewlett Packard 5890A gas chromatograph fitted with an HP-5MS capillary column (30 m x 0.24 mm i.d.) and operated with He carrier gas. Trimethylsilyl derivatives of individual phenolic products were identified with a Hewlett Packard 5972 mass selective detector and quantified by flame ionization detection (FID).

Amino acid analysis was performed with reverse-phase HPLC of hydrolysates versus charged-matched recovery standards based on the method of Cowie and Hedges (1992a) and described in detail by Aufdenkampe *et al.* (2001). In brief, samples were spiked with α-aminoadipic acid, γ-methylleucine, and δ-hydroxylysine as recovery standards, then hydrolyzed in 6 N HCl under N_2 in a sealed vial for 70 minutes at 150°C. Amino acids in neutralized hydrolysates were derivitized with *o*-phthaldialdehyde (OPA), resolved on a 15 cm x 4.6 mm ID C_{18} analytical column (Beckman ODS Ultrasphere, 5 μm pore size) using a binary solvent gradient of methanol versus aqueous sodium acetate, and detected with a Waters Model 420 fluorometer.

RESULTS

Sampling locations were chosen to follow a detailed transect down one Andean river system (Vilcanota-Urubamba-Ucayali) – from the altiplano, through erosive valleys, through depositional settings, to the Amazonian lowlands (Fig. 5.1). In addition, because the basin increases from 1,600 km^2 to 340,000 km^2 in area over this transect (Table 5.2), we sampled a number of important tributaries and tributary types. As such a wide diversity of physical environments are presented in this paper (Table 5.2), providing a relatively complete picture of the waters descending from the Peruvian Andes at the end of the dry season. On the other hand, this diversity of river sites also presents a challenge to simple interpretation of results and often requires placing data from each site into context.

Concentrations of suspended materials generally increased downstream, but were uncorrelated to basin properties such as average slope. At several sites, stagnant

local water conditions – such as in Lake Langui-Layo (U1), or in the wide and deep natural pool/lake at the Apurimac site (T1) – were reflected in low suspended sediment concentrations (Table 5.3). Even the Vilcanota at Tinta (U4), flowing down a steep gradient but upstream of any glacial inputs, only contained 4.5 mg FSS/L. On the other hand, waters carried by the glacial stream (U3) and the Rio Salcca (U5) appeared as "glacial milk", having FSS concentrations of 365 and 289 mg/L respectively. Through dilution and settling, these concentrations decreased downstream, even in river reaches exhibiting extreme local slopes and the highest mean basin slopes (U6-U10). At all lowland reaches (<300 m elevation), fine suspended sediment concentrations were uniformly high, from 179 to 338 mg/L (Table 5.3). CSS concentrations at these sites varied more, from 14 to 149 mg/L. However, these values do not come from flux-weighted sampling methods and CSS is known to show considerable variability with depth and laterally across the channel.

The distribution of organic carbon between coarse particulate, fine particulate and dissolved size fractions varied considerably from site to site (Fig. 5.3). In general, DOC and FPOC contributed equally to fluxes, with slightly more DOC at many Andean sites and slightly more FPOC in the lowlands. CPOC ranged from <1% of total organic carbon (TOC) to 67%, exceeding 450 μM in the the altiplano wetland and the Rio Salcca. High CPOC concentrations in waters at Andean sites were in part a consequence of CSS containing high percents of OC by weight ($\%OC_{CSS}$) (Table 5.3). Measured $\%OC_{CSS}$ values of 18%, 15% and 7.9% at the wetland (U2), the Vilcanota at Tinta (U4) and the Apurimac (T1) respectively are typical of streams with low suspended mineral content. However, in the Rio Salcca (U5), and lower Rio Vilcanota (U6 & U7) measured values of $\%OC_{CSS}$ of 9.0%, 8.2%

and 4.8% are much higher than downstream sites with similar CSS values that have a mean of 1.2% ±0.5% (Table 5.3, Fig. 5.4). In contrast, $\%OC_{FSS}$ concentrations increased from 0.6% in a small glacial stream (U3), to 1.2% in the glacial Rio Salcca (U5), to 1.6% and 3.8% in further downstream (U6 & U7). $\%OC_{FSS}$ values subsequently decreased from 2.7% and 2.5% in the foothills (U8 & U9) to uniform values of 1.4% ±0.28% at all sites downstream (Fig. 5.4). Thus, the downstream decreases in $\%OC_{FSS}$ lagged decreases in $\%OC_{CSS}$. At sites with low FSS (U1, U2, U4 & T1), $\%OC_{FSS}$ was high, ranging from 8.8% to 30%. The weight percent of organic carbon in ultrafiltration isolates ($\%OC_{UD}$) showed a very different trend. Despite the fact that the ultrafiltration membrane should pass essentially all free dissolved inorganic species, carbon comprised only 1.0% to 2.2% of UDOM (Table 5.3, Fig. 5.4). Values increased with decreasing mean basin elevation to ~12.5% in the Rio Marañón and Rio Napo (Fig. 5.4).

Weight percent OC associated with suspended riverine minerals exhibited much more consistent patterns when normalized to mineral surface area (Table 5.4, Fig. 5.5). The surface area of coarse suspended sediments ranged from 3.4 to 7.5 m^2/g for lowland sites (Table 5.4). In contrast, CSS collected at Andean sites exhibited much higher values, ranging from 17.2 to 43.5 m^2/g. Organic carbon to surface area ratios (OC:SA), excluding the wetland, were 1.9 ±0.6 mg C/m^2 in the lowlands versus 2.8 ±0.3 mg C/m^2 at Andean sites. Similar patterns were observed in the fine fraction. Aside from the 103 m^2/g measured for fine material suspended in the wetland, mineral surface area was much more uniform for the FSS fraction, ranging from 11.4 to 45.5 m^2/g but showing no distinct downstream trend (Table 5.4).

OC:SA ratios generally ranged from 0.34 to 0.84 mg C/m^2, except for Rio Urubamba sites in the highly depositional foothills (U8 & U9) and the wetland (U2) (Fig. 5.5).

Molar organic carbon to nitrogen ratios (C:N) were lowest for the FPOM fraction, ranging from 5.7 to 11.9 (Table 5.4, Fig. 5.6), whereas CPOM exhibited C:N ratios of 8.4 to 22.7. Regressions of the data for each particulate fraction (excluding Languna Langui-Layo) yield lines with equations $\%OC_{FSS} = (6.55 \pm 0.11) * \%N_{FSS} + (0.16 \pm 0.11)$ and $\%OC_{CSS} = (7.5 \pm 0.4) * \%N_{CSS} + (0.8 \pm 0.3)$ with $r^2 = 0.99$ and 0.96 respectively. However, the relationship between carbon and nitrogen in CPOM changes at %OC values less than ~2%. Excluding samples with $>2\%OC_{CSS}$ and also the Rio Yanatili (U10) changes the regression to $\%OC_{CSS} = (17.6 \pm 1.6) * \%N_{CSS} - (0.14 \pm 0.13)$ with $r^2 = 0.94$ and $n = 9$. Similarly, FPOM along the Urubamba corridor (U5, U6, U8, U9) shows a strong relationship with a different slope from the main FPOM trend: $\%OC_{FSS} = (10.0 \pm 0.6) * \%N_{FSS} - (1.0 \pm 0.2)$ with $r^2 = 0.99$. What is most striking about this last regression is an intercept that is statistically different than zero ($p = 0.03$), suggesting that FSS from these locations contain 0.10% ±0.01% of inorganic nitrogen. C:N ratios in UDOM appeared to increase steadily downstream (Table 5.4), from a mean of 12.8 ±2.0 at sites greater than 2,500 m in elevation to 27.8 ±1.8 at the three lowest sites near Iquitos (U13, M, N). Similar to CPOM, the relationship between %OC and %N for UDOM appeared to show a break in slope at ~2%, but in the opposite direction (Fig. 5.6). For all samples with <2.4% OC, the regression is $\%OC_{UD} = (9.5 \pm 2.6) * \%N_{UD} + (0.3 \pm 0.4)$ with $r^2 = 0.72$ and $n = 7$. For all samples with >1.3% OC (excluding the wetland), the regression is $\%OC_{UD} = (29.0 \pm 1.3) * \%N_{UD} - (2.8 \pm 0.4)$ with $r^2 = 0.98$ and $n = 11$. Again, it is worth noting that

this intercept is highly different from zero ($p = 0.00005$), suggesting that 0.098% ± 0.01% of the mass of dried UDOM is inorganic nitrogen.

Stable carbon isotope signatures ($\delta^{13}C$) of organic matter size fractions were generally greater than -27‰ at Andean sites and less than that downstream (Table 5.4). These values are best interpreted as a function of mean upstream basin elevation (Fig. 5.7a). Individual plant species analyzed from the altiplano, although monocot grasses, showed $\delta^{13}C$ values typical of plants that use the C3 photosynthetic pathway growing at high elevation (Korner and Arnone 1992; Ménot and Burns 2001). In general, at any given site, FPOM was enriched in ^{13}C relative to DOM and often relative to CPOM. The exceptions to this trend are generally at low sediment sites (U1, U4 & T1) but also at U7 and the Rio Salcca (U5) where UDOM is enriched by over 3% relative to FPOM (Table 5.4, Fig. 5.7a). Stable nitrogen isotope signatures were uniform as a function of elevation or distance downstream. UDOM was generally enriched over CPOM, with average $\delta^{15}N$ values of 4.0 ±0.8‰ and 2.8 ±0.3‰ respectively.

Total yields of the eight lignin phenols (Λ) were in general greatest for CPOM samples, ranging from 1.2 to 8.5 mg /(100 mg OC) (Table 5.5). Yields for FPOM and UDOM samples ranged from 0.3 to 2.2 mg /(100 mg OC). A number of samples exhibited ratios of cinnamyl to vanillyl phenols (C/V) that exceeded the range observed from leaf material of dicotyleonous plants and approached values typical of tropical monocotyleonous grasses (Fig. 5.8). In general, CPOM from the upper reaches of the Vilcanota-Urubamba system had the highest values of C/V, followed by FPOM from those same sites. Ratios of syringyl to vanillyl phenols for all samples fell in the range that is common to leaves of both monocotyleonous and

dicotyleonous plants. The ratio of vanillic acid to vanillin $(Ad/Al)_v$, which is an indicator of lignin degradation, was greater for all UDOM samples than for CPOM samples (Fig. 5.9). FPOM on the other hand showed a wide range of $(Ad/Al)_v$ values, with the greatest values at upstreams sites (U2, U4, U5).

Total hydrolyzable amino acid yields for 15 protein and 3 non-protein amino acids clearly decreased from Andean sites to the lowlands for both CPOM and FPOM fractions (Table 5.6, Fig. 5.10). From 5% to 28% of the carbon and 10% to 80% of the nitrogen in these samples could be identified chromatographically as these 18 compounds. In general, a larger percentage of nitrogen was identifiable in the CPOM fraction, whereas FPOM exhibited higher percentages of total amino acid carbon ($\%T_{AA}C$) (Fig. 5.10). FPOM samples were distinctly divided into two groups, with non-turbid waters (U1, U2, U4 & T1) and waters below Andean population centers (U7, U8 and U9) had the highest values of $\%T_{AA}C$ and $\%T_{AA}N$. The CPOM fraction from these same sites also exhibited the highest values. The UDOM fraction exhibited the lowest amino acids yields for at all sites and showed no apparent spatial trend.

The distributions of individual amino acids have often been used to as proxies for organic matter degradation, especially within marine sedimentary systems (Cowie and Hedges 1994; Dauwe et al. 1999). Two commonly used parameters are plotted in Figure 11. The sum of non-protein amino acids β-alanine (β-ala) and γ-aminobutyric acid (γ-aba), presented as mole percents of total amino acid yields, has been shown to increase with diagenesis in marine sediments. Similarly, an amino acid degradation index (DI), based on factor analysis of 14 protein amino acids from marine sedimentary sequences (Dauwe et al. 1999), is sensitive to subtle of compositional

changes that typically accompany degradation. High DI values correlate to relatively fresh sedimentary OM. Analyzed river samples cover the entire range of typical values for each proxy. Most FPOM samples contain less than 1.4 %(β-ala+γ-aba), with the three lowland samples near Iquitos showing values of 5.0% to 5.5%. These differences were not directly correlated to DI, although FPOM samples with DI >1 also had the highest values of $\%T_{AA}C$ and $\%T_{AA}N$ (Fig. 5.9, 5.10). CPOM values show wide scatter within 0 to 2.3 %(β-ala+γ-aba) (excluding the wetland) and 0.0 to 1.0 DI (Fig. 5.10). UDOM yielded the most apparent trends. Samples from Andean locations exhibit both low %(β-ala+γ-aba) and low DI values, which generally increase to high values of %(β-ala+γ-aba) and moderate DI in lowland samples (Fig. 5.11).

The amino acid paramenter, B/(B+A), has been used as a proxy for selective partitioning of organic components onto minerals due to electrostatic interactions (Hedges et al. 1994). B/(B+A) represents the ratio of basic amino acids, arginine and lysine, to the sum of these basic amino acids plus acidic amino acids, aspartic and glutamic acid. In general, values for both FPOM and UDOM appeared to decrease slightly from the Andean sites to the lowlands, from 0.25 ±0.03 and 0.09 ±0.05 to 0.14 ±0.05 and 0.04 ±0.04 for FPOM and UDOM respectively (Fig. 5.12). These values are considerably lower than those measured previously at three stations along the lower Amazon mainstem (Fig. 5.12).

DISCUSSION

Previous discussions of organic matter compositions in river systems (Hedges et al. 1994; Hedges et al. 2000; Devol and Hedges 2001) have divided isotopic and

biochemical evidence into classes of parameters that discern the sources of OM and its relative extent of degradation and most recently the likelihood of selective partitioning between dissolved and particulate phases. Two recent studies by our group demonstrate however that preferential association of certain biochemical classes over others leads to a wide array of compositional differences between dissolved and mineral-associated OM fractions that have previously been interpreted as indicators of source or diagenesis (Aufdenkampe et al. 2001; Aufdenkampe et al. in prep). This is not to say that these indicators, which were mostly developed to interpret sedimentary sequences in marine settings, are no longer useful. They certainly have a wide basis of evidence supporting comparisons between mineral-associated organic matter at different sites (Cowie and Hedges 1994; Cowie et al. 1995; Wakeham et al. 1997). Rather, the new findings on sorptive compositional fractionation highlight the difficulty in comparing indicators of source or diagenesis between dissolved and particulate fractions. The various processes that determine the isotopic and biochemical fractionation of organic matter are not clearly separable in systems where sorption and related processes are important.

The following discussion is directed toward answering the overall question of whether processes within the river system play an active role in transforming organic matter during transport or whether organic matter compositions merely reflect a mixing of materials from various sources. Therefore, particular attention is given to evaluating the likely mix of processes (source vs. degradation vs. partitioning) that determine OM compositions at given locations and whether this mix is consistent with observed downstream trends.

Organic matter distributions

The finding that coarse and fine sediments were generally most concentrated in waters at lowland sites (downstream of U10) – which exhibit both the lowest local slopes and mean basin slopes – is not immediately intuitive (Table 5.3). However, the Andean rivers were sampled late in the dry season. Typically, small erosive mountain rivers mobilize most of their annual sedimentary load during the severest storms of the year, leaving their beds scoured and armored with large grained material for the remainder of the year. On the other hand, rivers in net depositional environments are generally characterized by rapid channel migration in which more sediment are exchanged between banks than is transported downriver (Dunne et al. 1998). The seasonal range of sediment concentrations observed in the upper reaches of the Brazilian Amazon (i.e. at Vargem Grande) bracket CSS and FSS values from lowland sites in my study. Thus, observations during our sampling expedition in Oct.-Nov. 1996 are not inconsistent with observations elsewhere.

Particulate organic matter concentrations (Fig. 5.3) not only reflected these patterns in suspended sediments, but also the OM content associated with those sediments. Although most $\%OC_{CSS}$ and $\%OC_{FSS}$ values observed in my study were typical of those measured in turbid rivers throughout the Amazon lowlands (0.6-3.3% and 0.5-2.0% respectively) (Mayorga and Aufdenkampe in press), several sites in the Andes provided notable exceptions (Fig. 5.4). High %OC values, especially for CPOM, appear to be explainable in large part by variations in mineral surface area (Fig. 5.5). Although expected for FPOM, the strong relationship between %OC and SA came as a surprise for the coarse fraction. Data from the lower reaches of the Amazon show that most organic matter in the larger size fractions is found as discrete particles that have no physical associations with mineral material (Keil et al. 1997).

The surface areas of these larger fractions are also generally low (< 8 m^2/g). It thus appears that the >63 μm particle fraction at high altitude sites might be composed of robust aggregates of much finer material that are likely in close physical association with organic matter. That the OC:SA ratios are 2 to 4 times higher than is typically found lower in the river may be due to additional protection offered by these aggregates, which are known to protect OM in soils (Baldock and Skjemstad 2000).

Elemental composition

Relationships between the carbon and nitrogen contents of river samples offer a surprisingly informative look at OM dynamics. At lowland sites on the Amazon mainstem and major tributaries, C/N ratios of CPOM range from 18 to 30 (Hedges et al. 1986a; Hedges et al. 1994; Hedges et al. 2000), which is typical of the low density (<1.6), non-mineral associated fraction of soils (Oades 1989; Amelung et al. 1998) and only slightly lower than the leaves of most tropical plants (Hedges et al. 1986a). At sites >1,500 m elevation, however, CPOM exhibited C/N ratios that were substantially lower, and a regression of this data yielded a slope of 7.5 ±0.4 C/N (Fig. 5.6). This value is almost identical to the slope for all FPOM samples presented here and also for FPOM samples from the Amazon mainstem and major tributaries (Hedges et al. 1994). In contrast, the CPOM from sites <1,500 m followed a slope of 17.6 ±1.6 C/N (Fig. 5.6), which is nearly identical to CPOM values from the Amazon mainstem and major tributaries (Hedges et al. 1994). These observations, coupled with %OC and SA data, strongly support the hypothesis that CSS exported from altiplano and high altitude environments is composed of aggregations of finer minerals. Furthermore, two observations suggest that physical processes may disaggregate the CPOM into FPOM before it reaches the lowlands. The distinct

characteristics of high elevation CPOM disappear immediately after descending the short, steep and very turbulent reach between sites U7 and U8. At the same time, FPOM samples from U8 and U9 exhibit OC/SA ratios that are strickingly similar to those observed for the upstream CPOM samples.

FPOM samples exhibited relationships between %OC, %N and SA that are all very similar to previous observations of FPOM throughout the basin (Hedges et al. 1994; Keil et al. 1997). However, at many of the same locations, CPOM with similar surface areas and C/N ratios were associated with 2 to 4 times the amount of organic matter.

Dissolved organic matter at high elevation sites exhibited remarkably low %OC of 1-2%, which increased downstream to values at the Rios Napo and Marañón that are still half of what is typically observed further downstream in the Amazon mainstem (Hedges et al. 1994; Amon and Benner 1996a). This pattern was very similar to that observed for the Rio Beni system of Bolivia (Hedges et al. 2000). These data are consistent with the hypothesis that inorganic colloids are formed in colder environments by the physical breakdown of chemically unweathered substrates. While it is possible that these colloids dissolve once transported by the water to warmer regions, dilution with non-Andean waters could equally explain the trend.

Isotopic composition

Stable carbon isotopic signatures have a long history of use as a tracer of carbon sources. In addition to it's usefulness in distinguishing between tropical grasses and non-grass plants (C3 versus C4 photosynthetic pathways), and in identifying marine and freshwater planktonic sources, $\delta^{13}C$ is valuable as a tracer of

high elevation inputs. C3 plants typically exhibit increases of 0.7 to 1 ‰ in $\delta^{13}C$ values for every 1000 m gain in elevation (Korner and Arnone 1992; Bird et al. 1994; Ménot and Burns 2001). Samples from high altitude sites in my study reflect these enrichments, and others have observed similarly high $\delta^{13}C$ values in riverine particulates of –24 to –25 ‰ at other locations within the high Andes (Cai et al. 1988; Hedges et al. 2000). Based on such values and signatures of –27.4 ‰ for FPOM in the Amazon at Obidos, Hedges *et al.* (2000) estimate that >60% of FPOM originates in the lowlands despite the fact that >85% of FSS originates from the Andes.

The question here is whether the enriched Andean signal is the cause for the consistent 1-2 ‰ offset between FPOM and DOM (Fig. 5.7). One argument is that if FPOM exchanges with local OM pools more slowly that DOM, then this delay could cause FPOM to become more enriched than DOM as they are transported downstream. However recent experimental results demonstrate that sorption and related processes can be responsible for a 1 to 3 ‰ enrichment in newly mineral-associated OM relative to the parent DOM. One test of whether these fractionations are important in the Amazon River system is to see if the characteristic 1-2 ‰ offsets also occur at the highest elevation sites. In my study, only three out of the seven sites with mean basin elevations >3000 m show FPOM to be enriched over DOM (Fig. 5.7). On the other hand, $\delta^{13}C$ signatures of DOM are extremely variable between these samples with the highest values greatly exceeding measured values for plants in this region. It may be possible that the high inorganic carbon (IC) contents of these samples (roughly equivalent amounts of OC and IC; Table 5.4) may make isotopic measurement difficult. With a $\delta^{13}C$ signature of ~ 0 ‰, incomplete acidification and volatilization of even small amounts of inorganic carbon could strongly affect results.

Another test is to see whether downstream decreases in the $\delta^{13}C$ of FPOM lag decreases in the $\delta^{13}C$ of DOM. Clearly, the data do not show such a lag. The $\delta^{13}C$ of FPOM reaches a quasi-plateau almost immediately below 4000 m mean basin elevation, and $\delta^{13}C$ values for FPOM and DOM roughly run parallel to each other below this. In short, although the data from this study confirm values for the high elevation endmembers of each size fraction, there is not enough data to robustly determine whether offsets between fractions result from this altitudinal gradient.

Biochemical composition – The distributions of individual lignin-derived phenols offer a powerful tool for distinguishing between potential plant sources. Ratios of cinnamyl to vanillyl phenols in particular offer the potential to distinguish between dicots and monocots. This is particularly helpful in colder climates, such as the altiplano, where grass species use the C3 photosynthetic pathway and cannot be distinguished from dicots using stable carbon isotope measurements. As might be expected, CPOM and FPOM samples from high elevation sites showed elevated values of C/V, exceeding the range typical of dicots. UDOM samples were uniformly depleted in cinnamyl phenols, although dissolved samples from sites U4 and U7 had the highest C/V values as they did for the coarse and fine fractions. The trend of decreasing C/V from CPOM to FPOM to UDOM for any given sample may be evidence that C/V is sensitive to diagenetic alterations or selective partitioning.

Andean and lowland sites also distinguished themselves based on amino acid compositions of both coarse and fine particulates (Fig. 5.10). $\%T_{AA}C$ values for Andean CPOM was substantially higher than previously measured CPOM from the lower Amazon mainstem and major tributaries (Hedges et al. 1994) and from Bolivian rivers (Hedges et al. 2000). On the other hand, FPOM from these same sites

in the Peruvian Andes showed only slightly higher values than those from the Amazon mainstem and similar values to major lowland tributaries (Hedges et al. 1994). Because recent findings show amino acids exhibit strong preferential partitioning to minerals (Aufdenkampe et al. 2001), these results lend strong support to my earlier hypothesis that the CPOM fraction at these locations is composed of tightly associated organo-mineral aggregates. $\%T_{AA}N$ has also been shown to reflect to selective partitioning, although less so than $\%T_{AA}C$. However, $\%T_{AA}N$ is also sensitive to diagenesis (Cowie and Hedges 1994). Because differences between CPOM fractions from Andean and lowland sites in my study are minimal, I suggest that differences in $\%T_{AA}N$ between size fractions, particularly at the lowland sites, predominantly reflect differences in the extent of degradation.

The two paramenters – %(β-ala+γ-aba) and DI –also respond to both diagenisis (Cowie and Hedges 1994; Dauwe et al. 1999) and selective partitioning (Aufdenkampe et al. 2001). The cross-plot thus shows the complex interaction of the two processes on determining amino acid distributions in riverine OM. CPOM all plot in a cluster at relatively high DI values and relatively low %(β-ala+γ-aba), suggesting relatively fresh organic matter. DI values for FPOM are spread from 1.0 to –0.5, generally decreasing downstream with apparently increased biodegradation. %(β-ala+γ-aba) values are uniformly low for most FPOM samples. This could signal that these sediments have freshly partitioned OM associations that have not yet had time to develop the high %(β-ala+γ-aba) values that appear at the lowest three sites. DOM samples demonstrate best that these biochemical degradation proxies may be sensitive to other processes. Andean samples exhibit both very low DI and %(β-ala+γ-aba), which general increase as one moves downstream. This pattern reflects in

many ways the mirror image to the trend with FPOM samples. That is, sites that show highest DI values for FPOM show the lowest DI values for UDOM. Sites where DI values are the lowest for FPOM show the highest values for UDOM. This inverse pattern strongly suggests that partitioning reactions may determine DI values for the two fractions.

The one compositional parameter that has previously been used to infer selective partitioning is B/(B+A) (Hedges et al. 1994). In the Amazon mainstem, this parameter clearly shows that basic amino acids are enriched in FPOM and depleted in UDOM relative to CPOM, which is considered to most closely resemble the biochemical source of OM in these rivers (Fig. 5.12). For the entire Peruvian sample set, both values for B/(B+A) for FPOM and UDOM are depleted relative to CPOM, as was observed in Bolivia (Hedges et al. 2000). This may appear to suggest that partitioning reactions are less important in Andean systems than within the Amazon mainstem. However, it may simply suggest differences in mineralogy. For instance, high inorganic carbon contents in all the fractions, especially in the lower reaches, point to a strong influence on mineral surface characteristics by carbonates, which have a net positive surface charge. Such mineralogy has been shown to selectively enrich acidic amino acids onto surfaces (Carter 1978; Carter and Mitterer 1978; McKnight et al. 1992), which would draw down values of B/(B+A). Such low values for UDOM may offer evidence that the substantial inorganic colloid contents of this fraction might have a role in partitioning "dissolved" OM.

Overview

Elemental, isotopic and biochemical compositions of riverine organic matter clearly evolved from Andean source waters to large lowland rivers on their way to

joining the Amazon. Similar to previous results from the lower Amazon and from Bolivian tributaries, physical size was the most important factor in determining the composition and function of riverine organic matter. However, it has been shown that these distinctions can sometimes blur between size fractions. For instance, robust organo-mineral aggregates in Andean reaches appeared to function as mineral-associated OM similar to that typically found in the fine fraction, despite the larger size of these aggregates. Also dissolved organic matter in this region, with its high inorganic colloid content, in some ways behaves as a very fine particulate fraction. Associations between organic and inorganic constituents of this "dissolved" fraction may play an important role in the dynamics of DOM.

Table 5.1. Sampling locations and characteristics. Latitude and longitude was obtained in the field with handheld GPS, whereas elevation is our best estimate based on GPS, altimeter, a GIS digital elevation model and cartographic data. Distance to the Amazon mouth into the Atlantic is derived from our GIS river network model.

Site code	River system sampled	Sampling site	Lat (degrees S)	Lon (degrees W)	Elevation (m)	Distance to mouth (km)	River width (m)	River depth (m)
U1	Lake Langui-Layo	Langui	14° 26.08'	71° 17.08'	3,960	5,632	--	--
U2	Vilcanota	altiplano wetland	14° 21.79'	71° 19.11'	3,940	5,624	--	--
U3	Santa Maria - Urubamba	glacier stream	13° 09.45'	72° 16.49'	3,800	5,397	2-3	0.5
U4	Vilcanota - Urubamba	Tinta	14° 08.59'	71° 24.18'	3,490	5,582	19	0.9
U5	Salcca	confluence with Vilcanota	14° 05.76'	71° 26.27'	3,440	5,576	29	1.2
U6	Vilcanota - Urubamba	Huanbutio	13° 34.85'	71° 42.80'	3,040	5,499	24	0.8
U7	Vilcanota - Urubamba	Pachar	13° 16.45'	72° 13.02'	2,880	5,421	18	2.4
T1	Apurimac - Tambo	Cunyac	13° 03.78 '	72° 34.55'	1,850	5,441	79	5.1
U8	Vilcanota - Urubamba	Quillabamba	12° 51.96'	72° 41.77'	1,050	5,329	28	nd
U9	Vilcanota - Urubamba	Sahuayaoti	12° 38.90'	72° 32.10'	840	5,289	32	5.6
U10	Yanatili	Quellouno	12° 38.26'	72° 33.43'	830	5,288	~30	2.1
U11	Urubamba	Atalaya	10° 41.95'	73° 44.73'	290	4,889	350	5.2
T2	Tambo	Atalaya	10° 44.54'	73° 44.69'	290	4,892	~350	~6
U12	Ucayali	confluence with Pachitea	08° 47.05'	74° 33.14'	170	4,537	700	10.1
P	Pachitea	confluence with Ucayali	08° 45.25'	74° 32.58'	170	4,541	356	7.3
U13	Ucayali - Amazonas	confluence with Marañón	04° 28.29'	73° 25.96'	110	3,498	660	21.3
M	Marañón	confluence with Ucayali	04° 27.94'	73° 29.52'	110	3,500	1,400	25.9
N	Napo	confluence with Ucayali	03° 25.01'	72° 41.55'	100	3,280	850	12.2

Table 5.2. Average characteristics of the watersheds upstream of each sampling site. Mean data is derived from spatially averaging data from various GIS datasets.

Site code	Area (km2)	mean elevation (m)	% elevation <1000 m	% elevation >4000 m	slope (%)	mean % sand	mean % clay	Area % forest	Area % woodland	Area % grassland	mean temperature (C)	mean precipitation (mm yr-1)
U1	471	4,278	0	80.8	8.7	19.5	64.6	0.5	20.8	67.0	7.2	947
U2	3.6	4,212	0	91.7	4.4	17	67	0	25.0	75.0	8.2	1,038
U3	3.9	4,806	0	100	11.9	83	9	0	38.5	61.5	11.0	988
U4	1,610	4,240	0	70.5	8.3	21.9	62.4	0.6	22.2	73.8	7.8	1,013
U5	3,192	4,745	0	96.7	5.6	53.6	31.7	0.5	18.7	77.9	8.2	1,377
U6	7,371	4,424	0	75.9	8.3	53.2	33.8	0.5	22.9	73.8	8.7	1,223
U7	9,289	4,285	0	66.0	9.5	59.3	28.7	0.8	27.5	69.4	9.3	1,175
T1	22,763	4,106	0	61.2	9.4	57.6	31.2	2.7	35.7	61.4	7.8	848
U8	12,641	4,002	0.7	56.1	11.7	65.6	23.5	5.6	32.9	59.0	10.1	1,124
U9	13,918	3,791	3.2	51.0	11.7	67.2	22.1	11.4	32.5	53.9	10.9	1,124
U10	3,024	3,083	1.8	22.4	12.6	82.9	9.0	32.3	43.9	21.7	14.9	1,120
U11	61,067	1,890	49.3	16.0	7.5	51.9	34.4	63.1	17.6	18.1	18.1	1,403
T2	121,291	3,203	15.3	37.6	10.4	70.9	19.6	22.9	34.7	41.5	12.3	965
U12	205,519	2,500	34.4	27.0	8.6	59.2	29.2	42.7	26.2	29.9	15.4	1,205
P	27,498	830	79.1	1.8	4.4	18.1	64.9	86.2	10.7	2.3	22.1	1,782
U13	341,204	1,659	58.5	16.4	5.8	45.8	38.1	63.0	17.4	18.2	19.3	1,524
M	358,166	1,106	64.6	2.6	4.8	39.1	44.4	71.1	17.0	10.9	21.6	1,725
N	110,295	652	83.6	1.0	2.0	33.0	48.7	86.0	7.2	4.8	23.4	2,644

Table 5.3. Sampled water properties, chemistry and sediment load.

Site code	Temp (C)	pH	Conductivity uS/cm	Ca uM	Na uM	Mg uM	K uM	B uM	SiO4 uM	SO4 µM	Cl µM	CSS mg Sed/L	FSS mg Sed/L	DOC mg C/L
U1	11.9	8.46	588	2143	1296	514	46	9	87	1641	1091		1.5	1.90
U2	18.3	8.40	294	1277	326	193	26	6	21	81	194	32	10.4	10.65
U3	12.4	7.48	9	77	17	78	5	5	13				365	0.77
U4	18.7	7.69	1160	2580	4950	1024	207	92	118	1821	4923	0.5	4.5	2.63
U5	15.1	7.55	611	2448	974	543	79	129	163	2045	479	60	289	1.32
U6	16.2	8.10	1147	3084	4358	851	222	111	173	2369	4265	10	81.6	1.94
U7	17.6	7.89	1131	2982	4293	831	215	83	197	2130	4976	30	184	3.40
T1	22.1	8.75	685	1692	3197	387	105	28	214	996	3298	0.5	6.6	1.57
U8	19.7	8.21	428	1143	1422	358	84	28	155	726	2082	4.5	55.0	2.41
U9	23.5	8.28	418	1083	1379	354	79	28	161	692	1416	4.7	46.7	1.40
U10	23.3	7.67	74	277	200	210	26	7	151	230	1164	18	59.8	1.08
U11	27.0	8.06	146	554	222	128	31	6	165	160	142	56	268	1.81
T2	25.7	7.91	234	746	531	218	46	9	176	369	500	14	251	2.35
U12	26.1	7.70	192	701	348	160	38	<4.6	164	225	250	54	289	1.80
P	24.8	7.75	181	679	461	111	31	<4.6	127	147	351	55	269	2.21
U13	28.0	7.43	234	736	570	152	43	<4.6	154	354	951	31	338	2.65
M	26.0	6.97	134	447	331	78	31	<4.6	170	91	625	149	333	4.66
N	29.7	6.94	25	140	113	58	31	<4.6	229	38	560	64	179	2.44

Table 5.4. Bulk organic matter properties.

Site code	Size fraction	Sample symbol	Surface Area (m2/g)	OC (wt%)	IC (wt%)	N (wt%)	Organic C/N (molar)	OC:SA mg C/m2	$\delta^{13}C$ (‰)	$\delta^{15}N$ (‰)
U1	CPOM	C1								
U2	CPOM	C2	43.47	18.0	0.4	2.50	8.4	4.14	-23.8	
U3	CPOM	C3								
U4	CPOM	C4	46.04	14.8	0.3	1.62	10.6	3.21	-26.4	
U5	CPOM	C5	32.14	9.0	0	0.99	10.7	2.81	-25.9	
U6	CPOM	C6		8.2		0.61	15.6			
U7	CPOM	C7	17.17	4.8	3.6	0.62	9.1	2.82	-22.8	
T1	CPOM	CT1	31.80	7.9	1.7	1.05	8.7	2.48	-23.8	
U8	CPOM	C8		0.7	0	0.05	15.6		-26.2	
U9	CPOM	C9		2.0	0	0.12	19.0		-26.0	3.4
U10	CPOM	C10		1.1		0.13	10.2			
U11	CPOM	C11	7.01	1.7	0.1	0.11	18.5	2.47	-28.5	
T2	CPOM	CT2	3.42	0.8	0.5	0.05	17.0	2.22	-28.6	2.1
U12	CPOM	C12	7.49	1.4	0.2	0.09	16.9	1.81	-28.6	
P	CPOM	CP	4.91	0.4	0.4	0.03	16.7	0.85	-29.1	3.0
U13	CPOM	C13		0.8	0	0.06	15.8		-28.2	3.3
M	CPOM	CM	5.63	1.0	0.1	0.06	18.8	1.78	-27.7	2.7
N	CPOM	CN	7.43	1.7	0	0.09	22.7	2.33	-28.6	
U1	FPOM	F1		30.3		3.53	10.0		-26.7	
U2	FPOM	F2	103.9	17.0	1.0	2.63	7.6	1.64	-24.8	
U3	FPOM	F3		0.6		0.12	5.7			
U4	FPOM	F4		16.2	0.6	2.40	7.9		-24.6	
U5	FPOM	F5	24.57	1.2	0.4	0.22	6.2	0.47	-24.7	
U6	FPOM	F6		1.6		0.27	7.0			
U7	FPOM	F7	45.51	3.8	0.7	0.67	6.7	0.84	-23.2	
T1	FPOM	FT1		8.8	1.1	1.24	8.3		-23.7	
U8	FPOM	F8	18.45	2.7	0.4	0.38	8.4	1.48	-24.3	
U9	FPOM	F9	11.40	2.5	0.4	0.34	8.4	2.14	-24.4	
U10	FPOM	F10		1.0		0.16	7.2			
U11	FPOM	F11	25.63	1.7	0.1	0.19	10.4	0.65	-27.1	
T2	FPOM	FT2	27.48	1.5	0.3	0.18	9.5	0.53	-27.6	
U12	FPOM	F12	24.35	1.2	0.2	0.15	9.4	0.51	-28.0	
P	FPOM	FP		1.6		0.20	9.4			
U13	FPOM	F13	32.67	1.1	0.1	0.13	10.1	0.34	-28.6	
M	FPOM	FM	25.46	1.7	0.3	0.16	11.9	0.66	-28.2	
N	FPOM	FN	25.28	1.5	0.2	0.17	10.7	0.60	-28.5	
U1	UDOM	D1		1.4	1.8	0.15	10.6		-23.5	3.8
U2	UDOM	D2		17.0	5.2	1.44	13.8		-25.3	3.9
U3	UDOM	D3								
U4	UDOM	D4		2.2	1.2	0.21	12.1		-23.3	
U5	UDOM	D5		1.0	1.5	0.07	15.7		-21.9	3.2
U6	UDOM	D6								
U7	UDOM	D7		1.6	1.1	0.16	11.6		-22.6	5.7
T1	UDOM	DT1		2.0	1.0	0.16	14.5		-21.8	4.9
U8	UDOM	D8		1.1	2.1	0.08	15.0		-25.2	
U9	UDOM	D9		2.4	1.3	0.16	16.9		-24.8	4.8
U10	UDOM	D10								
U11	UDOM	D11		4.4	3.6	0.23	22.2		-29.0	2.9
T2	UDOM	DT2		5.1	2.8	0.28	21.0		-27.9	3.2
U12	UDOM	D12		4.8	3.5	0.26	21.0		-28.7	3.7
P	UDOM	DP								
U13	UDOM	D13		6.6	3.2	0.31	25.2		-29.5	3.8
M	UDOM	DM		12.5	2.7	0.51	28.8		-29.3	3.6
N	UDOM	DN		12.6	1.7	0.55	26.5		-29.6	4.2

Table 5.5. Lignin phenol yields, in mg/(100 mg OC), of the organic matter size fractions.

Site code	Size fraction	Lambda Λ	VAL	VON	VAD	SAL	SON	SAD	CAD	FAD
U1	CPOM									
U2	CPOM	1.21	0.33	0.13	0.21	0.17	0.12	0.08	0.07	0.10
U3	CPOM									
U4	CPOM	2.05	0.42	0.13	0.16	0.48	0.29	0.16	0.21	0.20
U5	CPOM	3.37	0.85	0.23	0.26	0.77	0.26	0.24	0.40	0.36
U6	CPOM									
U7	CPOM	3.19	0.61	0.28	0.36	0.45	0.32	0.39	0.39	0.38
T1	CPOM	3.31	0.92	0.24	0.28	0.91	0.28	0.24	0.22	0.23
U8	CPOM									
U9	CPOM									
U10	CPOM									
U11	CPOM	8.46	2.98	0.71	0.65	2.30	0.65	0.49	0.38	0.30
T2	CPOM									
U12	CPOM									
P	CPOM									
U13	CPOM									
M	CPOM									
N	CPOM									
U1	FPOM									
U2	FPOM	1.10	0.16	0.08	0.33	0.20	0.11	0.07	0.03	0.11
U3	FPOM									
U4	FPOM	0.67	0.10	0.03	0.16	0.11	0.06	0.06	0.05	0.10
U5	FPOM	0.45	0.08	0.03	0.08	0.09	0.07	0.04	0.03	0.04
U6	FPOM									
U7	FPOM	0.83	0.17	0.07	0.09	0.15	0.11	0.08	0.06	0.10
T1	FPOM									
U8	FPOM	1.50	0.30	0.08	0.20	0.38	0.18	0.13	0.07	0.15
U9	FPOM	1.74	0.43	0.13	0.23	0.44	0.15	0.14	0.08	0.16
U10	FPOM									
U11	FPOM	1.90	0.51	0.14	0.30	0.49	0.16	0.17	0.06	0.08
T2	FPOM									
U12	FPOM									
P	FPOM									
U13	FPOM	1.98	0.51	0.15	0.33	0.54	0.17	0.16	0.03	0.10
M	FPOM									
N	FPOM									
U1	UDOM									
U2	UDOM	1.00	0.23	0.12	0.24	0.14	0.12	0.07	0.02	0.07
U3	UDOM									
U4	UDOM	0.32	0.06	0.05	0.07	0.02	0.08	0.02	0.01	0.03
U5	UDOM									
U6	UDOM									
U7	UDOM	0.31	0.06	0.05	0.07	0.02	0.06	0.03	0.00	0.03
T1	UDOM									
U8	UDOM									
U9	UDOM	0.79	0.18	0.10	0.17	0.13	0.08	0.07	0.02	0.05
U10	UDOM									
U11	UDOM	2.24	0.49	0.24	0.48	0.43	0.21	0.24	0.05	0.10
T2	UDOM	1.80	0.41	0.22	0.44	0.29	0.16	0.18	0.02	0.08
U12	UDOM									
P	UDOM									
U13	UDOM	1.37	0.27	0.16	0.36	0.24	0.13	0.13	0.02	0.07
M	UDOM	1.81	0.40	0.21	0.43	0.33	0.16	0.19	0.02	0.07
N	UDOM	1.78	0.39	0.20	0.42	0.35	0.15	0.17	0.02	0.09

Table 5.6. Amino acid composition of the organic matter size fractions. Continued on next page.

Site code	Size fraction	THAA (mg / 100 mg OC)	%TAAC	%TAAN	ASP (mol%)	GLU (mol%)	SER (mol%)	GLY (mol%)	THR (mol%)	ALA (mol%)	TYR (mol%)	MET (mol%)	VAL (mol%)	PHE (mol%)	ILE (mol%)	LEU (mol%)	HIS (mol%)	ARG (mol%)	LYS (mol%)	βALA (mol%)	γABA (mol%)	αABA (mol%)
U1	CPOM																					
U2	CPOM	41.89	18.5	41.6	6.9	7.0	11.1	17.2	7.2	11.8	3.4	1.5	7.1	4.1	4.7	8.5	1.3	3.8	0.7	3.4	0	0.15
U3	CPOM																					
U4	CPOM	37.27	16.4	48.8	7.8	8.1	8.4	21.2	5.6	11.6	2.8	1.2	5.0	4.0	3.9	8.5	1.3	3.3	4.9	2.1	0.15	0.00
U5	CPOM	34.48	15.0	46.9	7.6	6.9	9.2	21.1	6.0	16.4	4.2	0.3	6.0	2.7	3.1	5.9	1.5	2.5	4.0	1.9	0.18	0.32
U6	CPOM																					
U7	CPOM	47.26	20.6	51.3	8.9	8.3	10.5	16.8	7.2	14.5	3.2	0.7	6.3	3.2	3.5	6.2	1.4	3.1	4.0	1.5	0.16	0.28
T1	CPOM	39.86	17.6	43.0	5.2	7.9	9.9	16.6	7.7	15.7	3.1	1.1	7.2	4.1	4.4	6.0	1.5	3.4	3.8	1.9	0.31	0.12
U8	CPOM	26.87	11.8	53.5	10.1	9.0	10.7	15.4	6.4	14.4	3.3	0.0	7.1	3.7	4.0	7.3	1.5	2.8	3.0	0.9	0	0.38
U9	CPOM	29.32	12.9	63.1	9.9	9.0	11.6	14.8	6.5	14.8	3.1	0.2	6.9	3.7	4.1	7.8	1.0	2.6	2.9	0.8	0	0.33
U10	CPOM	60.77	27.1	72.5	6.6	10.7	10.4	13.6	7.1	16.9	3.8	0.4	8.6	4.3	4.6	6.4	1.5	2.5	2.5	0	0	0.21
U11	CPOM	17.15	7.6	36.4	6.0	9.2	11.1	16.6	7.4	14.9	2.6	0.2	7.9	4.0	4.6	5.9	1.9	2.9	3.6	1.3	0	0
T2	CPOM	18.35	8.1	39.1	5.9	9.3	10.3	15.7	7.6	14.7	2.7	0.5	7.8	4.4	4.8	6.5	1.5	3.3	3.8	1.2	0	0
U12	CPOM	15.65	6.9	33.2	6.6	9.7	11.0	16.3	7.4	14.0	2.4	0.3	8.3	4.3	4.6	6.2	1.8	2.7	3.0	1.4	0	0
P	CPOM	18.22	8.1	44.4	5.6	8.6	11.1	15.2	6.7	12.8	2.9	0.5	7.5	3.7	4.4	6.1	2.1	2.8	8.1	1.8	0	0
U13	CPOM	13.60	6.0	29.2	6.6	10.0	10.7	15.7	7.2	13.6	2.6	0.5	7.9	3.8	4.6	6.2	2.3	2.8	4.1	1.5	0	0
M	CPOM	16.43	7.3	38.1	6.8	9.8	10.5	15.5	7.3	14.1	2.5	0.2	7.9	3.9	4.7	6.0	2.1	2.9	3.8	2.2	0	0
N	CPOM	13.59	6.0	40.1	6.7	9.3	11.6	16.0	7.7	14.3	2.2	0.2	7.9	4.0	4.4	5.8	2.1	2.6	3.3	1.8	0	0
U1	FPOM	34.71	15.4	41.5	6.0	13.0	7.8	13.0	7.5	17.0	0.9	0.5	8.1	4.9	5.4	8.3	0.6	4.1	2.2	0.6	0	0.11
U2	FPOM	41.77	18.7	36.4	7.3	14.1	7.4	12.0	7.4	13.9	0.8	1.4	8.5	5.2	6.4	8.1	0.9	3.3	2.0	1.0	0	0.16
U3	FPOM																					
U4	FPOM	39.41	17.4	36.8	6.6	10.4	8.9	13.3	9.4	15.7	0.4	1.1	8.7	4.8	5.7	7.5	0.9	3.5	1.5	1.4	0	0.12
U5	FPOM	13.98	6.1	10.3	6.8	10.2	9.2	14.1	8.7	17.4	0.5	0.5	8.3	4.6	5.3	6.8	0.0	3.3	3.0	0.9	0	0.20
U6	FPOM																					
U7	FPOM	54.71	24.3	45.1	6.2	11.4	7.3	13.4	6.9	16.1	0.8	1.4	8.1	4.7	5.7	7.6	1.1	4.2	3.6	1.4	0	0.07
T1	FPOM	32.15	14.1	31.7	6.5	10.3	8.8	15.0	9.0	15.8	0.4	1.1	8.8	4.7	5.5	7.2	0.6	3.6	1.5	1.1	0	0.12
U8	FPOM	37.93	16.7	38.2	6.5	11.4	8.5	14.2	8.0	15.8	0.4	1.3	8.2	4.8	5.5	7.3	1.0	3.7	2.3	1.3	0	0.14

Table 6 continued. Amino acid composition of the organic matter size fractions.

Site code	Size fraction	THAA (mg / 100 mg OC)	%TAAC	%TAAN	ASP (mol%)	GLU (mol%)	SER (mol%)	GLY (mol%)	THR (mol%)	ALA (mol%)	TYR (mol%)	MET (mol%)	VAL (mol%)	PHE (mol%)	ILE (mol%)	LEU (mol%)	HIS (mol%)	ARG (mol%)	LYS (mol%)	βALA (mol%)	γABA (mol%)	αABA (mol%)
U9	FPOM	33.84	14.9	33.7	6.7	11.0	8.8	14.9	8.3	16.2	0.3	0.9	8.8	4.8	5.6	7.2	0.5	3.3	1.9	0.7	0	0.12
U10	FPOM																					
U11	FPOM	13.56	5.9	16.6	7.1	10.8	8.4	15.0	8.5	16.2	0.4	0.4	9.1	4.3	5.2	6.6	0.6	2.7	2.0	2.5	0	0.19
T2	FPOM	17.70	7.7	18.5	12.9	11.0	8.1	14.8	8.1	15.6	0.6	0.5	7.9	3.6	4.4	8.6	0.5	1.2	0.9	0.8	0	0.51
U12	FPOM	16.96	7.3	17.9	12.1	10.5	7.6	18.5	7.7	15.1	0.6	0.1	7.2	3.8	4.2	8.0	0.3	1.4	1.4	1.1	0	0.39
P	FPOM																					
U13	FPOM	13.28	5.8	15.6	7.5	11.5	8.3	13.8	7.7	15.3	0.6	0.5	10.1	3.7	4.4	6.1	0.6	2.3	1.7	4.6	0.9	0.23
M	FPOM	12.54	5.5	17.1	7.7	12.1	8.8	14.0	7.7	15.4	0.6	0.6	9.3	3.8	4.6	6.1	0.7	1.7	1.6	4.2	0.9	0.20
N	FPOM	17.13	7.4	20.7	8.2	12.2	8.8	14.2	8.3	15.8	0.5	0.7	8.0	3.9	4.3	6.2	0.5	1.4	1.4	4.4	0.9	0.20
U1	UDOM	4.59	1.7	5.3	6.6	7.7	15.9	14.8	9.2	17.8	3.4	0.0	7.4	4.8	2.8	4.9	0.0	0.7	0.0	0.4	1.2	2.13
U2	UDOM	5.93	2.1	9.2	7.4	8.3	13.9	14.4	9.8	19.8	3.0	0.2	6.2	1.8	2.5	4.2	0.0	1.0	0.3	5.2	1.0	0.90
U3	UDOM																					
U4	UDOM	10.18	3.7	13.7	8.1	7.3	18.3	12.7	14.1	17.3	2.7	0.4	6.7	2.0	2.2	3.8	0.0	1.1	0.7	1.4	0.54	0.80
U5	UDOM	6.55	2.4	11.7	7.4	8.6	19.0	15.5	11.5	15.9	1.7	0.2	6.4	2.5	1.6	3.7	0.0	1.0	2.3	1.2	0	1.42
U6	UDOM																					
U7	UDOM	11.34	4.1	15.2	8.1	8.9	16.8	13.8	11.5	18.6	2.0	0.0	6.2	2.0	2.3	3.7	0.0	1.6	1.4	1.6	0.57	0.99
T1	UDOM	8.19	3.0	13.1	8.6	9.0	17.6	11.0	14.3	18.9	1.8	0.4	7.5	2.0	2.3	3.9	0.0	0.8	0.5	0.7	0	0.66
U8	UDOM	6.64	2.4	11.0	8.1	9.7	13.2	17.6	9.5	16.7	1.4	0.0	7.9	2.9	2.9	4.9	0.0	0.5	0.0	1.8	1.9	1.25
U9	UDOM	7.64	2.8	14.4	9.4	9.2	13.6	16.4	11.0	16.8	1.6	0.1	7.5	2.3	2.9	4.8	0.0	0.8	0.7	1.4	0.9	0.64
U10	UDOM																					
U11	UDOM	6.12	2.2	14.8	10.5	9.5	11.3	16.3	7.9	13.0	1.0	0.6	10.6	3.5	3.6	6.5	0.0	0.7	0.6	2.1	1.5	0.83
T2	UDOM	5.06	1.8	11.9	9.6	10.0	11.4	16.9	7.8	13.7	1.4	0.4	8.0	3.6	3.5	6.4	0.0	1.2	1.4	1.7	1.7	1.16
U12	UDOM	4.20	1.5	9.5	10.0	8.4	8.6	17.4	9.2	15.6	1.7	0.3	7.9	3.8	3.4	5.6	0.0	0.0	0.0	4.0	2.5	1.67
P	UDOM																					
U13	UDOM	4.05	1.5	11.2	10.8	8.5	8.9	19.7	8.0	15.1	1.4	0.2	8.1	3.2	3.5	6.0	0.0	0.3	0.0	3.9	1.8	0.74
M	UDOM	3.00	1.1	9.4	12.0	7.3	9.8	17.5	9.6	15.3	1.3	0.2	8.6	3.0	3.3	5.6	0.0	0.3	0.0	2.9	2.4	0.94
N	UDOM	3.48	1.3	10.0	11.0	8.6	7.8	17.1	8.0	15.3	1.3	0.3	9.2	3.2	4.0	6.6	0.0	0.0	0.6	4.3	1.8	0.85

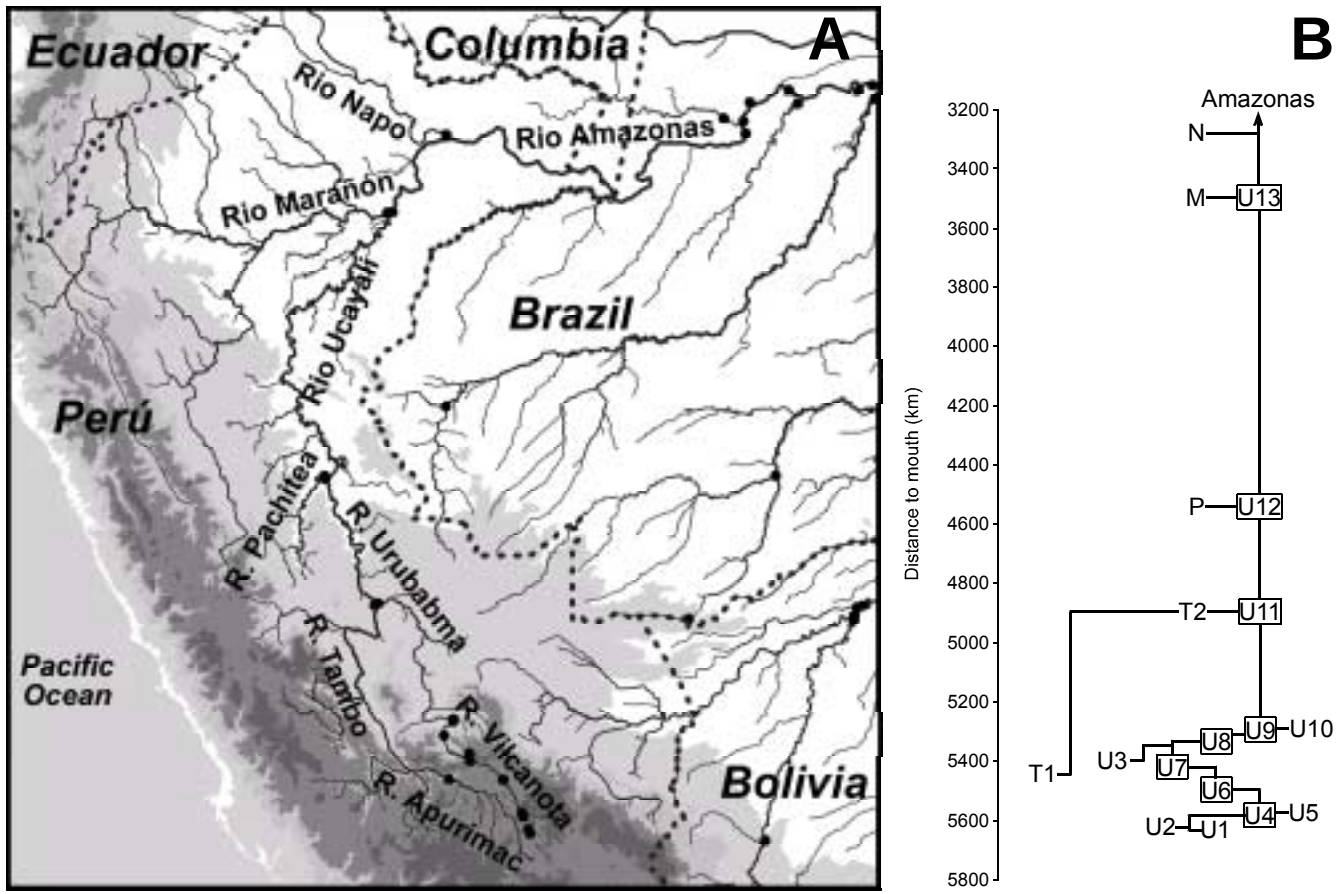

Figure 5.1. River sites sampled by the Carbon in the Amazon River Experiment (CAMREX) expedition to Amazon headwaters in Peru, presented A) in the geographic context of the region and B) by a schematic of the connections between sites. Vertical distances in B are scaled to actual flowpath distances between sites, which are described in Table 1 and in the text.

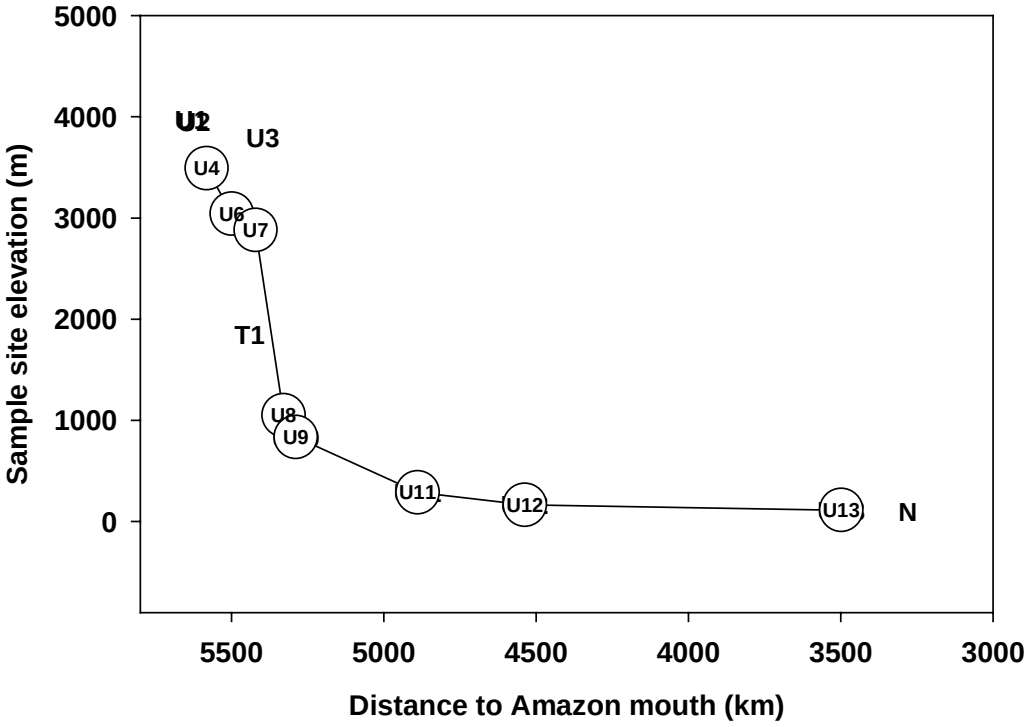

Figure 5.2. An elevation profile of the river surface between sampling sites along the confluent Rio Vilcanota – Rio Urubamba – Rio Ucayali flow path (linked symbols) and other sampling sites. See Table 5.1 for site codes.

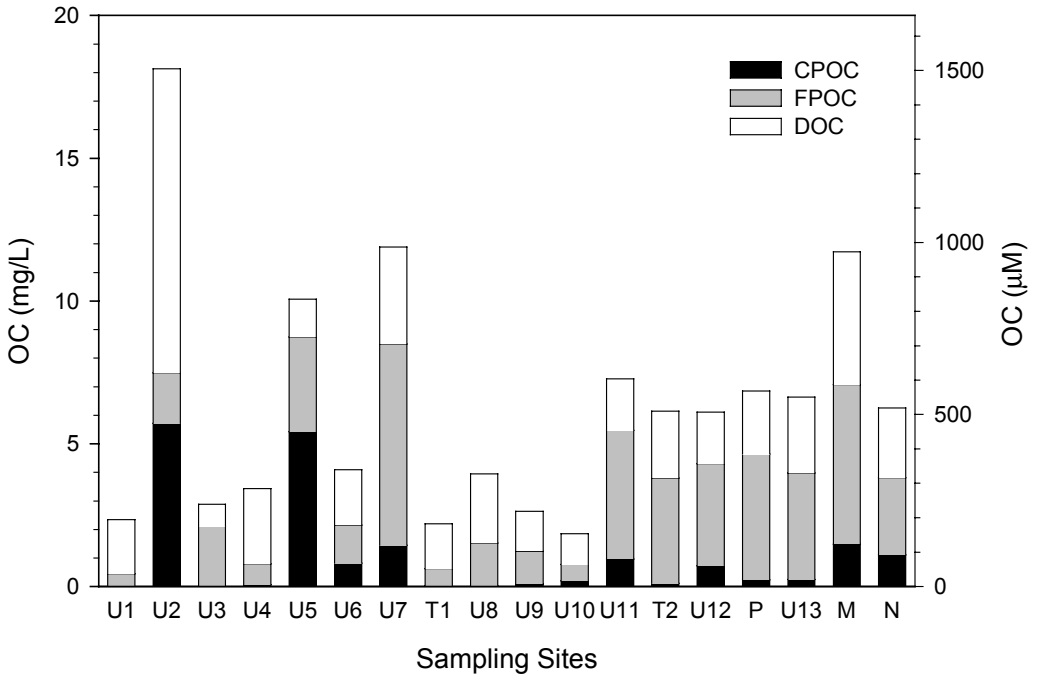

Figure 5.3. The concentration of total organic carbon (TOC) in waters sampled at each site, partitioned into contributions from each of the three principle size fractions. Coarse particulate organic carbon (CPOC) is that which is retained on a 63 µm sieve, fine particulate organic carbon (FPOC) passes the sieve but is retained on a 0.1 µm or 0.45 µm filter, and dissolved organic carbon (DOC) passes a 0.1 µm filter.

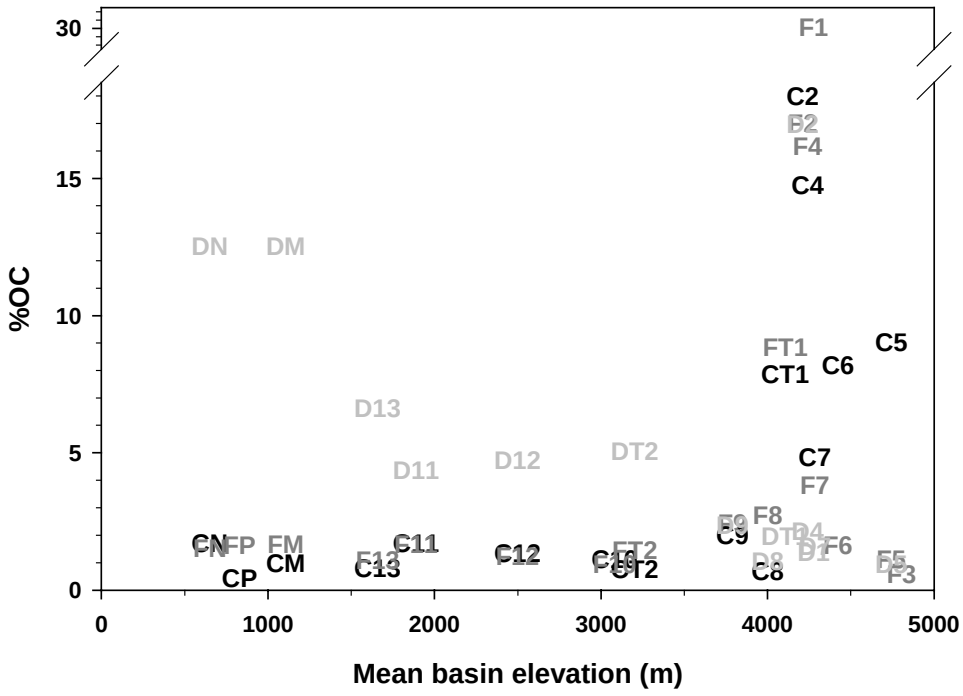

Figure 5.4. The percent by weight of organic carbon (%OC) in each of the principle size fractions, presented as function of mean basin elevation of the watershed upsteam from each sampling location. Sample codes are given in Table 5.4, where the prefixes C, F and D represent coarse particulate, fine particulate and dissolved fractions respectively.

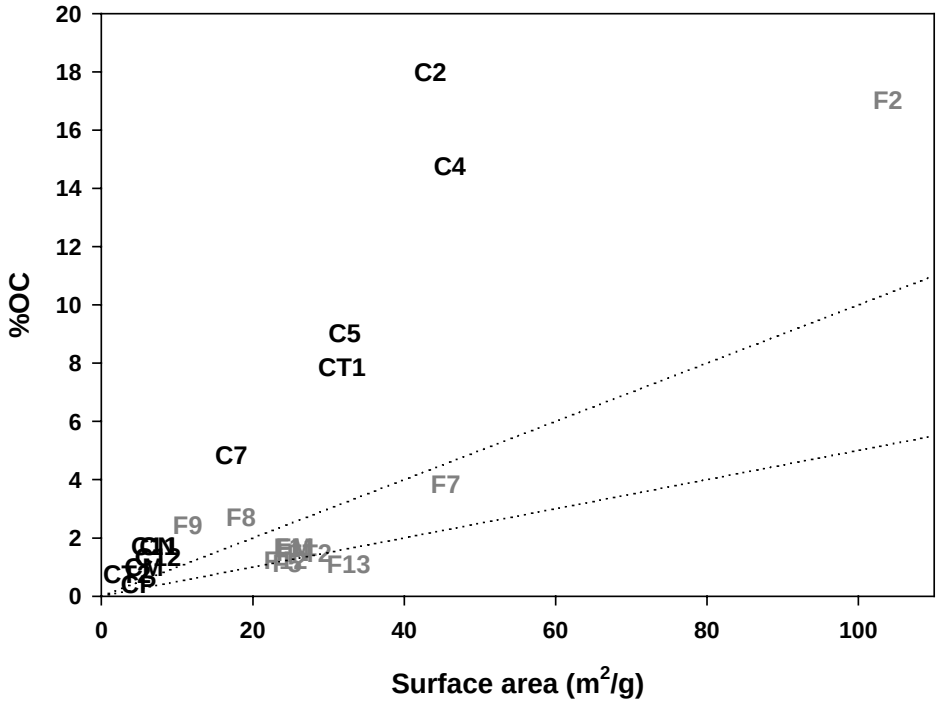

Figure 5.5. The weight percent of organic carbon (%OC) as a function of measured mineral surface area (SA) for coarse and fine riverine particulates. Dotted lines bound the region of organic carbon to surface area ratios (OC:SA) of 0.5 to 1.0 mg OC/m^2 SA. Sample codes are given in Table 5.4.

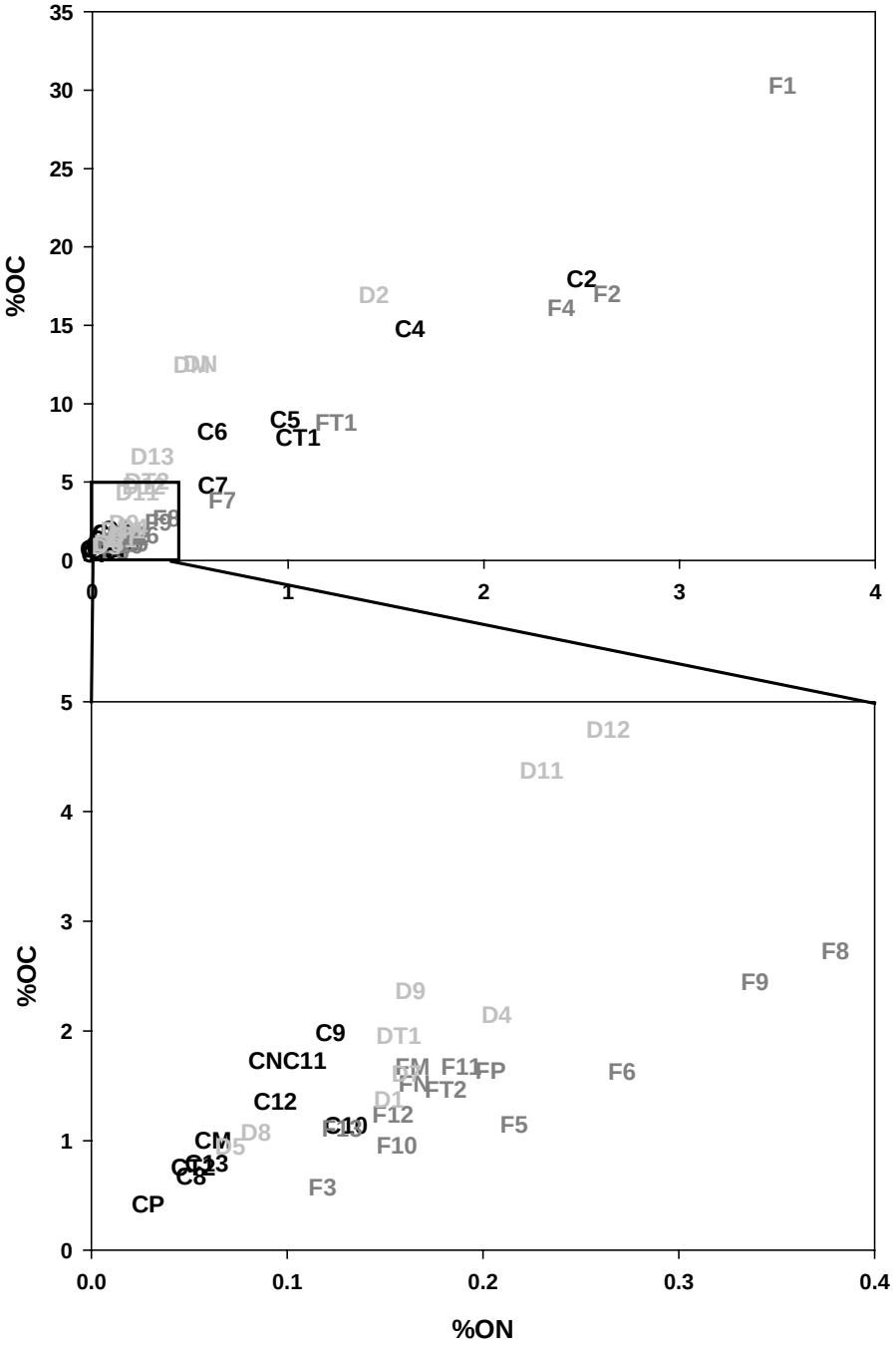

Figure 5.6. Weight percent organic carbon as a function of weight percent total nitrogen (%N) for A) all measured samples and B) expanded for those samples with lower percent organic concentrations. Sample codes are given in Table 5.4.

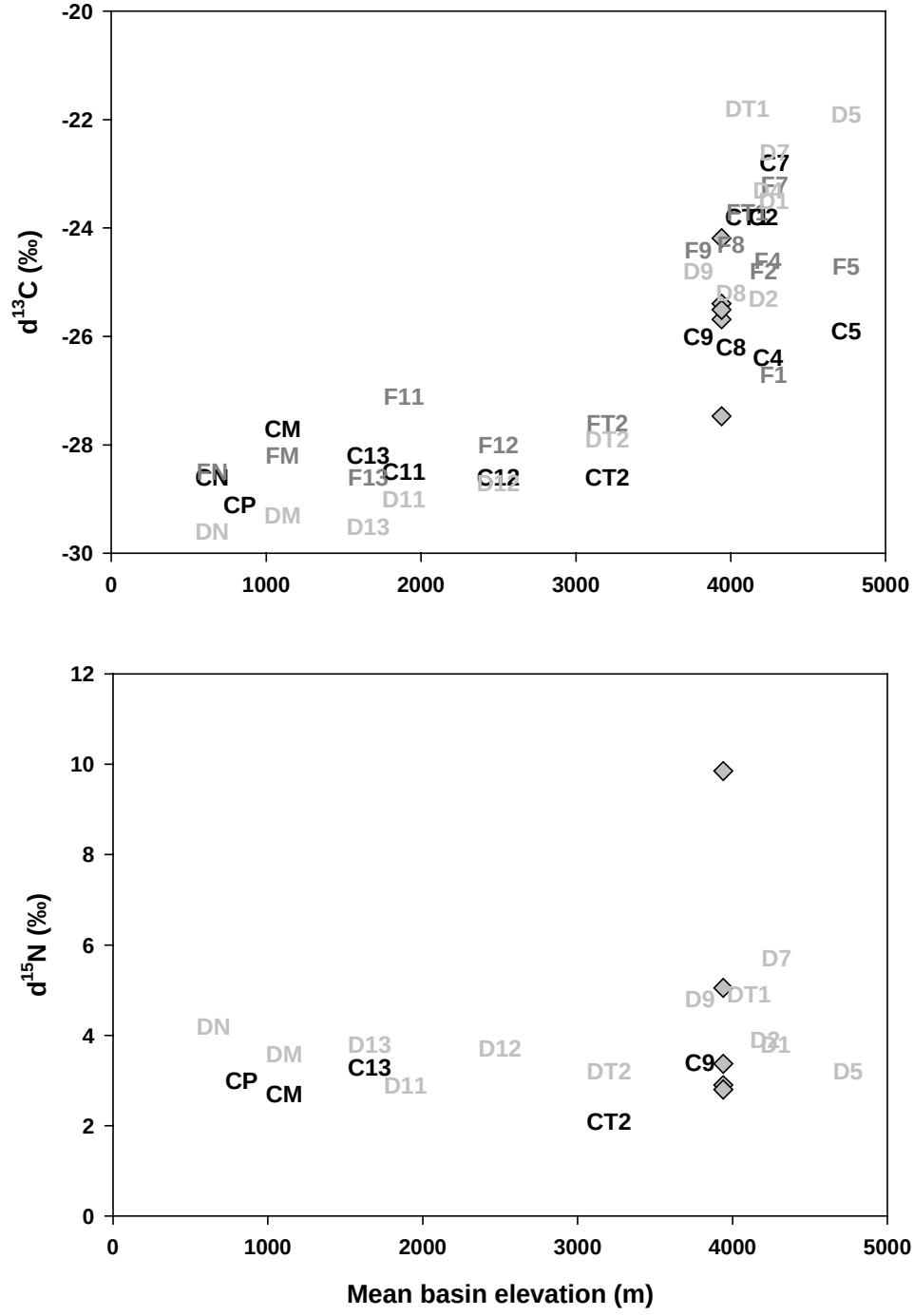

Figure 5.7. Stable isotope compositions of A) carbon ($\delta^{13}C$) and B) nitrogen ($\delta^{15}N$) for size fractions as a function of mean basin elevation. Diamonds show values measured for four different plant species (all grasses) collected near site U2.

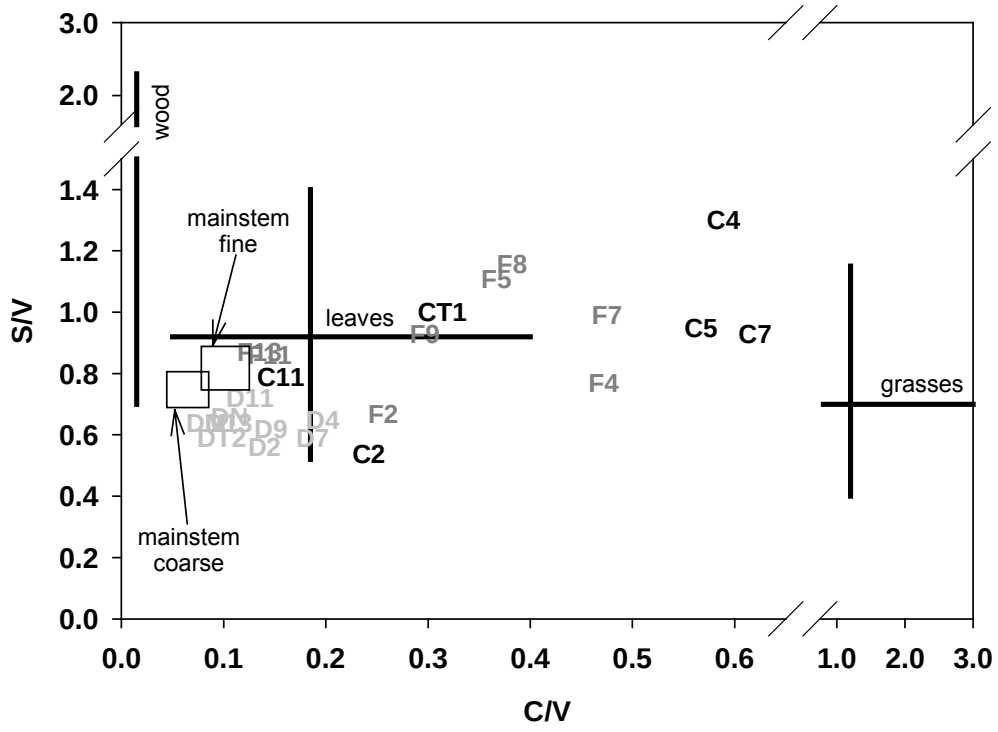

Figure 5.8. Lignin compositional parameters, the weight ratios of syringyl to vanillyl phenols (S/V) and cinnamyl to vanillyl phenols (C/V). Crosses represent the median and range of values measured for monocotylendonous grasses, dicotyledenous plant leaves and woody tissues by Hedges and Ertel (1986a). Boxes outline the mean ± standard deviation values for mainstem Amazon River samples measured in the same study.

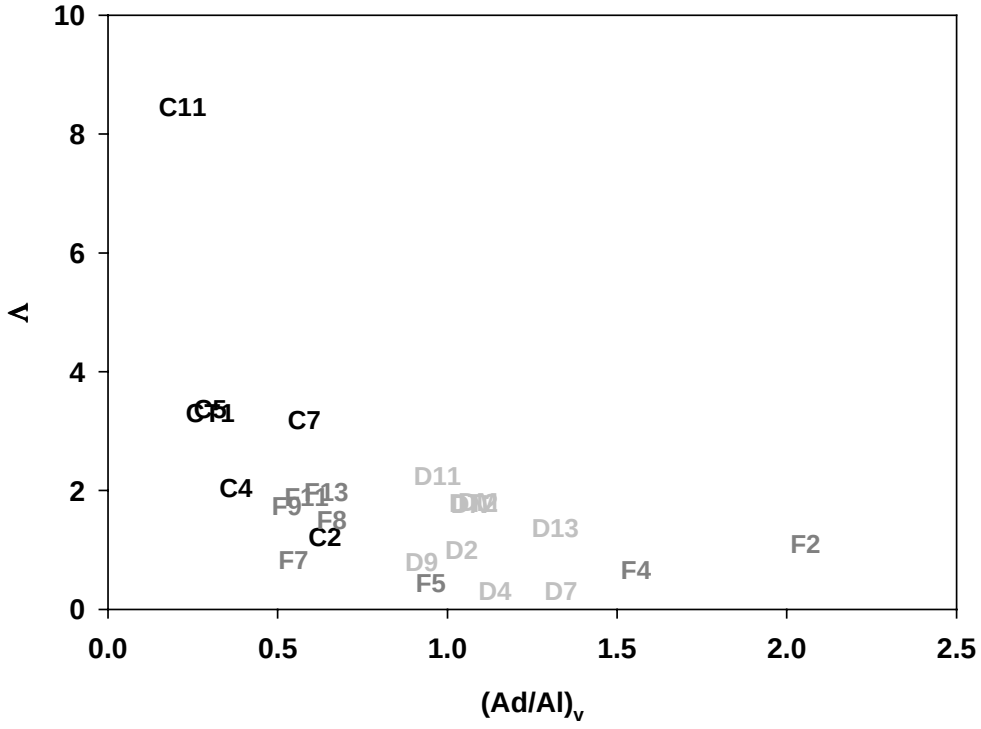

Figure 5.9. Total organic carbon normalized yield of lignin phenols (Λ, mg/100 mg OC) compared to the weight ratio of acidic to aldehyde lignin phenols (Ad/Al)v.

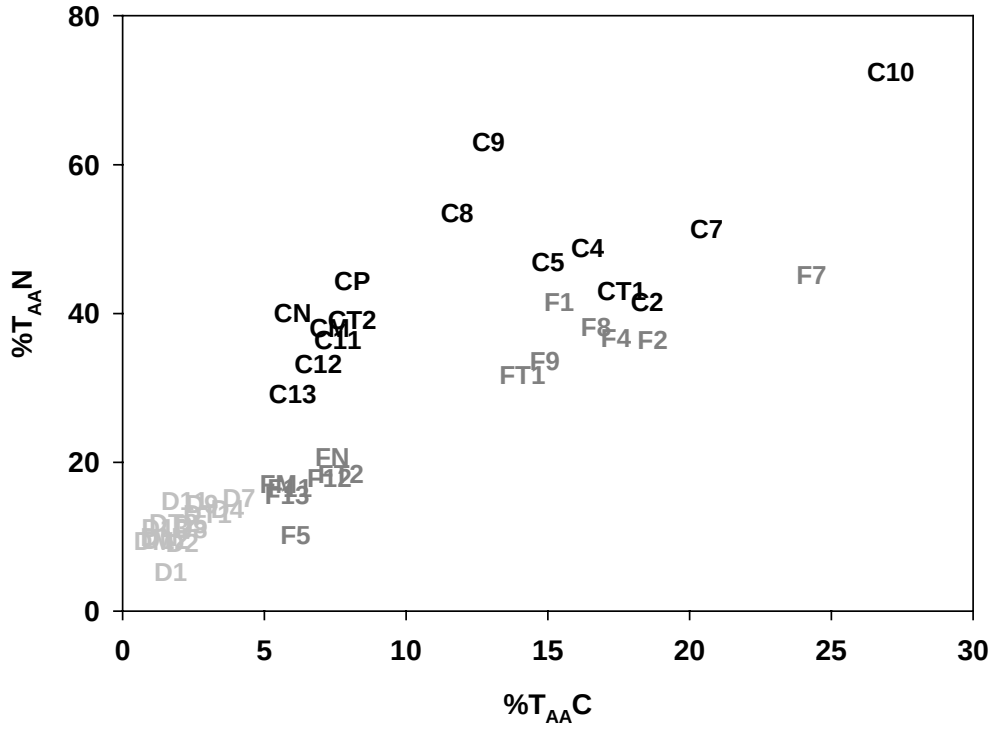

Figure 5.10. The percent of total organic nitrogen identifiable as amino acids ($\%T_{AA}N$) as a function of the corresponding percent total amino acid carbon ($\%T_{AA}C$).

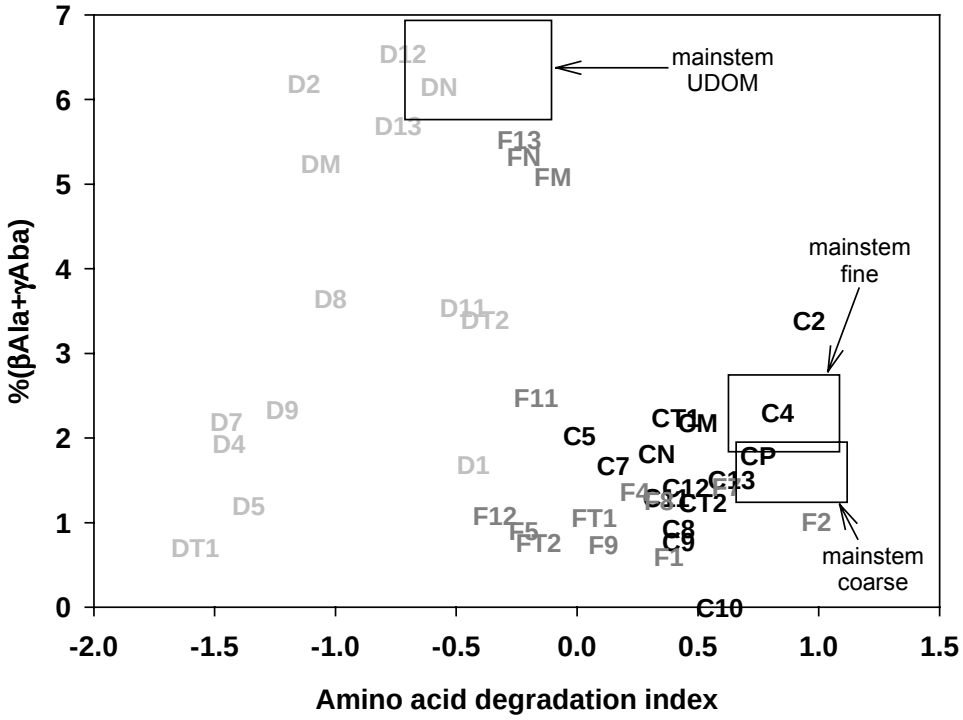

Figure 5.11. The percent contribution (to total amino acids) of non-protein amino acids β-alanine and γ-aminobutyric acid (%(βala+γaba)), as a function of an amino acid degradation index developed by Dauwe *et al.* (1999). Boxes outline the mean ± standard deviation values for mainstem Amazon River samples measured by Hedges *et al.* (Hedges et al. 1994).

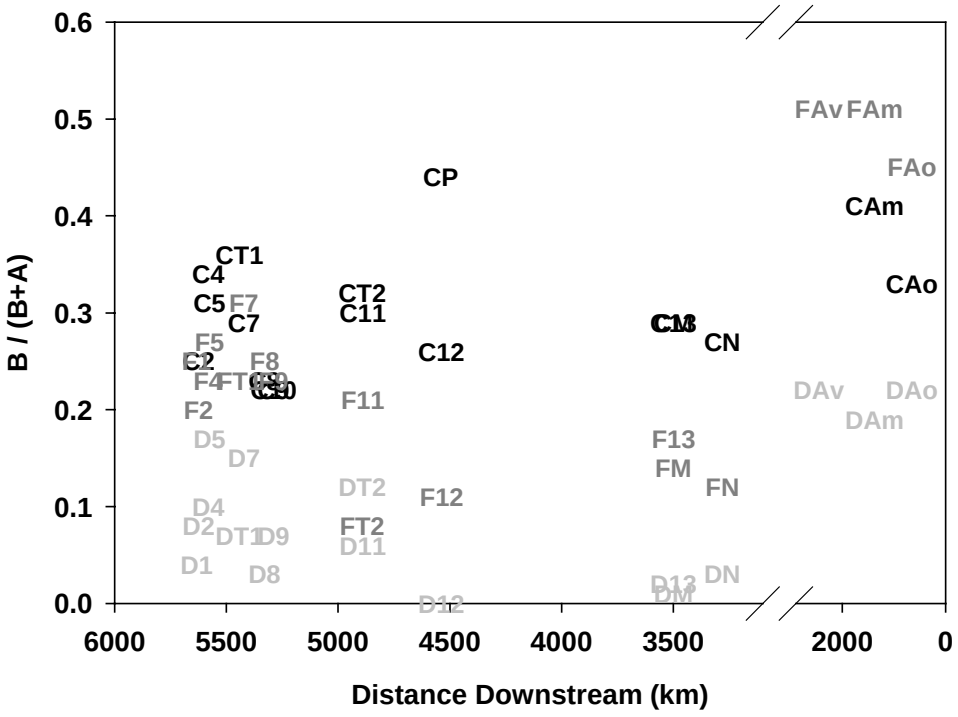

Figure 5.12. The ratio of basic amino acids, arginine and lysine, to the sum of these basic amino acids plus acidic amino acids, aspartic and glutamic acid, presented as a function of distance to the mouth of the Amazon River. Values measured at three sights for mainstem Amazon River by Hedges *et al.* (Hedges et al. 1994) are presented; Av, Am and Ao stand for the Amazon River at Vargem Grande, Manacapuru and Obidos respectively.

CHAPTER 6: OVERVIEW AND IMPLICATIONS

OVERVIEW

The driving question behind this dissertation has been: What processes determine observed contrasts in the elemental, isotopic and biochemical compositions of dissolved versus co-existing mineral-associated organic matter in aquatic systems? More specifically, do sorption and related processes produce compositional signatures that are discernable in dissolved and particulate natural organic matter fractions within the Amazon Basin? If so, how do patterns of selective partitioning affect signatures related to source or diagenesis?

In Chapter 2 and in the introduction of subsequent chapters, I reviewed previous observations and results regarding organic matter in the Amazon and other river systems. These findings were synthesized, along with related observations from soil and marine sciences, into a conceptual model of the processes important to the transport and fate of organic matter in rivers. A number of generalizations are clear. Dissolved, mineral-associated, and mineral-free particulate organic matter are compositionally distinct from one another in a wide range of environments. These OM fractions are separable by a combination of size and density, but size alone often suffices, as discrete mineral-free OM particles generally dominate in the sand size range (CPOM) but constitute a small fraction of OM found with silts and clays (FPOM). The low-density particulate fraction physically and biochemically represents partially degraded plant fragments or leaf litter and therefore can be thought to represent likely OM sources to the coexisting dissolved and mineral-associated fractions. Although CPOM is a small fraction of the total OM contained in

the flowing waters of rivers, biochemically similar materials abound on the bed, banks and riparian soils throughout a watershed. Compositional differences between low-density POM, mineral-associated OM and DOM at a given site could be due to different sources, as the three forms each have very different transport characteristics. However, consistent and strong contrasts in the composition of these fractions over such a wide range of environments point to an explanation based on universal processes rather than differential sources. Differences in the diagenesis of OM fractions have long been considered important in generating these patterns, but until this study, the role of sorption and related processes has largely been ignored in interpretations of compositional differences.

In Chapter 3, I demonstrated that essentially all of the characteristic organic nitrogen compositional differences observed between DOM and FPOM in the Amazon River could be recreated in a beaker by mixing natural DOM with aluminosilicate minerals. In each of nine laboratory experiments, nitrogen was preferentially taken into the FPOM fraction relative to the parent DOM, as were total hydrolyzable amino acids with respect to total organic carbon and to total nitrogen. The resulting distributions of indicated preferential sorption of OM containing basic amino acids with positively charged nitrogen side chains, and to a lesser extent amino acids with hydrophobic side chains. While conjectured from river samples, this was the first direct evidence for preferential uptake of naturally-occurring nitrogenous DOM by suspended riverine minerals.

These experimental observations also raised a number of important new questions. First, non-protein amino acids, which have a history of interpretation as diagenetic indicators, showed strong patterns of preferential retention in the dissolved

phase. Newly sorbed OM contained essentially none. Could this surprising result suggest that sorption and related processes might contribute to other compositional signatures that are commonly attributed to diagenetic processes? Second, the extent of elemental and biochemical fractionation during sorption appeared to increase as a function of increasing DOM freshness. Experimental "sorption" incubations were conducted with native microbial populations over a 24 hour period at ambient temperatures. Could bacteria and their exudates have played a role in creating observed FPOM compositions? Last, preliminary results showed differences in the stable carbon isotope signatures of FPOM and DOM that appeared to increase with increasing amino acid enrichment in these experiments. Given that proteins are generally enriched in ^{13}C by 1-3 ‰ relative to biomass, could sorptive processes be responsible for observed patterns of isotopic enrichment in FPOM relative to DOM in the Amazon Basin?

In Chapter 4, I present data from a second round of experiments that were designed to answer the outstanding questions raised by my first experimental results. Four suites of incubations were conducted to compare the isotherms and kinetics of DOM "sorption" in inoculated versus sterile systems. Inoculated incubations resulted in nearly twice as much organic matter associating with kaolinite compared to the sterile controls. However, only 0.2-6% of this difference could be directly attributed to bacterial biomass, suggesting that either microbial exudates were substantial or that attached bacterial biofilms might serve as new sites for additional sorption. Carbon-to-nitrogen ratios in both live and sterile incubations showed uniform and substantial enrichment of nitrogen onto particles (6-14 mol C mol^{-1} N) relative to initial dissolved OM (23.9 ± 1.6 mol C mol^{-1} N). Mineral-associated OM was enriched in

^{13}C relative to dissolved OM by on average 2.5‰ and 1.4 ‰ for the inoculated experiments and sterile controls respectively. These results demonstrate that, even over short time scales, the microbial community plays an important role in determining the extent of OM association with minerals as well as its biochemical and isotopic composition, despite the fact that biomass is an insignificant fraction of this OM. Furthermore, this study presents for the first time conclusive evidence that sorption and related processes are responsible for appreciable isotopic fractionations, which need to be considered when interpreting $\delta^{13}C$ differences between dissolved and mineral-associated fractions.

In Chapter 5, I examine the compositions of organic matter fractions from a diverse set of Andean environments near the source of the Amazon in Peru, down through a range of depositional reaches in the foreland basin, to the confluence of major lowland rivers that form the Rio Amazonas proper. The objective of the study was to evaluate the extent to which compositions of the three primary OM fractions evolve downsteam, with the overall goal of assessing the relative effects of various processes in the dynamics of OM within a large river system. Similar to previous results from the lower Amazon and from Bolivian tributaries, physical size was the most important factor in determining the composition and function of riverine organic matter. However, this study also shows that these distinctions can sometimes blur between size fractions. For instance, robust organo-mineral aggregates in Andean reaches functioned as mineral-associated OM similar to that typically found in the fine fraction, despite the larger size of these aggregates. Also dissolved organic matter in this region, with its high inorganic colloid content, might have behaved in some ways as a very fine mineral-associated particulate fraction. However, these

observations were all discerned from strong compositional signatures of sorptive processes. This study thus provides strong evidence that sorptive processes observed in the experimental studies of previous chapters are broadly applicable and quantitatively important in natural systems.

IMPLICATIONS

The biochemical composition of mineral-associated organic matter from all environments is generally quite distinct relative to either coexisting dissolved organic matter or local plant sources. In terrestrial environments, mineral-associated OM found in the fine particulate (0.1-63 μm) and high density ($\rho > 1.5$ g/cm^3) fractions of sediments and soils is consistently enriched in nitrogen and total amino acids relative to both DOM and coarse (>63 μm) or low density ($\rho < 1.5$ g/cm^3) terrestrial organic matter (POM) (Meybeck 1982; Oades 1989; Hedges et al. 1994). Biochemical signatures – such as relative proportions of individual amino acids, neutral sugars and lignin phenols – of mineral-associated OM is likewise distinct with respect to coexisting DOM (Hedges et al. 1994; Hedges et al. 2000). Mineral-associated OM in marine environments closely resembles that from terrestrial environments, with similar C/N ratios and amino acid and neutral sugar distributions (Wakeham et al. 1997; Keil et al. 1998; Lomstein et al. 1998). However, planktonic organic matter sources are typically even more enriched in N, amino acids and neutral sugars (Wakeham et al. 1997). Why is it that these compositionally very different organic matter sources converge to form mineral-associated OM fractions that are so similar? One hypothesis has been that bacteria modify these compositionally distinct to produce a more compositionally uniform pool of molecules consisting of their

byproducts. However, it is clear from observations presented in this dissertation that this is not the entire story. I propose that selective partitioning and association of dissolved OM onto mineral surfaces through both abiotic and microbially mediated processes may in fact be the dominant process. Last, in addition to exhibiting distinct biochemical compositional signatures, mineral-associated OM is also generally enriched in ^{13}C and ^{15}N and depleted in ^{14}C relative to DOM and POM that is not associated with minerals – in both rivers (Hedges et al. 1986b; Hedges et al. 2000; Raymond and Bauer 2001) and soils (Trumbore et al. 1995; Ehlreringer et al. 2000).

The results from this study demonstrate that many of these distinct compositional signatures of mineral-associated OM directly result from sorption and related processes. In fact, all of the signatures tested to date appear to be strongly affected by sorption. Therefore, it is quite possible that many more compositional signatures, once tested, might also prove to be imprinted onto minerals by these processes. If this is the case, the implications for our understanding of organic carbon cycling in the natural environment could be extraordinary. For instance, none of the mainstream terrestrial soil carbon and ecosystem models currently distinguishes between mineral-associated and low-density particulate OM (Parton et al. 1994; Schimel et al. 1994), yet all commonly use ^{13}C to constrain fluxes. Similarly, studies that interpret biochemical compositional traits would need to take sorptive processes into account.

A number of the field observations from Chapter 6 also considerably broaden our understanding of river systems. The compelling relationship between $\delta^{13}C$ and elevation in Andean drainages above 3500 m, which had only been hinted at in previous work (Cai et al. 1988; Hedges et al. 2000), is key to understanding OM

exchange on and off minerals during downriver transport. The observation of extremely high concentrations of inorganic colloids in high-altitude watersheds demonstrates how mountains can provide material that chemically weathers to nutrients once in warmer, downstream ecosystems. Finally, analysis of organic matter carried by Andean rivers considerably broadened the range of observed biochemical compositions for natural samples, especially C/V-based indications of grass contributions. The findings presented in this dissertation thus have considerable implications to organic matter studies in a wide range of natural settings and academic fields.

REFERENCES CITED

Abell, J., S. Emerson, and P. Renaud. 2000. Distributions of TOP, TON and TOC in the North Pacific subtropical gyre: Implications for nutrient supply in the surface ocean and remineralization in the upper thermocline. *J. Mar. Res.*, **58**: 203-222.

Abelson, P. H., and T. C. Hoering. 1961. Carbon isotope fractionation in formation of amino acids by photosynthetic organisms. *Proc. Natl. Acad. Sci.*, **47**: 623-632.

Amelung, W., W. Zech, X. Zhang, R. F. Follett, H. Tiessen, E. Knox, and K.-W. Flach. 1998. Carbon, nitrogen, and sulfur pools in particle-size fractions as influenced by climate. *Soil. Sci. Soc. Am. J.*, **62**: 172-181.

Amon, R. M. W., and R. Benner. 1996a. Bacterial utilization of different size classes of dissolved organic matter. *Limnol. Oceanogr.*, **41**: 41-51.

Amon, R. M. W., and R. Benner. 1996b. Photochemical and microbial consumption of dissolved organic carbon and dissolved oxygen in the Amazon River system. *Geochim. Cosmochim. Acta*, **60**: 1783-1792.

Armstrong, R. A., C. Lee, J. I. Hedges, S. Honjo, and S. G. Wakeham. in press. A new mechanistic model for organic carbon fluxes in the ocean: A quantitative role for the association of POC with ballast minerals. *Deep-Sea Res.*

Arnarson, T. S., and R. G. Keil. 2000. Mechanisms of pore water organic matter adsorption to montmorillonite. *Mar. Chem.*, **71**: 309-320.

Aufdenkampe, A. K., J. I. Hedges, P. D. Quay, A. V. Krusche, and J. E. Richey. in prep. The role of microbes in biochemical and isotopic fractionation of organic matter during association with clay minerals. *Limnol. Oceanogr.*

Aufdenkampe, A. K., J. I. Hedges, J. E. Richey, A. V. Krusche, and C. A. Llerena. 2001. Sorptive fractionation of dissolved organic nitrogen and amino acids onto fine sediments within the Amazon Basin. *Limnol. Oceanogr.*, **46**: 1921-1935.

Baldock, J. A., and J. O. Skjemstad. 2000. Role of the soil matrix and minerals in protecting natural organic materials against biological attack. *Org. Geochem.*, **31**: 697-710.

Bell, R. T. 1993. Estimating production of heterotrophic bacterioplankton via incorporation of tritiated thymidine, p. *In* P. F. Kemp, B. F. Sherr, E. B. Sherr, and J. J. Cole [eds.], *Handbook of Methods in Aquatic Microbial Ecology*. Lewis Publishers.

Benedetti, M. F., C. J. Milne, D. G. Kinniburgh, W. H. Van Riemsdijk, and L. K. Koopal. 1995. Metal ion binding to humic substances: Application of the non-ideal competitive adsorption model. *Environ. Sci. Technol.*, **29**: 446-457.

Benner, R. 1991. Ultra-Filtration for the concentration of Bacteria, Viruses, and Dissolved Organic Matter, p. 181-185. *In*, *Marine Particles: Analysis and Characterization*. American Geophysical Union.

Benner, R. in press. Chemical composition and reactivity, p. *In* D. A. Hansell and C. Carlson [eds.], *Biogeochemistry of Marine Dissolved Organic Matter*. Academic Press.

Benner, R., S. Opsahl, G. Chin-Leo, J. E. Richey, and B. R. Forsberg. 1995. Bacterial carbon metabolism in the Amazon River system. *Limnol. Oceanogr.*, **40**: 1262-1270.

Bergamaschi, B. A., E. C. Tsamakis, R. G. Keil, T. I. Eglinton, D. B. Montluçon, and J. I. Hedges. 1997. The effect of grain size and surface area on organic matter, lignin and carbohydrate concentration, and molecular compositions in Peru Margin sediments. *Geochim. Cosmochim. Acta*, **61**: 1247-1126.

Bernardes, M. C., L. A. Martinelli, A. V. Krusche, J. Gudeman, M. Moreira, R. L. Victoria, J. P. H. B. Ometto, M. V. R. Ballester, A. K. Aufdenkampe, J. E. Richey, and J. I. Hedges. in preparation. Organic matter composition of rivers of the Ji-Paraná basin (southwest Amazon basin) as a function of land use changes. *Ecol. Appl.*, **LBA Special Issue**.

Bird, M. I., S. G. Haberle, and A. R. Chivas. 1994. Effect of altitude on the carbon-isotope composition of forest and grassland soils from Papua New Guinea. *Global Biogeochem. Cycles*, **8**: 13-22.

Boulton, A. J., S. Findlay, P. Marmonier, E. H. Stanley, and H. M. Valett. 1998. The functional significance of the hyporheic zone in streams and rivers. *Annual Review of Ecology and Systematics*, **29**: 59-81.

Brandes, J. A., M. E. Mcclain, and T. P. Pimentel. 1996. ^{15}N evidence for the origin and cycling of inorganic nitrogen in a small Amazonian catchment. *Biogeochem.*, **34**: 45-56.

Burdige, D. J., and K. G. Gardner. 1998. Molecular weight distribution of dissolved organic carbon in marine sediment pore waters. *Mar. Chem.*, **62**: 45-64.

Burdige, D. J., and C. S. Martens. 1990. Biogeochemical cycling in an organic-rich coastal marine basin; II, The sedimentary cycling of dissolved, free amino acids. *Geochim. Cosmochim. Acta*, **54**: 3033-3052.

Burdige, D. J., and S. Zheng. 1998. The biogeochemical cycling of dissolved organic nitrogen in estuarine sediments. *Limnol. Oceanogr.*, **43**: 1796-1813.

Cai, D. L., F. C. Tan, and J. M. Edmond. 1988. Sources and transport of particulate organic carbon in the Amazon river and estuary. *Est. Coast. Shelf Sci.*, **26**: 1-14.

Carter, P. W. 1978. Adsorption of amino acid-containing organic matter by calcite and quartz. *Geochim. Cosmochim. Acta*, **42**: 1239-1242.

Carter, P. W., and R. M. Mitterer. 1978. Amino acid composition of organic matter associated with carbonate and non-carbonate sediments. *Geochim. Cosmochim. Acta*, **42**: 1231-1238.

Chin, W.-C., P. Verdugo, and M. Orellana. 1998. Spontaneous assembly of marine dissolved organic matter into polymer gels. *Nature*, **391**: 568-572.

Christensen, B. T. 1996. Carbon in primary and secondary organomineral complexes, p. 97-165. *In* M. R. Carter and B. A. Stewart [eds.], *Structure and Organic Matter Storage in Agricultural Soils*. CRC Press.

Cole, J. J., and N. F. Caraco. 2001. Carbon in catchments: Connecting terrestrial carbon losses with aquatic metabolism. *Marine and Freshwater Research*, **52**: 101-110.

Cole, J. J., N. F. Caraco, G. W. Kling, and T. K. Kratz. 1994. Carbon dioxide supersaturation in the surface waters of lakes. *Science*, **256**: 1568-1570.

Costerton, W. J., K.-J. Cheng, G. G. Geesey, T. I. Ladd, J. C. Nickel, M. Dasgupta, and T. J. Marrie. 1987. Bacterial biofilms in nature and disease. *Ann. Rev. Microbiol.*, **41**: 435-464.

Cowie, G. L., and J. I. Hedges. 1984. Determination of Neutral Sugars in Plankton, Sediments, and Wood by Capillary Gas Chromatography of Equilibrated Isomeric Mixtures. *Anal. Chem.*, **56**: 497-504.

Cowie, G. L., and J. I. Hedges. 1992a. Improved amino acid quantification in environmental samples: charge-matched recovery standards and reduced analysis time. *Mar. Chem.*, **37**: 223-238.

Cowie, G. L., and J. I. Hedges. 1992b. Sources and reactivities of amino acids in a coastal marine environment. *Limnol. Oceanogr.*, **37**: 703-724.

Cowie, G. L., and J. I. Hedges. 1994. Biochemical indicators of diagenetic alteration in natural organic matter mixtures. *Nature*, **369**: 304-307.

Cowie, G. L., J. I. Hedges, F. G. Prahl, and G. J. De Lange. 1995. Elemental and major biochemical changes across an oxidation front in a relict turbidite: An oxygen effect. *Geochim. Cosmochim. Acta*, **59**: 33-46.

Crump, B. C., and J. A. Baross. 2000. Characterization of the bacterially-active particle fraction in the Columbia River estuary. *Mar. Ecol. Prog. Ser.*, **206**: 13-22.

Crump, B. C., J. A. Baross, and C. A. Simenstad. 1998. Dominance of particle-attached bacteria in the Columbia River estuary, USA. *Aq. Microb. Ecol.*, **14**: 7-18.

Curtis, W. F., R. H. Meade, C. F. Nordin Jr., N. B. Price, and E. R. Sholkovitz. 1979. Non-uniform vertical distribution of fine sediment in the Amazon River. *Nature*, **280**: 381-383.

Dashman, T., and G. Stotzky. 1982. Adsorption and binding of amino acids on homionic montmorillonite and kaolinite. *Soil Biol. Biochem.*, **14**: 447-456.

Dauwe, B., J. J. Middelburg, P. M. J. Herman, and C. H. R. Heip. 1999. Linking diagenetic alteration of amino acids and bulk organic matter reactivity. *Limnol. Oceanogr.*, **44**: 1809-1814.

Davis, J. A. 1982. Adsorption of natural dissolved organic matter at the oxide/water interface. *Geochim. Cosmochim. Acta*, **46**: 2381-2393.

Davis, J. A., and R. Gloor. 1981. Adsorption of dissolved organics in lake water by aluminum oxide, effect of molecular weight. *Environ. Sci. Technol.*, **15**: 1223-1229.

Day, G. M., B. T. Hart, I. D. Mckelvie, and R. Beckett. 1994. Adsorption of natural organic matter onto goethite. *Colloid. Surf. A*, **89**: 1-13.

Devol, A. H., B. R. Forsberg, J. E. Richey, and T. P. Pimentel. 1995. Seasonal variation in chemical distributions in the Amazon (Solimões) River: a multiyear time series. *Global Biogeochem. Cycles*, **9**: 307-328.

Devol, A. H., and J. I. Hedges. 2001. Organic matter and nutrients in the mainstem Amazon River, p. 275-306. *In* M. E. McClain, R. L. Victoria, and J. E. Richey [eds.], *The Biogeochemistry of the Amazon Basin*. Oxford University Press.

Devol, A. H., J. E. Richey, B. R. Forsberg, and L. A. Martinelli. 1994. Environmental methane in the Amazon river floodplain, p. 151-165. *In* W. J. Mitsch [ed.], *Global Wetlands*. Elsevier.

Dunne, T., L. A. K. Mertes, R. H. Meade, J. E. Richey, and B. R. Forsberg. 1998. Exchanges of sediment between the flood plain and channel of the Amazon River in Brazil. *Geol. Soc. Am. Bull.*, **110**: 450-467.

Ehlreringer, J. R., N. Buchmann, and L. B. Flanagan. 2000. Carbon isotope ratios in belowground carbon cycle processes. *Ecol. Appl.*, **10**: 412-422.

Ertel, J. R., J. I. Hedges, A. H. Devol, and J. E. Richey. 1986. Dissolved humic substances of the Amazon River system. *Limnol. Oceanogr.*, **31**: 739-754.

Filius, J. D., D. G. Lumsdon, J. C. L. Meeussen, T. Hiemstra, and W. H. Van Riemsdijk. 2000. Adsorption of fulvic acid on geothite. *Geochim. Cosmochim. Acta*, **64**: 51-60.

Forsberg, B. R., A. H. Devol, J. E. Richey, L. A. Martinelli, and H. Dos Santos. 1988. Factors controlling nutrient concentrations in Amazon floodplain lakes. *Limnol. Oceanogr.*, **33**: 41-56.

Furch, K. 1984. Water chemistry of the Amazon basin: The distribution of chemical elements among freshwaters, p. 167-199. *In* H. Sioli [ed.], *The Amazon: Limnology and Landscape Ecology of a Mighty Tropical River and its Basin*. W. Junk Publishers.

Gibbs, R. J. 1967. The geochemistry of the Amazon River System: Part I. The factors that control the salinity and the composition and concentration of the suspended solids. *Geol. Soc. Am. Bull.*, **78**: 1203-1232.

Goni, M. A., and J. I. Hedges. 1992. Lignin dimers: Structures, distribution, and potential geochemical applications. *Geochim. Cosmochim. Acta*, **56**: 4025-4043.

Gu, B., T. L. Mehlhorn, L. Liang, and J. F. Mccarthy. 1996. Competitive adsorption, displacement, and transport of organic matter on iron oxide: I. Competitive adsorption. *Geochim. Cosmochim. Acta*, **60**: 1943-1950.

Gu, B., J. Schmitt, Z. Chen, L. Liang, and J. F. Mccarthy. 1994. Adsorption and desorption of natural organic matter on iron oxide: mechanisms and models. *Environ. Sci. Technol.*, **28**: 38-46.

Gu, B., J. Schmitt, Z. Chen, L. Liang, and J. F. Mccarthy. 1995. Adsorption and desorption of different organic matter fractions on iron oxide. *Geochim. Cosmochim. Acta*, **59**: 219-229.

Guggenberger, G., W. Zech, and H.-R. Schulten. 1994. Formation and mobilization pathways of dissolved organic matter: evidence from chemical structural studies of organic matter fractions in acid forest floor solutions. *Org. Geochem.*, **21**: 51-66.

Guyot, J. L. 1993. Hydrogeochimie des fleuves de l'Amazonie bolivienne [Etudes et Thèses]., Editions de l'ORSTOM.

Hayes, J. M. in press. Fractionation of the isotopes of carbon and hydrogen in biosynthetic processes, p. *In* J. W. Valley and D. R. Cole [eds.].

Hedges, J. I. 1978. The formation and clay mineral reactions of melanoidins. *Geochim. Cosmochim. Acta*, **42**: 69-76.

Hedges, J. I., W. A. Clark, P. D. Quay, J. E. Richey, A. H. Devol, and U. D. M. Santos. 1986a. Compositions and fluxes for particulate organic material in the Amazon River. *Limnol. Oceanogr.*, **31**: 717-738.

Hedges, J. I., G. L. Cowie, J. E. Richey, P. D. Quay, R. Benner, M. Strom, and B. R. Forsberg. 1994. Origins and processing of organic matter in the Amazon River indicated by carbohydrates and amino acids. *Limnol. Oceanogr.*, **39**: 743-761.

Hedges, J. I., and J. R. Ertel. 1982. Characterization of lignin by gas capillary chromatography of cupric oxide oxidation products. *Anal. Chem.*, **54**: 174-178.

Hedges, J. I., J. R. Ertel, P. D. Quay, P. M. Grootes, J. E. Richey, A. H. Devol, G. W. Farwell, F. W. Schmidt, and E. Salati. 1986b. Organic carbon-14 in the Amazon River system. *Science*, **231**: 1129-1131.

Hedges, J. I., and P. E. Hare. 1987. Amino acid adsorption by clay minerals in distilled water. *Geochim. Cosmochim. Acta*, **51**: 255-259.

Hedges, J. I., F. S. Hu, A. H. Devol, H. E. Hartnett, E. Tsamakis, and R. G. Keil. 1999. Sedimentary Organic Matter Preservation: a test for selective degradation under oxic conditions. *Am. J. Sci.*, **299**: 529-555.

Hedges, J. I., and R. G. Keil. 1995. Sedimentary organic matter preservation: An assessment and speculative synthesis. *Mar. Chem.*, **49**: 81-115.

Hedges, J. I., E. Mayorga, E. Tsamakis, M. E. Mcclain, A. K. Aufdenkampe, P. Quay, J. E. Richey, R. Benner, S. Opsahl, B. Black, T. Pimentel, J. Quintanilla, and L. Maurice. 2000. Organic matter in Bolivian tributaries of the Amazon River: A comparison to the lower mainstem. *Limnol. Oceanogr.*, **45**: 1449-1466.

Hedges, J. I., and J. M. Oades. 1997. Comparative organic geochemistries of soils and marine sediments. *Org. Geochem.*, **27**: 319-361.

Hedges, J. I., and J. H. Stern. 1984. Carbon and nitrogen determinations of carbonate containing solids. *Limnol. Oceanogr.*, **29**: 657-663.

Henrichs, S. M. 1995. Sedimentary organic matter preservation: An assessment and speculative synthesis -- a comment. *Mar. Chem.*, **49**: 127-136.

Henrichs, S. M., and S. F. Sugai. 1993. Adsorption of amino acids and glucose by sediments of Resurrection Bay, Alaska, USA: Functional group effects. *Geochim. Cosmochim. Acta*, **57**: 823-835.

Hoch, M. P., M. L. Fogel, and D. L. Kirchman. 1992. Isotope fractionation associated with ammonium uptake by a marine bacterium. *Limnol. Oceanogr.*, **37**: 1447-1459.

Ittekkot, V., S. Safiullah, and R. Arain. 1986. Nature of organic matter in rivers with deep-sea connections: The Ganges-Brahmaputra and Indus. *Sci. Tot. Environ.*, **58**: 93-107.

Janik, L. J., J. O. Skjemstad, and M. D. Raven. 1995. Characterization and analysis of soils using mid-infrared partial least squares I: Corrections with XRF-determined major element composition. *Aust. J. Soil Res.*, **33**: 621-636.

Jardine, P. M., N. L. Weber, and J. F. Mccarthy. 1989. Mechanisms of dissolved organic carbon adsorption on soil. *J. Soil Sci. Soc. Am.*, **53**: 1378-1385.

Johnsson, M. J., and R. H. Meade. 1990. Chemical weathering of fluvial sediments during alluvial storage: The Macuapanim Island point bar, Solimoes River, Brazil. *Journal of Sedimentary Petrology*, **60**: 827-842.

Kaiser, K. 1998. Fractionation of dissolved organic matter affected by polyvalent metal cations. *Org. Geochem.*, **28**: 849-854.

Kaiser, K., and G. Guggenberger. 2000. The role of DOM sorption to mineral surfaces in the preservation of organic matter in soils. *Org. Geochem.*, **31**: 711-725.

Kaiser, K., G. Guggenberger, L. Haumaier, and W. Zech. 1997. Dissolved organic matter sorption on subsoils and minerals studied by ^{13}C-NMR and DRIFT spectroscopy. *Euro. J. Soil. Sci.*, **48**: 301-310.

Kaiser, K., and W. Zech. 1997. Competitive sorption of dissolved organic matter fractions to soils and related mineral phases. *Soil. Sci. Soc. Am. J.*, **61**: 64-69.

Kaplan, L. A., and J. D. Newbold. 1993. Biogeochemistry of dissolved organic carbon entering streams, p. 139-165. *In* T. E. Ford [ed.], *Aquatic Microbiology: An Ecological Approach*. Blackwell Scientific Publications.

Keil, R. G., L. M. Mayer, P. D. Quay, J. E. Richey, and J. I. Hedges. 1997. Losses of organic matter from riverine particles in deltas. *Geochim. Cosmochim. Acta*, **61**: 1507-1511.

Keil, R. G., D. B. Montluçon, F. G. Prahl, and J. I. Hedges. 1994a. Sorptive preservation of labile organic matter in marine sediments. *Nature*, **370**: 549-552.

Keil, R. G., E. Tsamakis, J. C. Giddings, and J. I. Hedges. 1998. Biochemical distributions among size-classes of modern marine sediments. *Geochim. Cosmochim. Acta*, **62**: 1347-1364.

Keil, R. G., E. Tsamakis, and J. I. Hedges. 2000. Early diagenesis of particulate amino acids in marine systems, p. 69-82. *In* G. A. Goodfriend, M. J. Collins, M. L. Fogel, S. A. Macko, and J. F. Wehmiller [eds.], *Perspectives in Amino Acid and Protein Geochemistry*. Oxford University Press.

Keil, R. G., E. C. Tsamakis, C. B. Fuh, J. C. Giddings, and J. I. Hedges. 1994b. Mineralogical and textural controls on the organic composition of coastal marine sediments: Hydrodynamic separation using SPLITT-fractionation. *Geochim. Cosmochim. Acta*, **58**: 879-893.

Kennedy, M. J., D. R. Pevear, and R. J. Hill. 2002. Mineral surface control of organic carbon in black shale. *Science*, **295**: 657-660.

Korner, C., and J. A. I. Arnone. 1992. Responses to elevated carbon dioxide in artificial tropica ecosystems. *Science*, **257**: 1672-1675.

Küchler, I. L., N. Miekeley, and B. R. Forsberg. 1994. Molecular mass distributions of dissolved organic carbon and associated metals in waters from Rio Negro and Rio Solimoes. *Sci. Tot. Environ.*, **156**: 207-216.

Lee, C., and C. Cronin. 1982. The vertical flux of particulate nitrogen in the sea: decomposition of amino acids in the Peru upwelling area and the equatorial Pacific. *J. Mar. Res.*, **40**: 227-251.

Lewis, W. M., S. K. Hamilton, and J. F. Saunders. 1995. Rivers of northern South America, p. 219-256. *In* C. E. Cushing, K. W. Cummins, and G. W. Minshall [eds.], *River and Stream Ecosystems*. Elsevier.

Lobbes, J. M., H. P. Fitznar, and G. Kattner. 2000. Biogeochemical characteristics of dissolved and particulate organic matter in Russian rivers entering the Arctic Ocean. *Geochim. Cosmochim. Acta*, **64**: 2973-2983.

Lomstein, B. A., A.-G. U. Jensen, J. W. Hansen, J. B. Andreasen, L. S. Hansen, J. Berntsen, and H. Kunzendorf. 1998. Budgets of sediment nitrogen and carbon cycling in the shallow water of Knebel Vig, Denmark. *Aq. Microb. Ecol.*, **14**: 69-80.

Ludwig, W., and J.-L. Probst. 1996. Predicting the oceanic input of organic carbon by continental erosion. *Global Biogeochem. Cycles*, **10**: 23-41.

Macko, S. A., M. L. Fogel, P. E. Hare, and T. C. Hoering. 1987. Isotopic fractionation of nitrogen and carbon in the synthesis of amino acids by microorganisms. *Chem. Geol.*, **65**: 79-92.

Mannino, A., and H. R. Harvey. 2000. Biochemical composition of particles and dissolved organic matter along an estuarine gradient: Sources and implications for DOM reactivity. *Limnol. Oceanogr.*, **45**: 775-788.

Marengo, J. A., and C. A. Nobre. in press. General characteristics and variability of climate in the Amazon Basin and its links to the global climate system, p. *In* M. E. McClain, R. L. Victoria, and J. E. Richey [eds.], *The Biogeochemistry of the Amazon Basin and its Role in a Changing World*. Oxford University Press.

Martinelli, L. A., R. L. Victoria, J. L. I. Dematte, J. E. Richey, and A. H. Devol. 1993. Chemical and mineralogical composition of Amazon River floodplain sediments, Brazil. *Applied Geochemistry*, **8**: 391-402.

Mayer, L. M. 1994a. Relationships between mineral surfaces and organic carbon concentrations in soils and sediments. *Chem. Geol.*, **114**: 347-363.

Mayer, L. M. 1994b. Surface area control of organic carbon accumulation in continental shelf sediments. *Geochim. Cosmochim. Acta*, **58**: 1271-1284.

Mayer, L. M. 1999. Extent of coverage of mineral surfaces by organic matter in marine sediments. *Geochim. Cosmochim. Acta*, **63**: 207-215.

Mayer, L. M., R. G. Keil, S. A. Macko, S. B. Joye, K. C. Ruttenberg, and R. C. Aller. 1998. Importance of suspended particulates in riverine delivery of bioavailable nitrogen to coastal zones. *Global Biogeochem. Cycles*, **12**: 573-579.

Mayer, L. M., and B. Xing. 2001. Organic matter-surface area relationships in acid soils. *Soil. Sci. Soc. Am. J.*, **65**: 250-258.

Mayorga, E., and A. K. Aufdenkampe. in press. The processing of bioactive elements by the Amazon River system, p. *In* M. E. McClain [ed.], *The Ecohydrology of South American Rivers and Wetlands*.

Mccarthy, M., J. I. Hedges, and R. Benner. 1996. Major biochemical composition of dissolved high molecular weight organic matter in seawater. *Mar. Chem.*, **55**: 281-297.

Mcclain, M. E., J. E. Richey, J. A. Brandes, and T. P. Pimentel. 1997. Dissolved organic matter and terrestrial-lotic linkages in the central Amazon Basin of Brazil. *Global Biogeochem. Cycles*, **11**: 295-311.

Mcclain, M. E., J. E. Richey, and T. P. Pimentel. 1994. Groundwater nitrogen dynamics at the terrestrial-lotic interface of a small catchment in the Central Amazon Basin. *Biogeochem.*, **27**: 113-127.

Mcknight, D. M., K. E. Bencala, G. W. Zeliweger, G. R. Aiken, G. L. Feder, and K. A. Thorn. 1992. Sorption of dissolved organic carbon by hydrous aluminum and iron oxides occuring at the confluence of Deer Creek with the Snake River, Summit County, Colorado. *Environ. Sci. Technol.*, **26**: 1388-1396.

Meade, R. H. 1994. Suspended sediments of the modern Amazon and Orinoco Rivers. *Quaternary International*, **21**: 29-39.

Meade, R. H., T. Dunne, J. E. Richey, U. M. Santos, and E. Salati. 1985. Storage and remobilization of sediment in the lower Amazon River of Brazil. *Science*, **228**: 488-490.

Ménot, G., and S. J. Burns. 2001. Carbon isotopes in ombrogenic peat bog plants as climatic indicators: calibration from an altitudinal transect in Switzerland. *Org. Geochem.*, **32**: 233-245.

Mertes, L. A. K., T. Dunne, and L. A. Martinelli. 1996. Channel-floodplain geomorphology of the Solimões-Amazon River, Brazil. *Geol. Soc. Am. Bull.*, **108**: 1089-1107.

Meybeck, M. 1982. Carbon, nitrogen, and phosphorus transport by world rivers. *Am. J. Sci.*, **282**: 401-450.

Moran, M. A., and R. G. Zepp. 1997. Role of photoractions in the formation of biologically labile compounds from dissolved organic matter. *Limnol. Oceanogr.*, **42**: 1307-1316.

Moran, S. B., M. A. Charette, S. M. Pike, and C. A. Wicklund. 1999. Differences in seawater particulate organic carbon concentration in samples collected using small- and large-volume methods: the importance of DOC adsorption to the filter blank. *Mar. Chem.*, **67**: 33-42.

Mounier, S., R. Braucher, and J. Y. Benaïm. 1999. Differentiation of organic matter's properties of the Rio Negro basin by crossflow ultra-filtration and UV-spectrofluorescence. *Water Res.*, **33**: 2363-2373.

Nelson, P. N., J. A. Baldock, and J. M. Oades. 1993. Concentration and composition of dissolved organic carbon in streams in relation to catchment soil properties. *Biogeochem.*, **19**: 27-50.

Nelson, P. N., J. A. Baldock, and G. Soulas. 1994. Availability of organic carbon in soluble and particle-sized fractions from a soil profile. *Soil Biol. Biochem.*, **26**: 1549-1555.

Oades, J. M. 1988. The retention of organic matter in soils. *Biogeochem.*, **5**: 35-70.

Oades, J. M. 1989. An introduction to organic matter in mineral soils, p. 89-159. *In* J. B. Dixon and S. B. Weed [eds.], *Minerals in Soil Environments*. Soil Science Society of America.

Parton, W. J., D. S. Ojima, C. V. Cole, and D. S. Schimel. 1994. A general model for soil organic matter dynamics: Sensitivity to litter chemistry, texture and management, p.

147-167. *In* R. B. Bryant and R. W. Arnold [eds.], *Quantitative modeling of soil forming processes*. SSSA Special Pub. no. 39.

Patel, N., S. Mounier, J. L. Guyot, C. Benamou, and J. Y. Benaïm. 1999. Fluxes of dissolved and colloidal organic carbon, along the Purus and Amazonas Rivers (Brazil). *Sci. Tot. Environ.*, **229**: 53-64.

Peterson, M. L., S. Lang, A. K. Aufdenkampe, and J. I. Hedges. submitted. Dissolved organic carbon measurement using a modified high temperature DOC analyzer. *Mar. Chem.*

Puhakka, M., R. Kalliola, M. Rajasilta, and J. Salo. 1992. River types, site evolution and successional vegetation patterns in Peruvian Amazonia. *Journal of Biogeography*, **19**: 651-665.

Qualls, R. G., and B. L. Haines. 1992. Biodegradability of dissolved organic matter in forest throughfall, soil solution, and stream water. *Soil. Sci. Soc. Am. J.*, **56**: 578-586.

Quay, P., S. King, D. Wilbur, S. Wofsy, and J. Richey. 1989. $^{13}C/^{12}C$ of atmospheric CO_2 in the Amazon Basin: forest and river sources. *J. Geophys. Res.*, **94**: 18327-18336.

Quay, P. D., D. O. Wilbur, J. E. Richey, A. H. Devol, R. Benner, and B. R. Forsberg. 1995. The $^{18}O/^{16}O$ of dissolved oxygen in rivers and lakes in the Amazon Basin: a tracer of respiration and photosynthesis. *Limnol. Oceanogr.*, **40**: 718-729.

Quay, P. D., D. O. Wilbur, J. E. Richey, J. I. Hedges, A. H. Devol, and R. L. Victoria. 1992. Carbon cycling in the Amazon River: Implications from the ^{13}C composition of particles and solutes. *Limnol. Oceanogr.*, **37**: 857-871.

Ransom, B., R. H. Bennett, R. J. Baerwald, and K. Shea. 1997. TEM study of in situ organic matter on continental margins: Occurrence and the "monolayer" hypothesis. *Mar. Geol.*, **138**: 1-9.

Räsänen, M., R. Neller, J. Salo, and H. Junger. 1992. Recent and ancient fluvial deposition systems in the Amazonian foreland basin, Peru. *Geol. Mag.*, **129**: 293-306.

Raymond, P. A., and J. E. Bauer. 2001. Riverine export of aged terrestrial organic matter to the North Atlantic Ocean. *Nature*, **409**: 497-499.

Richey, J. E., A. H. Devol, S. C. Wofsy, R. Victoria, and M. N. G. Ribeiro. 1988. Biogenic gases and the oxidation and reduction of carbon in the Amazon River and floodplain waters. *Limnology and Oceanograpy*, **33**: 551-561.

Richey, J. E., J. I. Hedges, A. H. Devol, P. D. Quay, R. L. Victoria, L. Martinelli, and B. R. Forsberg. 1990. Biogeochemistry of carbon in the Amazon River. *Limnol. Oceanogr.*, **35**: 352-371.

Richey, J. E., R. H. Meade, E. Salati, A. H. Devol, C. F. Nordin, Jr., and U. Dos Santos. 1986. Water discharge and suspended sediment concentrations in the Amazon River: 1982-1984. *Water Resour. Res.*, **22**: 756-764.

Richey, J. E., J. M. Melack, A. K. Aufdenkampe, V. M. Ballester, and L. L. Hess. In Press. Outgassing from Amazonian rivers and wetlands as a large tropical source of atmospheric CO_2. *Nature*.

Richey, J. E., S. R. Wilhelm, M. E. Mcclain, R. L. Victoria, J. M. Melack, and C. Araujo-Lima. 1997. Organic matter and nutrient dynamics in river corridors of the Amazon Basin and their response to anthropogenic change. *Ciencia e Cultura*, **49**: 98-110.

Salo, J., R. .Kalliola, I. Häkkinen, Y. Mäkinen, P. Niemelä, M. Puhakka, and P. D. Coley. 1986. River dynamics and the diversity of Amazon lowland forest. *Nature*, **322**: 254-258.

Schimel, D. S., B. H. Braswell, E. A. Holland, R. Mckeown, D. S. Ojima, T. H. Painter, W. J. Parton, and A. R. Townsend. 1994. Climatic, edaphic, and biotic controls over storage and turnover of carbon in soils. *Global Geochemical Cycles*, **8**: 279-293.

Schimel, D. S., J. I. House, K. A. Hibbard, P. Bousquet, P. Ciais, P. Peylin, B. H. Braswell, M. J. Apps, D. Backer, A. Bondeau, J. Canadell, G. Churkina, W. Cramer, A. S. Denning, C. B. Field, P. Friedlingstein, C. Goodale, M. Heimann, R. A. Houghton, J. M. Melillo, B. Moore, Iii, D. K. Murdiyarso, I. Noble, S. W. Pacala, I. C. Prentice, M. R. Raupach, P. J. Rayner, R. J. Scholes, W. L. Steffen, and C. Wirth. 2001. Recent patterns and mechanisms of carbon exchange by terrestrial ecosystems. *Nature*, **414**: 169-172.

Sioli, H. 1984a. The Amazon and its main affluents: Hydrography, morphology of the river courses, and river types, p. 127-165. *In* H. Sioli [ed.], *The Amazon: Limnology and Landscape Ecology of a Mighty Tropical River and its Basin*. W. Junk Publishers.

Sioli, H. 1984b. The Amazon: Limnology and Landscape Ecology of a Mighty Tropical River and its Basin.]. W. Junk Publishers, 763.

Sokal, R. R., and F. J. Rohlf. 1995. Biometry: The Principles and Practice of Statistices in Biological Research, W. H. Freeman and Company.

Stallard, R. F. 1998. Terrestrial sedimentation and the carbon cycle: coupling weathering and erosion to carbon burial. *Global Biogeochem. Cycles*, **12**: 231-257.

Stallard, R. F., and J. M. Edmond. 1981. Geochemistry of the Amazon. 1. Precipitation chemistry and the marine contribution to the dissolved load at the time of peak discharge. *J. Geophys. Res.*, **86**: 9844-9858.

Stallard, R. F., and J. M. Edmond. 1983. Geochemistry of the Amazon: 2. The influence of geology and weathering environment on the dissolved load. *J. Geophys. Res.*, **88**: 9671-9688.

Stallard, R. F., and J. M. Edmond. 1987. Geochemistry of the Amazon. 3. Weathering chemistry and limits to dissolved inputs. *J. Geophys. Res.*, **92**: 8293-8302.

Sternberg, H. O. 1975. *The Amazon River of Brazil*, Franz Steiner Verlag GMBH.

Sun, L., E. M. Perdue, J. L. Meyer, and J. Weis. 1997. Use of elemental composition to predict bioavailability of dissolved organic matter in a Georgia river. *Limnol. Oceanogr.*, **42**: 714-721.

Taylor, J. R. 1997. An Introduction to Error Analysis: The Study of Uncertainties in Physical Measurements, University Science Books.

Trumbore, S. E., E. A. Davidson, P. B. D. Camargo, D. C. Nepstad, and L. A. Martinelli. 1995. Belowground cycling of carbon in forests and pastures of Eastern Amazonia. *Global Biogeochem. Cycles*, **9**: 515-528.

Van De Weerd, H., A. Leijnse, and W. H. Van Riemsdijk. 1999. Modeling the dynamic adsorption/desorption of a NOM mixture: Effects of physical and chemical heterogeneity. *Environ. Sci. Technol.*, **33**: 1675-1681.

Victoria, R. L., L. A. Martinelli, P. C. O. Trivelin, E. Matsui, B. R. Forsberg, J. E. Richey, and A. H. Devol. 1992. The use of stable isotopes in studies of nutrient cycling: Carbon isotope composition of Amazon varzea sediments. *Biotrop.*, **24**: 240-249.

Wakeham, S. G., C. Lee, J. I. Hedges, P. J. Hernes, and M. L. Peterson. 1997. Molecular indicators of diagenetic status in marine organic matter. *Geochim. Cosmochim. Acta*, **61**: 5363-5369.

Wallace, A. R. 1853. Narrative of travels on the Amazon and Rio Negro, Reeve.

Wang, X.-C., and C. Lee. 1993. Adsorption and desorption of aliphatic amines, amino acids and acetate by clay minerals and marine sediments. *Mar. Chem.*, **44**: 1-23.

Williams, P. M. 1968. Organic and inorganic constituents of the Amazon River. *Nature*, **218**: 937-938.

Wissmar, R. C., J. E. Richey, R. F. Stallard, and J. M. Edmond. 1981. Plankton metabolism and carbon processes in the Amazon River, its tributaries, and floodplain waters, Peru-Brazil, May-June 1977. *Ecology*, **62**: 1622-1633.

Zhou, J. L., S. Rowland, R. F. C. Mantoura, and J. Braven. 1994. The formation of humic coatings on mineral particles under simulated estuarine conditions -- a mechanistic study. *Water Res.*, **28**: 571-579.

Vita
ANTHONY K. AUFDENKAMPE

EDUCATION

Ph.D. 2002. Chemical Oceanography, University of Washington. Advisor: John I. Hedges. Dissertation: *The Role of Sorptive Processes in the Organic Carbon and Nitrogen Cycles of the Amazon River Basin*.

M.Sc. 1998. Chemical Oceanography, University of Washington. Advisors: John I. Hedges and James W. Murray. Thesis: *Controls on New Production Along the Equator in the Western and Central Pacific*.

B.A. 1991, *cum Laude*. Chemistry, Dartmouth College. Advisor: Dean E. Wilcox. Senior Honors Thesis: *Solid-Phase Synthesis and Characterization of the β-Domain of Human Liver Metallothionein II*.

PUBLICATIONS

Richey, J. E., J. M. Melack, **A. K. Aufdenkampe**, V. M. Ballester and L. L. Hess. In Press. Outgassing from Amazonian rivers and wetlands as a large tropical source of atmospheric CO_2. *Nature*.

Aufdenkampe, A. K., J. J. McCarthy, C. Navarette, M. Rodier, J. Dunne and J. W. Murray. In Press. Biogeochemical controls on new production in the tropical Pacific. *Deep-Sea Research II* Equatorial Pacific Synthesis Special Issue.

Aufdenkampe, A. K., and J. W. Murray. In Press. Controls on new production: The role of iron and physical processes. *Deep-Sea Research II* Equatorial Pacific Synthesis Special Issue.

Mayorga, E. and **A. K. Aufdenkampe**. In Press. The processing of bioactive elements by the Amazon River system. *The Ecohydrology of South American Rivers and Wetlands*. M. E. McClain, ed.

Aufdenkampe, A. K., J. I. Hedges, A. V. Krusche, C. Llerena and J. E. Richey. 2001. Sorptive fractionation of dissolved organic nitrogen and amino acids onto sediments within the Amazon Basin. *Limnology and Oceanography*, **46**(8), 1921-1935.

Aufdenkampe, A. K., J. J. McCarthy, M. Rodier, C. Navarette, J. P. Dunne and J. W. Murray. 2001. Estimation of new production in the tropical Pacific. *Global Biogeochemical Cycles*, **15**(1): 101-113.

Hedges, J. I., E. Mayorga, E. Tsamakis, M. E. McClain, **A. K. Aufdenkampe**, P. Quay, J. E. Richey, R. Benner, S. Opsahl*, et al.* 2000. Organic matter in Bolivian tributaries of the Amazon River: A comparison to the lower mainstem. *Limnology and Oceanography* **45**(7): 1449-1466.

Dunne, J. P., J. W. Murray, **A. K. Aufdenkampe**, S. Blain and M. Rodier. 1999. Silicon-nitrogen coupling in the equatorial Pacific upwelling zone. *Global Biogeochemical Cycles* **13**(3): 715-726.